Bioengineering Strategies to Enhance Myoglobin Expression in 3D C2C12 Muscle Constructs

Vom Promotionsausschuss der

Technischen Universität Hamburg

zur Erlangung des akademischen Grades

Doktor-Ingenieur (Dr.-Ing.)

genehmigte Dissertation (Monografie)

von

Mojtaba Khozaei Ravari

aus

Kerman, Iran

2026

Die Gutachter:

Prof. Dr. rer. nat. An-Ping Zeng

Prof. Dr.-Ing. Ralf Pörtner

Tag der mündlichen Prüfung:

04.06.2026

DOI: https://doi.org/10.15480/882.17649

ORCID: https://orcid.org/0000-0001-7362-7988

Acknowledgments

I would like to express my deepest gratitude to Prof. Dr. rer. nat. An-Ping Zeng, former Head of the Institute of Bioprocess and Biosystems Engineering (IBB) at Hamburg University of Technology (TUHH), for his invaluable supervision, continuous guidance, and unwavering support throughout my doctoral studies.

My sincere thanks also go to Prof. Dr.-Ing. Ralf Pörtner, former Chief Engineer of the Institute of Bioprocess and Biosystems Engineering, for his guidance, constructive discussions, and for kindly serving as a reviewer of this thesis. His critical insights and encouragement have been of great value throughout both my experimental work and the preparation of this dissertation.

I am deeply grateful to my colleague Christiane Schaffer, whose unwavering support, patience, and dedication in the laboratory were instrumental in overcoming numerous experimental challenges. I would also like to thank my colleagues Xinyi, Lukas, Tom, Philipp, Jan, Tyll, Chijian, and Giovanni for generously sharing their knowledge and experience and for fostering a collaborative and supportive working environment. Working alongside such talented and kind colleagues has been one of the most rewarding aspects of my doctoral journey.

I would also like to express my heartfelt gratitude to my family, whose love, sacrifices, and constant encouragement have provided the foundation for my achievements.

Finally, I owe my deepest thanks to my beloved wife, Fatemeh Zarei, for her unwavering love, patience, and support throughout these years. Her encouragement and steadfast belief in me have been my greatest source of strength, both in times of success and in moments of challenge. Without her, this achievement would not have been possible.

To all those who contributed directly or indirectly to this work, I extend my sincere appreciation. Your support has been invaluable and is deeply appreciated.

Abstract

Developing physiologically relevant *in vitro* models of skeletal muscle tissue remains a central and persistent challenge across tissue engineering, regenerative medicine, and cultivated meat research. A critical barrier to achieving both scalability and advanced function is the absence of a simple, cost-effective fabrication strategy, coupled with insufficient clarity regarding the control mechanisms governing tissue maturation and key metabolic parameters like oxygenation. Myoglobin, the crucial oxygen-binding protein in muscle, serves as a vital functional biomarker for metabolic capacity and tissue maturity. This thesis directly addresses these fundamental obstacles through three integrated studies. First, a novel, scaffold-free protocol was successfully developed for fabricating three-dimensional (3D) skeletal muscle constructs with good structural integrity from C2C12 myoblasts. This innovative method leverages a spontaneous delamination phenomenon induced solely by serum starvation, offering a distinct advantage in simplicity and cost-effectiveness over conventional techniques. The resulting constructs were characterized for high viability, structural integrity determined via histology and scanning electron microscopy, and successful myogenic differentiation confirmed through myosin heavy chain expression. Second, to overcome inherent scalability limitations, computational modeling was integrated computational modeling with meticulous experimental validation to estimate a critical size constraint for these dense, cell-only constructs. Finite element simulations, validated by experimental measurements, established a maximum viable thickness of 5 mm based on the model's prediction that oxygen concentration at the construct's core would drop to zero at this boundary. This constraint is fundamentally driven by the inherent biophysical characteristics of the engineered tissue, thus establishing an important, data-informed design parameter for all future upscaling efforts. Finally, a a broad range of biochemical and physical parameters was systematically investigated to enhance myoglobin protein synthesis, the central indicator of tissue maturation and coloration.

The findings showed that myoglobin synthesis is not solely driven by supplementation with iron, creatine, or Insulin-like Growth Factor-I (IGF-I), but is instead profoundly regulated by the physical and chemical microenvironment. Specifically, culture vessel size was inversely correlated with myoglobin content, with smaller vessels yielding significantly higher levels. Controlled bioreactor experiments identified a moderate dissolved oxygen (DO) concentration of 30 % air saturation as most favorable for myoglobin synthesis. Furthermore, applying a

cyclic mechanical stretching regimen, when combined with optimal DO, induced a synergistic increase in myoglobin levels, resembling physiological responses to muscle exercise.

Altogether, this work presents an integrated framework to creating, optimizing, and functionally enhancing scaffold-free muscle constructs. Four critical parameters, culture vessel size, culture time, dissolved oxygen levels, and mechanical stimulation, were identified that collectively govern myoglobin synthesis. These findings provide a useful foundation for developing physiologically relevant engineered muscle constructs with potential applications, from disease modeling to sustainable food production.

Table of contents

List of figures

List of tables

List of Abbreviations

ECM	Extracellular matrix
PNIPAAm	Poly(N-isopropylacrylamide)
3D	Three-dimensional
GM	Growth medium
PBS	Phosphate-buffered saline
H&E	Hematoxylin and Eosin
MHC	Myosin heavy chain
SEM	Scanning electron microscopy
D_{eff}	Effective oxygen diffusion coefficient
OUR	Oxygen uptake rate [$mol.L^{-1}.h^{-1}$]
k_La	Volumetric mass transfer coefficient
q_{O2}	Specific oxygen consumption rate [$mol.cells^{-1}.h^{-1}$]
ROS	Reactive oxygen species
DO	Dissolved oxygen
NRU	Neutral red uptake assay
OD	Optical density
DCFH-DA	(2′− 7′- dichlorodihydrofluorescein diacetate) assay
RFU	Relative fluorescence units
PI	Propidium Iodide
I_2KI	Iodine potassium iodide
IGF-I	Insulin-like Growth Factor-I

1. Chapter One: Introduction

1.1. Background

Skeletal muscle, as a highly organized, contractile tissue, plays a vital role in voluntary movement, posture, metabolism, and regeneration. Muscle injuries arising from trauma, degenerative diseases, or surgical resections often require therapeutic interventions beyond the body's natural regenerative capacity. This has driven growing interest in skeletal muscle tissue engineering, a field that aims to restore or replace damaged muscle tissue by integrating principles from cell biology, materials science, and biomedical engineering [1].

The engineering of functional skeletal muscle tissue typically involves three essential components: myogenic cells, a scaffold or supporting structure, and a suitable biochemical and mechanical environment. These elements work together to recapitulate the architecture and physiological function of native muscle. However, the complexity of skeletal muscle, particularly its hierarchical structure and mechanical anisotropy, poses substantial engineering challenges. One critical issue remains the alignment and maturation of myotubes *in vitro*, a necessary feature for developing contractile and physiologically relevant muscle tissues [2]. Another major hurdle is the vascularization of thick constructs, as sufficient oxygen and nutrient supply becomes limiting in larger tissue volumes [3].

To address these limitations, various strategies have been proposed, including the use of anisotropic scaffolds, conductive biomaterials, and dynamic culture systems. Conductive and mechanically tunable biomaterials have demonstrated potential to enhance electrical and mechanical cues that promote myogenic differentiation and maturation [4]. Yet, while scaffold-based approaches have achieved significant milestones, they are often constrained by issues such as immunogenicity, degradation byproducts, and limited cell–cell interactions.

In response to the limitations posed by traditional scaffold-based systems, researchers have increasingly turned toward scaffold-free tissue engineering. This strategy seeks to exploit the cells' intrinsic capacity to self-organize and produce their own extracellular matrix (ECM), thus mimicking natural tissue development more closely [5]. By eliminating the scaffold, these methods offer several advantages, such as improved biocompatibility, enhanced cell signaling, and a lower risk of introducing foreign material into the body.

Scaffold-free techniques include spheroid assembly, cell aggregation, and bio-printing of tissue-like structures, often relying on external forces (e.g., gravity, magnetic fields) to guide the spatial organization of cells. In the context of cardiac and skeletal muscle engineering, scaffold-free methods have yielded promising results in terms of both tissue structure and function. For instance, Stevens et al. demonstrated the physiological functionality of scaffold-free, vascularized cardiac tissues suitable for transplantation, while Fujita et al. utilized magnetite-incorporated C2C12 cells to fabricate contractile skeletal muscle tissue without exogenous scaffolds [6,7].

Nevertheless, creating robust and functional muscle tissues using scaffold-free approaches remains challenging. Achieving proper alignment, mechanical strength, and integration with host tissues still requires careful design of the culture system and stimulation protocols. Moreover, thick 3D tissues often suffer from oxygen diffusion limitations, leading to necrotic cores or incomplete differentiation in the central regions.

Among scaffold-free techniques, cell sheet engineering has emerged as a particularly promising platform for tissue reconstruction, offering precise control over cell organization and tissue layering without the need for enzymatic dissociation or synthetic materials [8,9]. Originally developed for myocardial applications, the technique involves culturing cells on temperature-responsive surfaces that allow intact sheets of cells and ECM to be harvested simply by lowering the temperature.

Cell sheet engineering enables the fabrication of aligned and functionally relevant tissues by stacking multiple sheets of myogenic cells. This approach preserves crucial cell–cell and cell–ECM interactions, which are essential for maintaining tissue integrity and promoting differentiation. Furthermore, layering multiple sheets facilitates the creation of three-dimensional structures with improved thickness and contractile performance compared to monolayer cultures [7].

Tissue engineering strategies, particularly those involving cell sheet technology, have advanced significantly in the last two decades. One of the pioneering approaches, developed by Okano et al., introduced the use of temperature-responsive culture surfaces to harvest intact cell sheets without enzymatic treatment [10]. While this technique preserves cell-cell junctions and ECM components, critical for functional tissue architecture, it is not without its technical limitations. The reliance on thermo-responsive polymers, such as poly(N-isopropylacrylamide) (PNIPAAm), necessitates precise thermal control and often specialized cultureware, which can

be both costly and difficult to scale. Moreover, the delamination process, although non-enzymatic, still requires careful manipulation and timing to avoid sheet tearing or uneven detachment. These limitations present challenges for both standardization and translation to larger-scale or 3D tissue constructs.

In light of these limitations, there has been growing interest in enhancing the physiological functionality of 3D muscle constructs, moving beyond the mechanical aspects of tissue assembly and focusing on cellular metabolism and oxygen dynamics. At the center of this interest lies myoglobin, a heme-containing oxygen-binding protein predominantly found in striated muscle cells. Myoglobin plays a critical role in oxygen storage, delivery, and buffering, especially under hypoxic or energetically demanding conditions. It acts as an intracellular reservoir and facilitator of oxygen diffusion, thereby sustaining aerobic metabolism in muscle tissue [11]. Structurally, myoglobin is composed of a globular polypeptide chain with a central heme prosthetic group, which binds molecular oxygen via its iron atom [12]. This structure is highly conserved across species, reflecting its evolutionary importance in vertebrate muscle physiology. Developmentally, myoglobin expression begins early during myogenesis, with studies showing induction at the mRNA and protein levels during the initial stages of muscle cell differentiation [13,14]. Its expression is tightly coordinated with the maturation of contractile elements such as myosin heavy chains, marking it as both a functional and maturation biomarker in muscle tissue engineering.

The regulation of myoglobin is multifaceted. It is influenced by hypoxia, exercise, and various signaling molecules. Kanatous and Mammen emphasized the role of PGC-1α and oxidative signaling pathways in upregulating myoglobin, which are relevant targets in tissue engineering and regenerative therapies [15]. Interestingly, even outside of classic muscle tissue, myoglobin has been shown to play developmental roles, as seen in zebrafish models where its absence led to developmental abnormalities [16]. This reinforces its importance not just as an oxygen buffer, but as a regulator of cellular differentiation and tissue organization.

1.2. Research objectives

The primary aim of this research was to explore and optimize strategies for enhancing myoglobin protein synthesis in three-dimensional (3D) muscle-like constructs derived from myoblasts. From a process engineering perspective, the study sought to identify and fine-tune culture parameters that improve myoglobin expression and contribute to the development of more physiologically relevant muscle constructs. The research was guided by the following

interconnected objectives, each rooted in potential applications across medicine, research, and biotechnology.

First, the study aimed to generate foundational knowledge relevant to future therapeutic applications in regenerative medicine. Engineered muscle constructs with higher oxidative capacity, achieved through elevated myoglobin expression, are hypothesized to be better suited for transplantation, particularly in ischemic or metabolically stressed environments. This has potential implications for treating volumetric muscle loss, traumatic injuries, or progressive degenerative conditions such as Duchenne muscular dystrophy. By promoting the resilience and function of the grafted tissue, such constructs could better integrate and survive in the host.

Second, the research explored the feasibility of developing a more physiologically relevant *in vitro* model of skeletal muscle. The generated 3D muscle constructs enriched in myoglobin represent an initial step toward models that better reflect the oxidative characteristics of mature muscle. Such models are valuable for basic biological studies as well as for preclinical drug screening targeting oxidative stress or muscle metabolism. Crucially, to ensure the physiological relevance and viability of these models, the study also aimed to define the critical physical parameters, such as oxygen diffusion limitations, through computational modeling. This modeling component was essential for guiding the design of viable 3D constructs and ensuring their relevance as *in vitro* platforms.

Third, the research demonstrated potential relevance to cultured meat technologies. Myoglobin plays a crucial biological role and influences the color, taste, and nutritional quality of meat. Enhancing myoglobin levels in lab-grown muscle tissue could therefore improve visual appeal and nutritional content, contributing to the scientific basis for future food biotechnology applications. This is particularly relevant since cultivated muscle typically appears pale due to its low myoglobin content [17]. While adding edible colorants is the simplest solution to this issue, it may negatively affect how consumers perceive lab-grown meat.

Finally, the research aimed to support the functional maturation of engineered muscle tissues by promoting myoglobin synthesis as a metabolic and structural regulator. Myoglobin expression is not just a molecular marker but is closely associated with fiber type specification, oxidative capacity, and contractile function. Promoting its synthesis could thus help drive the metabolic and structural development of muscle constructs, ultimately bringing them closer to the physiological characteristics of native skeletal muscle.

Together, these objectives guided the experimental design and analytical approaches throughout the project, with the overarching goal of advancing the scientific understanding and future application potential of engineered muscle tissues.

1.3. Outline and structure

This thesis is logically structured across six distinct chapters, designed to systematically progress from the foundational background and platform development to the integrated analysis and functional optimization of the engineered muscle tissue. The flow of the chapters directly reflects the research objectives, ensuring a clear, a structured narrative that guides the reader through the entire scope of the project.

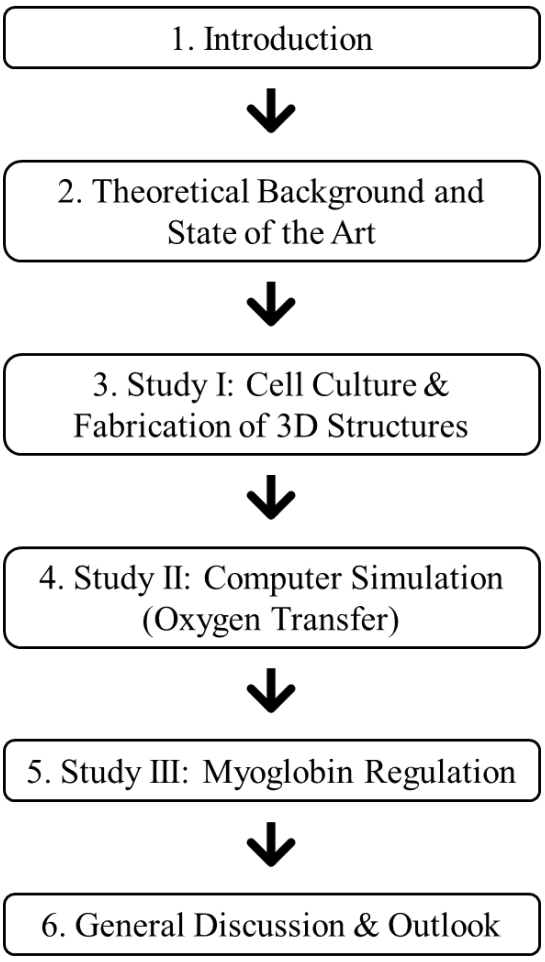

Figure 1 - Visual outline of the thesis structure. (Note: Each methodology chapter contains integrated Results & Discussion.)

Chapter One - This chapter establishes the contextual and scientific imperative for the research. It provides an overview of the current state-of-the-art in muscle tissue engineering, focusing on the challenges inherent to large-scale, scaffold-free fabrication. This section discusses the key knowledge gaps concerning oxygen transport limitations and the lack of native pigmentation in cultivated muscle, which directly informs the specific aims of the thesis.

Chapter Two - This chapter is dedicated to the scientific and mathematical principles underpinning the experimental and computational work. It presents the theoretical frameworks governing cell biology, myogenesis, and essential transport phenomena. Key areas covered include the principles of cell sheet engineering, the biophysics of oxygen diffusion (Fick's laws), the mechanism of myoglobin synthesis, and the principles of colorimetric and spectroscopic analysis used for quantification.

Chapter Three - This chapter meticulously details the foundational experimental procedures. It describes the preparation, maintenance, and differentiation of C2C12 myoblasts and introduces a non-enzymatic, scaffold-free protocol developed for fabricating the cohesive, three-dimensional muscle constructs. All protocols related to the structural and cellular characterization (e.g., histology, viability assays) that affirm the platform's utility are documented here.

Chapter Four - This chapter addresses the crucial issue of tissue scalability by detailing the computational and biophysical modeling strategy. It outlines the establishment of the finite element model (FEM) used to simulate oxygen transfer within the dense 3D constructs. The methodology for experimentally determining the system-specific biophysical parameters, such as the Oxygen Uptake Rate (OUR), effective diffusion coefficient (), and porosity, which are essential for model validation and determining the critical size limit, is fully described.

Chapter Five - This chapter details the comprehensive array of functional optimization experiments. It presents the methodologies used to investigate the regulatory factors influencing myoglobin synthesis, including the specific protocols for biochemical supplementation (e.g., iron, creatine, IGF-I), environmental manipulation (e.g., Dissolved Oxygen control in the bioreactor), and the application of mechanical stretching. All associated analytical techniques, such as the myoglobin ELISA, iron uptake assay, and ROS analysis, are thoroughly described.

Chapter Six - This final, pivotal chapter provides a comprehensive “Integration of Findings Across Studies and Literature Review”. It synthesizes the major conclusions from the scaffold-free fabrication, oxygen transport modeling, and myoglobin regulation studies, discussing their collective implications within the broader context of current literature. The chapter concludes with a concise section on “Concluding Remarks”, which summarizes the thesis's primary contributions to scientific knowledge and outlines essential future research directions necessary to translate the established principles into industrial and therapeutic applications.

In summary, the thesis follows a logical progression, as visually outlined in Figure 1. The research begins with a foundational phase dedicated to developing a novel, scaffold-free 3D muscle tissue fabrication method. This is followed by a crucial analytical phase focused on assessing the physical limitations imposed by oxygen diffusion through computational modeling. The work concludes with a comprehensive experimental evaluation of strategies to enhance myoglobin production *in vitro*, an intrinsic approach to overcome the limitations identified earlier. This stepwise structure reflects the interconnected nature of tissue engineering challenges and provides a holistic view of designing functional skeletal muscle constructs.

2. Chapter Two: Theoretical background and State of the Art

This chapter first introduces the theoretical foundations of skeletal muscle tissue engineering, oxygen transport, and myoglobin function. It then reviews current scaffold-free approaches and recent developments in engineered muscle and cultivated meat to position the present work within the state of the art.

2.1. Foundations of Skeletal Muscle Tissue Engineering

Skeletal muscle, a highly complex and dynamic tissue, is essential for virtually all voluntary movements, from subtle facial expressions to powerful exertions. Its intricate hierarchical organization, from individual myofibers bundled into fascicles encased by connective tissue, allows for both immense strength and precise control. Nevertheless, this very complexity poses a significant challenge for its repair and regeneration following substantial injury due to trauma, disease, or surgical intervention. For decades, researchers have sought methods to restore or replace damaged muscle, progressing from basic repair techniques to the sophisticated realm of tissue engineering (TE).

This chapter delineates the theoretical underpinnings of skeletal muscle tissue engineering, establishing the context for the novel approaches investigated in this thesis. The following sections trace the evolution of TE, emphasizing its core principles and the key components—cells, scaffolds, and signals—that govern its success. A particular focus will be placed on skeletal muscle tissue engineering (SMTE), discussing both conventional scaffold-based strategies and the emerging scaffold-free methodologies, such as cell sheet engineering, which constitutes a technological cornerstone of the present research.

Crucially, this chapter extends beyond a mere compilation of existing literature. Instead, it serves as a foundational narrative, critically evaluating the strengths and limitations of current methodologies in relation to the specific research objectives of this work. The chapter explores how a deeper comprehension of muscle physiology, particularly the intricate role of myoglobin in oxygen dynamics and cellular metabolism, directly informs the development of more functional and resilient engineered muscle constructs. This integration of the research aims within the broader scientific discourse is paramount, as the study seeks to address current knowledge gaps and contribute relevant contributions to the field.

Ultimately, this theoretical exposition aims to elucidate why the pursuit of enhanced myoglobin synthesis is not merely an academic exercise, but an important step toward creating muscle constructs that could be more robust for future therapeutic applications, more accurate as *in vitro* models for disease investigation, and more appealing for innovative food technologies.

2.1.1. The Evolution and Core Principles of Tissue Engineering

The human body possesses remarkable self-healing capabilities, yet there are instances where these natural processes are insufficient, leading to debilitating tissue loss or organ failure. Confronted with challenges such as chronic conditions, the severe shortage of donor organs, and the inherent limitations of prosthetic devices, scientists and engineers have long envisioned solutions that could actively regenerate or replace damaged biological structures. This ambition coalesced into the multidisciplinary field now recognized as Tissue Engineering (TE).

While the conceptual foundations of utilizing biological materials for repair were established much earlier, TE formally emerged in the late 20th century. A pivotal moment arrived in 1993 with the seminal publication by Langer and Vacanti [17], which articulated a revolutionary vision: combining living cells with engineered scaffolds to develop functional biological substitutes. This foundational work catalyzed a scientific movement, providing the intellectual framework for contemporary TE. The subsequent decades witnessed rapid growth, transitioning from rudimentary cell transplantation experiments to sophisticated constructs integrating 3D scaffolds and advanced bioreactor systems [6]. Initial clinical successes, such as the development of engineered skin for burn patients and pioneering cartilage repair techniques, provided experimental validation, demonstrating that these "biological substitutes" were not merely theoretical constructs but tangible therapeutic realities.

As breakthroughs in stem cell technologies, genetic engineering, and advanced biomaterials continued to emerge, the field expanded its scope, addressing increasingly complex tissues and organs. Notably, the period from 1998 to 2006 saw landmark advances such as the isolation of human embryonic stem cells and the development of induced pluripotent stem cells, both of which significantly expanded the cellular toolkit available for TE applications. While stem cell research has continued well beyond this timeframe, these years mark a pivotal inflection point in their relevance to the field. Khademhosseini and Langer (2016) aptly characterized the early 21st century as a period of significant progress in synergizing microengineering and biofabrication methods, enabling unprecedented control over tissue architecture [18].

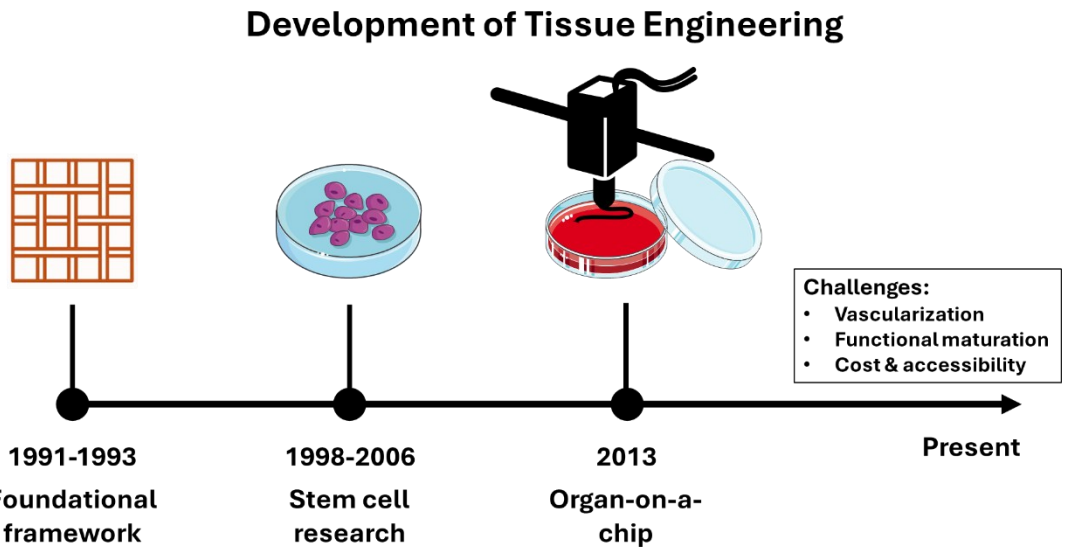

Figure 2 - Chronological progression of major milestones in tissue engineering (TE) from 1991 to the present. Key developments include the establishment of the foundational framework by Langer and Vacanti (1991), pivotal advances in stem cell biology between 1998–2006, including the isolation of human embryonic stem cells and the advent of induced pluripotent stem cells, followed by the emergence of organ-on-a-chip systems and 3D bioprinting (2010). The timeline concludes with ongoing challenges such as vascularization, functional maturation, cost, and accessibility.

At its essence, TE is often defined as "an interdisciplinary field that applies the principles of engineering and life sciences toward the development of biological substitutes that restore, maintain, or improve tissue function or a whole organ" [19]. In essence, it leverages scientific and technological ingenuity to augment the body's inherent healing potential or to construct replacements for compromised tissues. The success of any tissue engineering endeavor hinges upon the synergistic interplay of three fundamental components, frequently referred to as the "triad of tissue engineering":

- Cells: These are the living building blocks, the biological architects responsible for synthesizing new tissues. They can be sourced directly from the patient (autologous cells, minimizing immune rejection), from donors (allogeneic cells, offering scalability but necessitating immunosuppression), or, increasingly, from highly versatile stem cells. The latter, particularly mesenchymal stem cells (MSCs) and induced pluripotent stem cells (iPSCs), are highly attractive due to their remarkable capacity for self-renewal and their potential to differentiate into various cell types.
- Scaffolds: Serving as a temporary or permanent framework, scaffolds provide the requisite structural support for cells to attach, proliferate, and mature into organized tissues. These structures must be biocompatible (not eliciting an adverse immune response), ideally biodegradable (gradually dissolving as the new tissue forms), and

meticulously designed to mimic the extracellular matrix (ECM), the native environment surrounding cells in vivo.

- Signals: These are the critical biochemical and biomechanical cues that orchestrate cell behavior and guide tissue formation. Biochemical signals encompass growth factors, cytokines, and other soluble molecules that regulate cell proliferation, differentiation, and survival. Biophysical signals include mechanical forces (e.g., stretching, compression, fluid flow) and electrical stimuli, all of which play crucial roles in shaping tissue development and function.

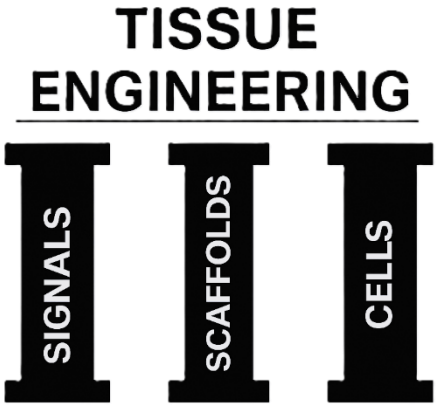

Figure 3 - The triad of tissue engineering, Cells, Scaffolds, and Signals, illustrated as interdependent pillars essential for functional tissue regeneration.

The delicate balance and precise combination of these three elements are paramount to replicating the intricate complexity and functionality of the body's natural environment within an engineered construct.

2.1.2. Methods in Tissue Engineering

The multifaceted nature of tissue engineering has led to the development of a diverse array of methodologies, each tailored to address specific challenges in creating functional tissue substitutes. These techniques span from fundamental scaffold design to cutting-edge biofabrication processes.

Scaffold-Based Techniques. Historically, scaffold-based approaches have formed the cornerstone of tissue engineering. Scaffolds are biomimetic frameworks that provide essential structural support for newly forming tissues. Their design is critical; they must be

biocompatible, allowing cells to thrive without adverse reactions, and ideally bioresorbable, degrading at a rate that matches new tissue formation. Importantly, they must also accurately mimic the native extracellular matrix (ECM), providing appropriate mechanical cues and attachment sites for cells.

A variety of materials are employed for scaffold fabrication. Natural polymers, such as collagen, fibrin, and gelatin, offer excellent biocompatibility and cell recognition sites due to their inherent biological origins. However, they often exhibit limited mechanical strength and rapid degradation rates, making them less suitable for load-bearing applications. In contrast, synthetic polymers like poly(lactic acid) (PLA), polycaprolactone (PCL), and poly(glycolic acid) (PGA) provide greater control over mechanical properties, degradation kinetics, and scaffold architecture. Techniques such as freeze-drying, electrospinning, and gas foaming are utilized to create scaffolds with precise porosity, pore interconnectivity, and mechanical stiffness, all of which are critical for guiding cell infiltration, nutrient transport, and tissue maturation [20]. Hydrogels, highly hydrated polymeric networks, are particularly valuable for soft tissue engineering applications due to their elasticity and ability to encapsulate cells in a 3D environment.

Cell-Based Constructs. The selection and meticulous preparation of the appropriate cell source are arguably the most critical determinants of success in tissue engineering. Autologous cells, derived directly from the patient, offer the significant advantage of eliminating immune rejection, making them the gold standard for many clinical applications. However, their acquisition can be invasive, and their limited expansion potential *in vitro* often restricts their widespread use. Allogeneic cells, harvested from donors, provide greater scalability and off-the-shelf availability, but they necessitate immunosuppression to prevent rejection. In this study, it was opted to use C2C12 cells, a well-established murine myoblast cell line. This choice provides a highly reproducible and easily expandable cell source for *in vitro* studies, allowing for consistent experimental conditions to investigate fundamental aspects of muscle tissue engineering without the complexities associated with primary human cell isolation at this foundational stage of research.

The advent of stem cells has revolutionized cell-based therapies. Mesenchymal stem cells (MSCs), readily isolated from various adult tissues, and induced pluripotent stem cells (iPSCs), reprogrammed from somatic cells, are highly attractive due to their remarkable proliferative capacity and their ability to differentiate into multiple cell lineages. The challenge, however,

lies in precisely controlling their differentiation pathways to ensure commitment to the desired tissue type [21].

A powerful alternative to scaffold-based approaches is cell sheet engineering. This technique involves culturing cells on temperature-responsive polymer surfaces, allowing them to form confluent, extracellular matrix-rich sheets without the use of scaffolds or enzymatic digestion. These intact cell sheets can then be harvested and stacked to create three-dimensional tissue constructs, preserving cell-cell junctions and deposited extracellular matrix. In this study, cell sheet engineering approach was utilized to create pre-vascularized muscle constructs by co-culturing muscle cells with endothelial cells. This method allows the construction of complex tissue structures while maintaining cell viability and native tissue architecture, aiming to overcome the limitations of nutrient and oxygen diffusion often encountered in thicker engineered tissues.

Bioreactor Systems. To truly foster the development of functional engineered tissues, merely providing cells and scaffolds is often insufficient. Bioreactor systems are indispensable tools that create and maintain controlled environments, actively mimicking the physiological conditions found *in vivo*. These sophisticated devices meticulously regulate critical parameters such as oxygen tension, pH, temperature, and, crucially, mechanical forces and fluid flow, all of which profoundly influence cell behavior and tissue development. Different bioreactor designs are optimized for specific tissue types; for instance, rotating wall bioreactors are often used for cartilage constructs to facilitate uniform cell distribution, while perfusion systems are ideal for bone tissue engineering, ensuring efficient nutrient and waste exchange within dense constructs [22]. The latest generation of bioreactors incorporates real-time sensors and automated control systems, enabling continuous monitoring and dynamic modulation of culture conditions, thereby pushing the boundaries of tissue maturation and quality control. In the study, a fully controlled DASbox bioreactor system was employed to precisely manage the culture conditions of the 3D cell-based constructs, with a particular focus on controlling the dissolved oxygen concentration, as will be explained in detail in the Materials and Methods section.

3D Bioprinting and Microfabrication. Perhaps the most transformative advancement in recent tissue engineering is 3D bioprinting. This additive manufacturing technology allows for the precise, layer-by-layer placement of cells and biomaterials (known as bioinks) to construct complex, pre-designed tissue architectures. This level of spatial control is particularly advantageous for engineering tissues with intricate vascular networks or for fabricating organoids that recapitulate specific tissue functions [23]. Recent breakthroughs in developing

novel bioinks with tunable properties and significant improvements in printing resolution are rapidly expanding the capabilities of bioprinting. However, significant challenges remain, particularly ensuring the viability and long-term functionality of cells during and after the printing process, as well as scaling up for clinically relevant tissue sizes [24,25].

Organs-on-Chips and Microfluidics. Moving beyond therapeutic applications, the convergence of tissue engineering with microfluidics has given rise to "organ-on-chips." These miniature, sophisticated devices are designed to replicate the physiological functions of human organs on a microscale, making them invaluable tools for drug discovery, toxicology screening, and fundamental biological research. By precisely simulating tissue interfaces, fluid dynamics, and even mechanical forces, organ-on-chips allow scientists to study complex biological interactions in a highly controlled and high-throughput manner [26]. Prominent examples include liver-on-a-chip platforms for hepatotoxicity testing, heart-on-a-chip models for cardiac pharmacology, and tumor-on-a-chip systems for personalized cancer drug screening. These platforms represent a significant shift from traditional 2D cell culture, offering a more physiologically relevant *in vitro* environment.

Biochemical and Biophysical Cues. Beyond merely providing cells and a scaffold, engineered muscle tissue development is profoundly influenced by a complex interplay of biochemical and biophysical cues. These signals act as the cellular language, orchestrating the intricate processes of myogenesis and tissue maturation.

Biochemical factors, particularly growth factors, play a pivotal role. Insulin-like growth factor 1 (IGF-1), basic fibroblast growth factor (bFGF), hepatocyte growth factor (HGF), and transforming growth factor-β (TGF-β) are commonly incorporated into SMTE protocols due to their known roles in promoting myoblast proliferation, differentiation, and survival. These factors can be delivered in a sustained manner through controlled-release systems embedded within scaffolds or directly supplemented into the culture medium to achieve desired concentrations [27,28].

Equally important are biophysical cues. Mechanical loading (e.g., cyclic stretching or compression) and electrical stimulation are critical for inducing myotube alignment, enhancing their maturation, and promoting robust contractility, mirroring the physical demands placed on native muscle. Electrical stimulation, in particular, has emerged as an indispensable tool in the *in vitro* phase of muscle tissue development. It not only accelerates myotube fusion and

maturation but also improves their contractile force and force generation capacity by promoting sarcomere organization and the expression of mature muscle proteins [29].

2.2. Scaffold-Free Approaches in Skeletal Muscle Tissue Engineering

Tissue engineering has continuously evolved, seeking to create functional biological substitutes that can repair, replace, or enhance damaged tissues and organs. While early efforts largely relied on exogenous scaffolds to provide structural support for cells, a compelling paradigm shift has emerged in the field: scaffold-free tissue engineering. This research directly contributes to this exciting area by developing 3D cell structures from cell sheets, an approach that leverages the cells' inherent ability to self-organize and produce their own extracellular matrix, thereby circumventing many challenges associated with traditional scaffold-based methods.

Cell sheet engineering (CSE), pioneered by the Okano group [30], stands as a example of this scaffold-free approach. The fundamental principle of CSE lies in a unique biological mechanism: cultivating cells on surfaces designed for non-enzymatic harvesting. Unlike conventional cell culture, which often requires harsh enzymatic digestion (like trypsin) to detach cells, a process that damages crucial cell-cell junctions and deposited extracellular matrix (ECM), CSE allows intact cell monolayers, or "cell sheets," to be gently released.

The most common method for achieving this relies on temperature-responsive polymer-coated surfaces, typically utilizing poly(N-isopropylacrylamide) (PNIPAAm). PNIPAAm exhibits a unique characteristic known as a lower critical solution temperature (LCST), which is approximately 32°C. This property dictates its behavior:

- Above the LCST (e.g., at 37°C for cell culture): The PNIPAAm chains dehydrate and become hydrophobic. This provides a suitable surface for cells to adhere, spread, and proliferate, forming a confluent monolayer. Crucially, during this growth phase, cells actively deposit their own native ECM (e.g., collagen, fibronectin, laminin) on the basal surface of the sheet and establish robust cell-cell junctions.
- Below the LCST (e.g., typically 20°C for harvesting): When the temperature is lowered, PNIPAAm rapidly rehydrates, causing the polymer chains to swell and the surface to become hydrophilic. This change in surface property triggers the spontaneous detachment of the entire cell monolayer as an intact sheet [31]. The preservation of these vital cell-cell junctions and the inherent ECM is a key advantage, as these components

are essential for maintaining tissue integrity, promoting differentiation, and facilitating the complex intercellular signaling necessary for functional tissue development.

For this study, the ability to harvest these intact cell sheets is particularly advantageous because it allows the construction of complex, 3D structures that closely mimic native tissues without the need for external scaffolding. These cohesive cell sheets, once harvested, can be precisely layered or rolled to form dense, multi-layered 3D constructs. This "bottom-up" assembly provides enhanced control over cellular density and the overall architecture of the final construct, enabling the creation of more physiologically relevant models for investigations into muscle tissue regeneration and potential applications in drug testing.

Applications of Cell Sheet Engineering in Muscle Tissue Engineering and Myogenesis. Cell sheet engineering (CSE) offers remarkable advantages for skeletal muscle tissue engineering (SMTE) due to its ability to create organized, scaffold-free constructs that closely mimic the native muscular environment. The inherent preservation of cell-cell junctions and deposited extracellular matrix (ECM) during non-enzymatic harvesting is particularly important for myogenesis, as native skeletal muscle is characterized by highly organized myofibers interconnected by a rich ECM. Enzymatic dissociation, common in traditional cell harvesting, damages these crucial structures, impairing the cells' ability to self-organize into functional tissue. CSE, by maintaining these natural connections, facilitates the formation of more mature and organized myotubes [32].

Myoblasts, the precursor cells for muscle, when cultured on temperature-responsive dishes, proliferate and fuse to form nascent myotubes. Furthermore, if the culture surface is modified with micro-patterns or grooves, myoblasts can be guided to align uniaxially, faithfully mimicking the parallel organization of native muscle fibers [33,34]. When these aligned cells are harvested as an intact sheet, this intrinsic alignment is retained, a feature paramount for generating directional contractile force, which is the hallmark of functional muscle tissue.

A key strength of CSE lies in its versatility for fabricating three-dimensional (3D) constructs. Individual cell sheets, once harvested, are highly cohesive and can be precisely layered or rolled to form dense, multi-layered 3D muscle constructs without the need for additional exogenous scaffolds or synthetic glues. This "bottom-up" assembly provides greater control over the cellular density and potentially the anisotropy of the final construct, facilitating enhanced cell-cell interactions across the layers and promoting overall tissue formation. Muscle sheet constructs can be layered via centrifugation to achieve 3D architecture, as shown by Hasegawa

et al. (2015), who established a rapid stacking technique that preserved cellular integrity while improving construct thickness and uniformity [35]. This method proves valuable in volumetric muscle loss models, where functional integration and large tissue volumes are required.

Beyond simply muscle cells, the power of CSE extends to incorporating other vital cell types through co-culture strategies. For instance, human umbilical vein endothelial cells (HUVECs) can be co-cultured to promote vascularization, or induced pluripotent stem cell (iPSC)-derived neurons can be integrated to facilitate innervation, by integrating them in myoblast sheets [36–38]. This layered co-culture approach helps in mimicking the complex multicellular environment of native muscle, where muscle fibers are closely associated with blood vessels and nerves, thereby enhancing the biomimicry of these constructs and their potential for functional integration in vivo. Moreover, by eliminating the need for foreign scaffold materials, CSE significantly reduces the risk of host inflammatory responses or scaffold-related complications upon implantation, leading to more biocompatible and potentially less immunogenic engineered tissue.

Despite these advancements, achieving the full functional maturity of native skeletal muscle, including robust, sustained contractility, force generation, and fatigue resistance, remains a significant challenge. Myoglobin, a heme-containing protein crucial for oxygen storage and transport within muscle cells, plays a pivotal role in oxidative metabolism and is a direct indicator and driver of this functional maturation. Therefore, the fourth research objective, which focuses on studying the factors that regulate myoglobin synthesis from a process engineering point of view, is directly aimed at addressing this challenge. By understanding and optimizing myoglobin expression within the 3D cell-based muscle constructs, the reasearch seeks to enhance their oxygen handling capacity and, consequently, their functional maturation and long-term viability, moving closer to developing truly robust and physiologically relevant engineered muscle tissues.

2.3. The Critical Role of Oxygen in Tissue Engineering

Oxygen is an indispensable nutrient for nearly all living cells, and its availability is a rate-limiting factor in the development and survival of engineered tissues, particularly for thicker, more metabolically active constructs like skeletal muscle. While significant strides have been made in optimizing scaffolds, cell sources, and mechanical stimulation, the fundamental challenge of ensuring adequate oxygen diffusion within 3D tissue constructs remains a pervasive bottleneck. This section will delve into the critical importance of oxygen in tissue

engineering, highlight the problem of hypoxia in dense constructs, and introduce how understanding myoglobin and its oxygen-binding properties becomes central to overcoming these limitations.

2.3.1. Oxygen Diffusion Limitations in 3D Tissue Constructs

Native tissues benefit from a highly organized and efficient vascular network that ensures a continuous supply of oxygen and nutrients to every cell. In engineered tissues, especially those developed *in vitro* without immediate vascularization, cells rely solely on passive diffusion from the surrounding culture medium. This process is inherently limited by diffusion distances. Oxygen, being relatively insoluble in aqueous solutions, can only travel short distances before being consumed by metabolically active cells.

For muscle tissue, which is highly metabolically active and requires substantial oxygen for contraction and energy production, this limitation is particularly acute. Myoblasts and differentiating myotubes exhibit high oxygen consumption rates, especially as they mature and develop contractile machinery. Consequently, engineering physiologically relevant muscle constructs of clinically relevant sizes (often millimeters to centimeters in thickness) demands innovative strategies to overcome oxygen transport barriers. This direct challenge underscores the importance of the first research objective: to create engineered muscle constructs with higher oxidative capacity for therapeutic applications. Without sufficient oxygen, even the most promising engineered tissue will fail to survive transplantation.

2.3.2. Strategies for Overcoming Hypoxia in Engineered Tissues

Numerous strategies have been proposed to mitigate hypoxia in 3D tissue constructs. These can broadly be categorized into:

- **Pre-vascularization:** This involves creating a rudimentary vascular network within the engineered tissue *in vitro* before implantation. This can be achieved by co-culturing endothelial cells with tissue-specific cells, using angiogenic growth factors (e.g., VEGF), or fabricating microchannel networks within scaffolds via 3D bioprinting [39–42].
- **Perfusion Bioreactors:** These systems actively pump culture medium through the construct, ensuring continuous and uniform delivery of oxygen and nutrients, and efficient removal of waste products [43–45].

- **Oxygen Carriers:** Incorporating oxygen-carrying molecules or oxygen-generating materials directly into the construct or culture medium can provide a transient or sustained supply of oxygen. Examples include perfluorocarbons or oxygen-releasing nanoparticles [46–48].
- **Cell Density and Geometry Optimization:** Careful control of initial cell seeding density and designing constructs with optimized geometries (e.g., thin sheets, hollow tubes) can maximize the surface-to-volume ratio, facilitating better oxygen exchange.

While these strategies primarily focus on external factors to deliver oxygen, this research introduces a novel, intrinsic approach to enhance oxygen handling. By employing cell sheet engineering, a 3D construct from cohesive cell monolayers was created, which were randomly crumpled to form a scaffold-free structure. This approach focused on studying factors that regulate myoglobin synthesis, a protein crucial for oxygen storage and transport within muscle cells. By investigating how to enhance myoglobin expression within the myoblast cell sheets themselves, this study aimed to intrinsically improve the cells' capacity to manage oxygen. It is acknowledged that increased myoglobin content alone may not fully compensate for the lack of a vascular network, but it was hypothesized that it may allow for the viability of cells in thicker constructs. This internal, process-engineered solution complements the external strategies mentioned above, offering a potential new tool for improving the viability and functional maturation of engineered muscle.

2.3.3. Computational Modeling of Oxygen Transport in 3D Bioconstructs

To overcome the inherent limitations of oxygen diffusion in dense, vessel-free engineered tissues, and to provide a quantitative understanding of oxygen availability within the constructs, computational modeling of oxygen diffusion has become an indispensable tool in tissue engineering. This approach, often employing techniques such as Finite Element Analysis (FEA) or Computational Fluid Dynamics (CFD), allows for the simulation of oxygen transport and consumption within complex 3D geometries, predicting oxygen profiles and identifying regions prone to hypoxia [49–51].

In this work, this simulation was essential to predict whether larger tissue volumes, such as those generated by layering cell sheets, would suffer from central hypoxia or necrosis. It was recognized that relying on input parameters from the existing literature, which were often derived from different cell types and culture conditions, could introduce errors and lead to misleading results [52,53]. Furthermore, it was understood that even these experimental

measures would be subject to certain assumptions. Therefore, to ensure the highest possible reliability, it was decided to experimentally measure key input parameters specific to this engineered constructs. These parameters included the oxygen diffusion coefficient within the tissue matrix, the volumetric mass transfer coefficient at the tissue-medium interface, and, critically, the cellular oxygen uptake rate of the specific muscle cells as they differentiated and matured. By experimentally feeding these measured values into the computational model, more reliable predictions of oxygen distribution could be generated. The outcome of the simulation provided a precise estimate for the maximum construct thickness that would maintain viable oxygen levels, allowing the experimental protocols to be proactively designed and all subsequent experiments to be constrained accordingly, thereby preventing costly and time-consuming failures due to hypoxia. This upfront computational analysis is a powerful component of the rational design strategy, directly informing the physical dimensions and expected viability of the muscle constructs relevant to the first research objective concerning therapeutic applications and the second research objective for accurate *in vitro* models. It allows the study to move beyond qualitative observations to quantitative predictions, optimizing construct design for maximal viability and functionality.

2.3.4. Myoglobin: Structure, Function, and Physiological Significance

To overcome the oxygen diffusion limitations in engineered tissues, particularly in the 3D muscle constructs, this study introduces a novel, intrinsic approach that complements existing external strategies. While methods such as pre-vascularization and perfusion bioreactors focus on external oxygen delivery, this research focuses on intrinsically enhancing the cells' ability to manage oxygen by regulating the synthesis of a key protein: myoglobin.

At the core of the muscle's remarkable ability to function under varying oxygen conditions lies myoglobin (Mb) which is a heme-containing oxygen-binding protein found predominantly in striated muscle cells (skeletal and cardiac muscle). It acts as an intracellular reservoir, facilitator of oxygen diffusion, and an oxygen buffer, particularly crucial during periods of high metabolic demand or limited oxygen supply.

Structurally, myoglobin is a relatively small (approximately 17 kDa) globular protein composed of a single polypeptide chain folded into eight alpha-helices, encapsulating a central heme prosthetic group. It is this heme group, with its central iron atom, that reversibly binds molecular oxygen (O2). This structure is highly conserved across vertebrate species, underscoring its profound evolutionary importance in muscle physiology [54–56]. The oxidation state of this

iron atom, which is typically in the ferrous (+2) state, determines myoglobin's oxygen-binding capacity. The protein can exist in several forms depending on its binding state. Deoxymyoglobin is the form of myoglobin without an oxygen molecule bound to the heme iron. When an oxygen molecule binds to the heme group, it forms oxymyoglobin. This binding causes the iron atom to change its position, moving into the plane of the porphyrin ring and shifting from a high-spin to a low-spin state. A third form, metmyoglobin, is created when the iron atom is oxidized to the ferric (+3) state, rendering it unable to bind oxygen [11,57].

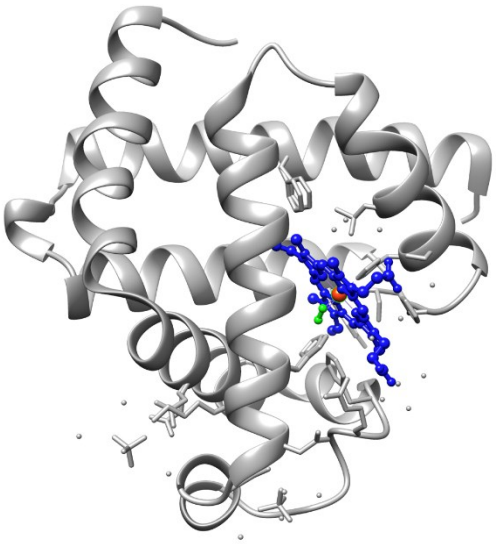

Figure 4 - Ribbon diagram of oxy-myoglobin, illustrating the conformational change of the iron atom upon oxygen binding to the heme group. The bound oxygen molecule is shown in green, the iron atom in red, and the heme group in blue. (Image source: Wikimedia Commons, public domain.)

Functionally, myoglobin serves several critical roles:

- **Oxygen Storage:** Myoglobin can bind and store a significant amount of oxygen within the muscle cell, providing a readily available local supply during bursts of activity when blood flow cannot meet immediate oxygen demands.
- **Facilitated Diffusion:** It acts as a "molecular shuttle," facilitating the diffusion of oxygen from the cell membrane to the mitochondria, where it is consumed for aerobic respiration. This is particularly important under conditions of high metabolic flux or low oxygen partial pressure.
- **Oxygen Buffering:** Myoglobin buffers intracellular oxygen levels, protecting oxygen-sensitive enzymes from fluctuations in oxygen supply.

- **Nitric Oxide (NO) Metabolism:** Beyond oxygen, myoglobin also interacts with nitric oxide (NO), an important signaling molecule. Myoglobin can metabolize NO, contributing to its regulation within muscle cells.

Developmentally, myoglobin expression is intricately linked with muscle maturation. Its synthesis begins relatively early during myogenesis, with studies demonstrating an upregulation of myoglobin mRNA and protein levels during the initial stages of muscle cell differentiation [13, 14]. This makes myoglobin not only a functional component but also a powerful biomarker of muscle maturation. Its expression is tightly coordinated with the development of key contractile elements, such as myosin heavy chains, signifying progression towards a more oxidative and functionally mature muscle phenotype. This direct association with functional maturation strongly supports the fourth research objective: to support the functional maturation of engineered muscle tissues by promoting myoglobin synthesis.

The regulation of myoglobin expression is complex and multifaceted, influenced by various physiological and environmental cues. Hypoxia is a potent inducer of myoglobin, as cells adapt to low oxygen environments by increasing their capacity for oxygen storage and diffusion. Exercise and increased muscle activity also upregulate myoglobin, reflecting the muscle's adaptive response to increased metabolic demand. Kanatous and Mammen (2007) emphasized the critical role of key signaling pathways, notably PGC-1α (Peroxisome Proliferator-Activated Receptor Gamma Coactivator 1-alpha) and various oxidative signaling pathways, in mediating myoglobin upregulation [15]. These pathways are particularly relevant targets in tissue engineering and regenerative therapies, as modulating them could enhance myoglobin synthesis. Interestingly, myoglobin's influence extends beyond its classic role in oxygen transport. Studies in zebrafish models have shown that the absence of myoglobin can lead to developmental abnormalities [16], underscoring its broader importance as a regulator of cellular differentiation and tissue organization, not just a simple oxygen buffer. This multifaceted role of myoglobin directly ties into the second research objective: developing a more accurate *in vitro* model of skeletal muscle physiology and pathophysiology, as a model with enhanced myoglobin more closely mimics native muscle's oxidative characteristics, making it more relevant for studying hypoxia, ischemia-reperfusion, and metabolic disorders.

In the context of process engineering, this study aims to identify and manipulate the factors that govern myoglobin expression within the 3D cell-based muscle constructs. While it is acknowledged that an increase in myoglobin content might not fully compensate for the inherent lack of vascularization in thicker engineered tissues, it was hypothesized that it may

significantly contribute to enhancing cell viability and overall metabolic robustness under oxygen-limited conditions. This targeted approach to myoglobin regulation represents a crucial step towards improving the functional longevity and performance of the engineered muscle constructs.

2.4. Strategic Role of Myoglobin in Advancing Tissue Engineering Applications

The profound importance of myoglobin in native muscle physiology provides a compelling rationale for its targeted enhancement in engineered muscle constructs. This section will expand on how optimizing myoglobin levels directly addresses key limitations in the field, further elaborating on the research objectives.

2.4.1. Myoglobin for Enhanced Therapeutic Outcomes in Engineered Muscle

Addressing the critical need for more resilient and functional engineered tissues in regenerative medicine is the primary driver behind the focus of this study on myoglobin. Current muscle tissue engineering efforts, while promising, often struggle to create constructs that can withstand the harsh, often ischemic or metabolically stressed environments encountered upon transplantation into a host. This environment is frequently characterized by ischemia (restricted blood flow) and hypoxia, especially immediately after implantation before host vascularization can establish. Muscle tissue engineered *in vitro*, often grown in well-oxygenated culture conditions, may be ill-prepared for this abrupt shift.

Here, myoglobin serves as a biological safeguard. By increasing myoglobin protein synthesis within the 3D muscle-like constructs, this research aims to augment their intrinsic capacity for oxygen storage and facilitated diffusion. This means that even in a low-oxygen environment post-transplantation, the engineered muscle would have a built-in oxygen reserve and a more efficient system for delivering what little oxygen is available to mitochondria, sustaining aerobic metabolism for a longer crucial period. This directly supports the first research objective: to contribute to therapeutic applications in regenerative medicine. Engineered muscle with higher myoglobin levels would be inherently more resilient, potentially reducing early cell death upon implantation and improving long-term graft survival and functional integration. This has direct implications for addressing volumetric muscle loss (VML), traumatic injuries, or even providing robust cellular grafts for conditions like Duchenne muscular dystrophy where muscle degeneration is chronic and widespread. The ability of the engineered tissue to better

withstand initial ischemic stress would significantly enhance its therapeutic potential, enabling it to "hold its breath" until a new blood supply can be established.

2.4.2. Myoglobin as a Biomarker and Functional Enhancer in *In Vitro* Models

Recognizing the limitations of current *in vitro* models in faithfully replicating complex muscle physiology, the second research objective centers on developing a more accurate and physiologically relevant model of skeletal muscle. Traditional 2D cell cultures often fail to replicate the complex physiological nuances of real tissues, particularly regarding oxygen gradients and metabolic responses. Even many 3D engineered muscle models often lack the mature oxidative characteristics of native skeletal muscle, which is rich in myoglobin.

A 3D muscle model robustly enriched in myoglobin would more closely mimic the oxidative metabolism of mature *in vivo* muscle, making it an invaluable tool for studying complex biological phenomena. For instance, such a model could be used to precisely investigate:

- **Hypoxia-reperfusion injury:** Simulating conditions where muscle experiences oxygen deprivation followed by reoxygenation, allowing for the study of cellular damage and protective mechanisms.
- **Mitochondrial dysfunctions:** Examining how genetic mutations or environmental toxins affect mitochondrial health and energy production in a more physiologically relevant context.
- **Fiber type specification:** Studying how different stimuli influence the shift between oxidative (slow-twitch, myoglobin-rich) and glycolytic (fast-twitch, myoglobin-poor) muscle fiber types.

These myoglobin-enhanced models would represent a significant advancement over current systems, offering a more predictive platform for drug screening. Companies could test compounds targeting oxidative stress, metabolic disorders, or muscle regeneration with greater confidence, potentially reducing the need for costly and time-consuming animal trials. The ability to create a model that intrinsically responds to oxygen cues, much like native muscle, opens up entirely new avenues for understanding muscle biology and disease.

2.4.3. Myoglobin's Influence on Functional Muscle Maturation

The next overarching motivation stems from the aspiration to achieve true functional maturation in engineered muscle tissues, which is directly addressed by the fourth research objective: to

support the functional maturation of engineered muscle tissues. This is not just about cells surviving or differentiating into myotubes; it is about these myotubes becoming truly contractile, organized, and metabolically active like their native counterparts.

Myoglobin expression is not merely a molecular marker; it is intrinsically linked to several critical aspects of muscle development and function:

- **Fiber Type Specification:** Myoglobin is predominantly found in oxidative (Type I, slow-twitch) muscle fibers, which are fatigue-resistant and rely heavily on aerobic metabolism. Promoting myoglobin synthesis could encourage a shift towards a more oxidative phenotype, which is desirable for engineered constructs requiring sustained function.
- **Oxidative Capacity:** Higher myoglobin levels directly translate to an enhanced capacity for aerobic respiration, meaning the muscle can produce more energy (ATP) efficiently in the presence of oxygen. This is crucial for sustained contractile activity and overall tissue viability.
- **Contractile Function:** The metabolic efficiency supported by myoglobin is fundamental to robust and sustained contractile function. Well-matured muscle with high oxidative capacity can generate and maintain force more effectively.

Therefore, promoting myoglobin synthesis within the 3D muscle constructs is not an isolated endpoint but a strategic leverage point. It acts as a driver for the metabolic and structural development of the tissue, bringing it closer to the complex physiological characteristics and robust contractile performance of native skeletal muscle. By optimizing conditions for myoglobin production, the engineered tissue is nudged along its natural developmental pathway, fostering a more complete and functionally superior construct.

2.4.4. Myoglobin's Contribution to Cultivated Meat: Aesthetic and Nutritional Implications

Extending the impact of the findings beyond therapeutic applications, the third research objective addresses the burgeoning field of cultured meat technologies. This emerging field aims to produce meat directly from animal cells, offering a sustainable and ethical alternative to traditional livestock farming. However, one of the significant hurdles for widespread consumer acceptance of cultured meat lies in its sensory attributes, particularly its appearance and taste.

Myoglobin plays a crucial role not only in the biological function of muscle but also as the primary determinant of meat's characteristic red color and a significant contributor to its flavor profile. Native muscle, particularly red meat, is rich in myoglobin, which imparts its distinct reddish hue. In contrast, lab-grown muscle tissue typically appears pale and lacks the robust "meaty" flavor notes due to its inherently low myoglobin content [17]. This lack of visual appeal and familiar taste can be a major deterrent for consumers accustomed to traditional meat products. While adding artificial edible colorants might seem like a simple fix, such additives could negatively affect consumer perception, leading to concerns about the "naturalness" or "wholesomeness" of the product.

By increasing myoglobin synthesis in cultivated muscle tissue through optimized culture parameters, its visual appeal can be naturally enhanced, making it more appetizing and familiar. Furthermore, myoglobin is a significant source of heme iron, a highly bioavailable form of iron crucial for human nutrition. Elevating myoglobin levels would therefore also boost the nutritional quality of cultured meat, making it a more comprehensive and appealing food source. This objective represents a fascinating intersection of biomedical engineering, food science, and sustainability, demonstrating the broad impact of understanding fundamental biological processes like myoglobin expression. This work provides a biological, intrinsic solution to an aesthetic and nutritional challenge in a nascent industry.

2.5. Cultivated Meat

The enhancement of myoglobin synthesis in engineered muscle tissues directly relates to emerging technologies in cultivated meat, often referred to as lab-grown or cell-based meat. Cultivated meat is produced by culturing animal muscle cells *in vitro*, bypassing traditional livestock farming methods. This research aims to optimize the physiological properties of engineered muscle constructs, specifically targeting enhanced myoglobin levels, to improve nutritional and sensory characteristics such as color, taste, and nutritional quality, essential attributes influencing consumer acceptance.

Cultivated meat technology is increasingly recognized for its potential to significantly mitigate the ethical and environmental issues inherent to conventional livestock production. Datar and Betti (2010) highlighted the promising possibilities of cultivated meat, including reduced animal suffering, decreased environmental impacts, and potential public health benefits stemming from controlled, pathogen-free production environments [58].

Environmental Impact and Sustainability Considerations. Traditional livestock farming contributes substantially to global greenhouse gas emissions, land degradation, deforestation, and water resource depletion. Cultivated meat presents a sustainable alternative capable of addressing these environmental concerns. In an influential study, Tuomisto and Teixeira de Mattos (2011) reported that cultivated meat production systems could potentially reduce greenhouse gas emissions by up to 96%, land use by 99%, and water usage significantly compared to traditional farming practices [59]. Further studies, including recent ex-ante lifecycle assessments, reinforce the environmental advantages of scaling up cultivated meat production [60].

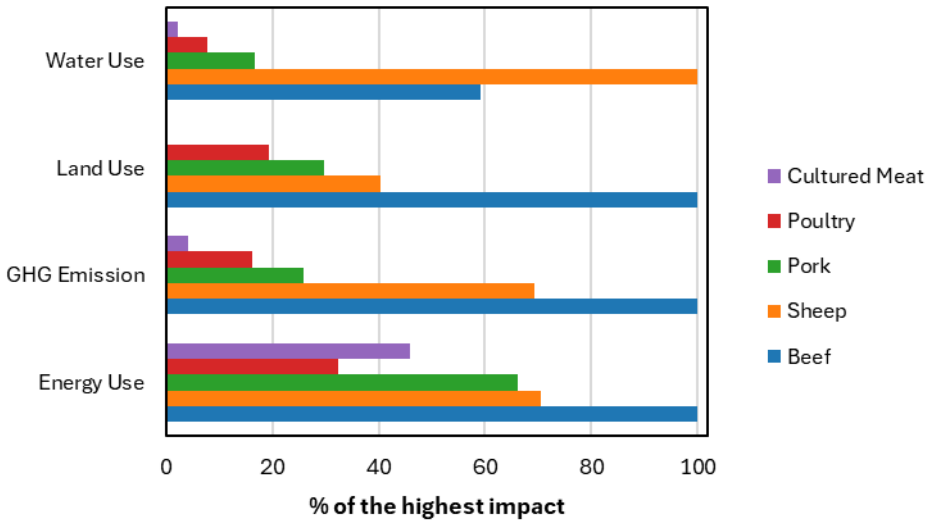

Figure 5 - Comparative environmental impacts of traditional versus cultivated meat production. Adapted from Tuomisto and Teixeira de Mattos (2011)

Technological Approaches and Methodologies. Cultivated meat production encompasses several interconnected technological processes, including muscle progenitor cell isolation, scalable cell expansion, scaffold development, and tissue maturation within bioreactors. Sharma et al. (2015) elaborated on methods to efficiently isolate and propagate muscle progenitor cells, aligning closely with the research methodology employed in this study, which aimed at optimizing myogenic differentiation and muscle-specific protein expression [61].

Advanced methodologies also involve scaffold technologies essential for supporting three-dimensional muscle tissue formation. Acevedo et al. (2018) introduced micropatterned edible films designed to facilitate the organized growth of muscle cells, effectively replicating the texture and structural properties of conventional meat products [62]. In parallel, Ben-Arye et al. (2020) demonstrated that plant-derived textured soy protein scaffolds can support the growth

and maturation of bovine skeletal muscle tissues, reinforcing the viability of plant-based scaffold materials in cultivated meat production [63].

Emerging Role of 3D Printing Technologies. The incorporation of additive manufacturing or 3D printing technologies represents a significant innovation in cultivated meat production, offering unprecedented control over tissue architecture, cellular distribution, and final product appearance. Ramachandraiah (2021) reviewed current developments in sustainable 3D-printed meat analogs, highlighting their potential to enhance product appeal through improved texture, nutritional quality, and consumer acceptance [64]. The research emphasis on myoglobin enrichment directly contributes to the sensory and nutritional improvements achievable through these 3D-printed cultivated meat analogues.

Commercialization and Consumer Acceptance. Despite technical progress, the widespread commercialization and market acceptance of cultivated meat face several notable barriers. Choudhury et al. (2020) critically examined the business landscape, identifying challenges such as high production costs, scalability limitations, regulatory complexities, and consumer skepticism. Enhancing visual and nutritional attributes through optimized myoglobin content, as targeted in this research, is a key strategy for improving consumer perceptions and facilitating market entry [65].

Key Challenges and Future Research Directions. The potential of cultivated meat to transform global food production is substantial. Progress in cell biology, tissue engineering, and scalable manufacturing methods positions cultivated meat as a viable solution to future challenges in food security, environmental sustainability, and animal welfare. Targeted research, such as these investigations into optimizing physiological characteristics like myoglobin content, plays a pivotal role in advancing the feasibility and acceptance of cultivated meat technologies. However, significant technical and scientific challenges still impede the broad adoption of cultivated meat. Pandurangan and Kim (2015) emphasized the critical need for optimized bioreactor systems, improved cell viability, differentiation protocols, and cost-effective scalability [66]. Further, Bomkamp et al. (2022) identified substantial hurdles concerning scaffold biomaterials, efficient and sustainable cell sourcing, and the development of effective vascularization strategies, areas where the insights from this research may inform further developments [67].

3. Chapter Three: Study I - Cell Culture & Fabrication of 3D Structures

The field of tissue engineering has long sought to replicate the complexity and functionality of native tissues for a wide range of applications, from regenerative medicine and disease modeling to the emerging sector of cultivated meat. A persistent challenge has been the fabrication of three-dimensional (3D) tissues that are both physiologically relevant and scalable for production. While conventional methods often rely on biomaterial scaffolds to provide structural support, these materials can introduce challenges related to cost, biocompatibility, and the complexity of their removal. An alternative approach, scaffold-free tissue engineering, harnesses the inherent ability of cells to self-assemble and secrete their own extracellular matrix (ECM), thereby creating a more natural microenvironment.

This chapter details the comprehensive development and characterization of a novel, scaffold-free protocol for fabricating robust 3D skeletal muscle constructs from murine C2C12 myoblasts. The developed approach uniquely capitalizes on an unexpected cellular response to serum starvation, which was discovered to induce the spontaneous delamination of intact cell sheets from standard tissue culture surfaces. This non-enzymatic and non-thermo-responsive method offers significant advantages in simplicity, cost-effectiveness, and the preservation of cell-cell and cell-ECM interactions, which are critical for maintaining tissue integrity and function.

The methodology presented herein systematically addresses the key steps from cell culture to the formation of complex 3D structures. The following section outlines the protocols for cell handling and the precise conditions required to induce the spontaneous detachment of cell sheets. The subsequent sections are dedicated to the rigorous characterization of the fabricated constructs. The section details the analytical methods employed to confirm the high viability and health of the cells throughout the process using live-dead assays. Furthermore, the techniques for evaluating structural integrity and successful myogenic differentiation are described, including histological analysis with Hematoxylin and Eosin (H&E) staining, immunostaining for the muscle-specific protein myosin heavy chain (MHC), and high-resolution imaging via Scanning Electron Microscopy (SEM). By establishing this robust and reproducible fabrication and characterization pipeline, a solid foundation was laid for

subsequent investigations into the environmental and biochemical factors that influence muscle development and maturation.

3.1. Materials and Methods

3.1.1. Cell Culture and Aseptic Technique

Maintaining a sterile environment is paramount in cellular biology to prevent contamination and ensure the reproducibility of experimental results. In this study, all cell culture manipulations were meticulously conducted within a Class II Microbiological Safety Cabinet (HERAsafe KS12, Thermo Scientific, USA). This specialized laminar flow hood provides a controlled, aseptic workspace by continuously filtering the air through High-Efficiency Particulate Air (HEPA) filters, thereby protecting both the cell cultures from environmental contaminants and the researcher from potential biohazards.

For the consistent growth and maintenance of the cell lines, a CO_2-humidified incubator (HeraCell 150i, Thermo Scientific, USA) was utilized. This incubator precisely regulated the critical parameters of temperature, humidity, and atmospheric gas composition. A constant temperature of 37 °C was maintained to mimic the physiological conditions of the organism from which the cells were derived, while a 5% CO_2 atmosphere was established to buffer the culture medium and maintain a stable physiological pH. This precise control over the cellular microenvironment is essential for supporting optimal cell proliferation and metabolic function.

Routine monitoring of cell health and confluency was a vital part of the culture protocol. Cell growth was systematically assessed every 24 to 48 hours using an inverted light microscope (Diaphot, Nikon, Japan). The inverted configuration of this microscope allowed for the observation of cells from below the culture vessel, enabling non-invasive, real-time assessment of cell morphology, proliferation, and the overall health of the monolayer without disrupting the culture environment. This regular visual inspection ensured that the cell cultures remained in a healthy state, providing a robust foundation for all subsequent experiments.

3.1.2. C2C12 Myoblast Cell Line

For this research, the C2C12 murine skeletal muscle myoblast cell line was acquired from a reputable and established bioresource center, the German Collection of Microorganisms and Cell Cultures (DSMZ). This specific cell line was selected due to its well-documented and robust capacity for myogenic differentiation, a critical attribute for studies focused on muscle

tissue engineering. The C2C12 line is a sub-clone of the original C2 parental cell line, which was originally derived from the leg muscle of an adult C3H mouse following a crush injury. This origin makes C2C12 cells a highly relevant and widely used model for *in vitro* studies of myogenesis [68].

To ensure the long-term viability, genetic stability, and consistency of the cells throughout the experimental period, a tiered cell banking system was meticulously established. A Master Cell Bank (MCB) was created at passage 3, and a Working Cell Bank (WCB) was subsequently generated from the MCB at passage 6. These cell banks were cryopreserved in liquid nitrogen, which provides an ultra-low-temperature environment, effectively halting all cellular metabolic activity and preserving cell integrity until the cells were needed for a specific experiment.

To support cell proliferation and expansion, the C2C12 myoblasts were cultured in a specialized growth medium (GM). This medium was formulated to provide all the essential nutrients for cell growth and consisted of RPMI-1640 basal medium (PAN-Biotech GmbH, Germany). To this basal medium, 10% Fetal Bovine Serum (FBS) (PAN-Biotech GmbH, Germany) was added, a complex mixture of proteins, growth factors, and hormones that promotes cell proliferation. To prevent microbial contamination that could compromise the integrity of the cell cultures, the medium was also supplemented with 1% penicillin-streptomycin (Corning, USA), an antibiotic-antimycotic solution. The cells were maintained and expanded within this GM until they reached 80–90% confluence, a state where the cell monolayer is dense but not so crowded as to inhibit further growth. To ensure a continuous supply of fresh nutrients and to prevent the accumulation of metabolic waste products, the growth medium was carefully replenished every other day.

3.1.3. Cell Counting and viability assessment

Following the enzymatic dissociation of the cell monolayer using trypsin (Lonza, Switzerland), a crucial step to release cells from their adherent state, the resulting cell suspension was meticulously homogenized. This was accomplished by carefully pipetting the suspension up and down to ensure a uniform distribution of single cells, which is essential for obtaining an accurate and representative cell count.

To determine both the total cell concentration and viability, a classic and robust method was employed: manual counting using a Neubauer hemocytometer in conjunction with the trypan blue exclusion method. This technique is based on the principle that the chromophore trypan blue (Sigma-Aldrich, USA) can only permeate the compromised cell membranes of non-viable

cells, staining them with a distinctive dark blue hue. Conversely, viable cells with intact membranes actively exclude the dye and remain unstained.

A small, representative aliquot of the cell suspension, specifically 10 µL, was carefully mixed with an equal volume of a 0.4% trypan blue stain, creating a 1:1 dilution ratio. This mixture was then immediately and carefully introduced into both counting chambers of the hemocytometer via capillary action, ensuring an even distribution of cells within the grid. The hemocytometer's grid is etched with a precise pattern that allows for the counting of cells within a known volume.

Under an inverted light microscope, the cells were systematically counted within the eight large corner squares of the hemocytometer grid. Viable cells were identified as being small, refractile, and unstained, while non-viable cells appeared larger, darker, or stained blue. Any cellular debris was explicitly excluded from the final count.

The final cell concentration was calculated based on the mean cell count from the counted grids. Specifically, the average count from the eight grids was determined, representing the number of cells per 0.1 mm^3. This average was then adjusted by a dilution factor of 2 (to account for the initial 1:1 dilution with trypan blue). Finally, to convert the count to the standard unit of cells per milliliter, this value was multiplied by 10^4 (the conversion factor from 0.1 mm^3 to 1 cm^3). The total number of viable cells in the initial suspension was then calculated by multiplying this final cell concentration by the total volume of the cell suspension. This rigorous process ensured a precise and reliable assessment of the cell population, which is fundamental for all subsequent experiments.

$$cells/mL = Average\ of\ 8\ grids \times dilution\ factor \times 10^4\ cells/mL \quad [1]$$

$$Total\ number\ of\ cells = cells/mL \times cell\ suspension\ volume\ (mL) \quad [2]$$

3.1.4. Cell Sheet Production and Fabrication of 3D Constructs

The foundational protocol for the formation of C2C12 cell sheets was serendipitously discovered during a separate investigation focused on cell cycle synchronization. A critical requirement for that study was to arrest C2C12 myoblasts in the quiescent G_0/G_1 phase of the cell cycle. This was achieved by culturing the cells to a state of high confluency and then subjecting them to serum starvation for a period of 48 hours. Upon subsequent microscopic examination, an unexpected and remarkable observation was made: the cell monolayers had begun to spontaneously and partially delaminate from the surface of the tissue culture plates.

This pivotal finding led to the development of an innovative, scaffold-free method for cell sheet engineering that circumvented the need for specialized substrates, such as expensive thermo-responsive surfaces. The convenience and cost-effectiveness of this approach represent a significant advancement in the field.

Further analysis of this method revealed that it shares certain conceptual similarities with techniques previously reported in the literature, particularly the work of Shahin-Shamsabadi et al. [69], but it incorporates substantial and distinct modifications to the process.

The refined protocol for cell sheet production and subsequent 3D construct fabrication is outlined as follows. Initially, C2C12 myoblasts were seeded onto new culture dishes at a specific, high density of 120,000 cells/cm². The cells were cultured in a standard growth medium (GM) for a period of 24 hours, designated as day 0 (d0), to allow for complete adherence and initial proliferation. Following this initial period, the GM was carefully aspirated and replaced with a differentiation medium (DM). This DM was a low-serum formulation consisting of RPMI-1640 supplemented with only 0.1% horse serum (PAN-Biotech GmbH, Germany) and 1% ITS (insulin-transferrin-selenium, Gibco, USA). The low-serum conditions were maintained for 48 hours to induce a state of partial myogenic differentiation and promote the self-assembly of a cohesive cell sheet. At the conclusion of this 48-hour period, on day 3 (d3), the DM was fully replenished. It was at this stage that the cell sheets could be manually detached by gently and carefully manipulating the medium along the edges of the sheet using a sterile pipette. This technique resulted in the complete and intact detachment of the cell sheets, which were then left floating freely within the culture dish until further use. The entire protocol, from initial seeding to detachment, is comprehensively illustrated in Figure 6.

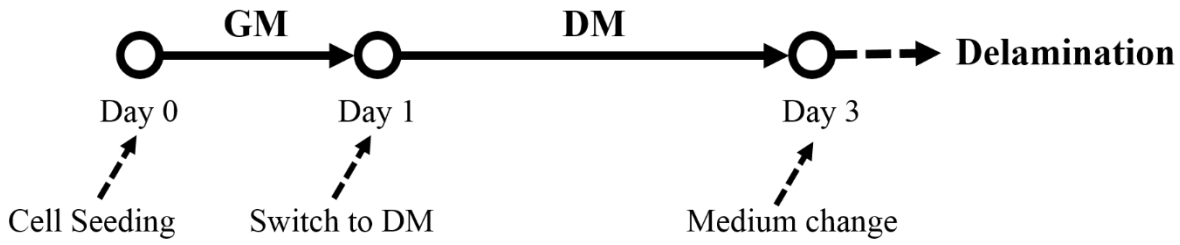

Figure 6 - Cell sheet formation and delamination

To create more complex and robust 3D constructs, a specific number of the detached cell sheets were assembled through a process of manual stacking. Once all the individual sheets were successfully detached on d3, one sheet was designated as the "host sheet" and allowed to remain flat while floating on the medium's surface. The remaining sheets were then sequentially and

carefully positioned on top of the host sheet's center. This precise alignment and stacking procedure promoted direct cell-to-cell contact between the layers. The resulting stacked, multi-layered structure was then incubated at 37°C for a further 24 hours. During this period, the multiple layers naturally compacted and integrated, forming a single, dense 3D structure. This process takes advantage of the intrinsic contractile forces of the cells and their self-secreted extracellular matrix to create a cohesive and robust construct.

3.1.5. Cell Viability Assay

To rigorously evaluate the health and viability of the engineered cell sheets at critical stages of the protocol, a fluorescence-based live-dead assay was performed. This assay provides a clear and reliable distinction between living and dead cells by utilizing a combination of two distinct fluorescent probes: Calcein AM and Propidium Iodide (PI). This dual-stain method is widely recognized as a gold standard for assessing cell viability without the need for destructive sampling.

The mechanism of this assay hinges on the integrity of the cell membrane and the presence of intracellular enzymatic activity. Calcein AM is a non-fluorescent, cell-permeant dye that can freely diffuse across the membranes of all cells. Once inside a viable cell, however, the dye is a substrate for ubiquitous intracellular esterase enzymes. These enzymes hydrolyze the dye's acetoxymethyl (AM) groups, converting it into a highly fluorescent product, Calcein. Calcein is a hydrophilic molecule that is retained within the cytoplasm of cells with intact membranes, causing them to emit a bright green fluorescence. This signal serves as a direct indicator of both cell membrane integrity and metabolic activity.

In stark contrast, Propidium Iodide (PI) is a nucleic acid-staining dye that is cell-impermeant. It can only enter cells where the plasma membrane has been compromised, a hallmark of non-viable or dead cells. Once inside, PI intercalates with the DNA, producing a distinct and intense red fluorescence. Because living cells actively exclude PI, the absence of a red signal confirms a cell's viability. This combination of a bright green signal for living cells and a bright red signal for dead cells provides a robust and unambiguous readout of the cell sheet's overall health.

This assay was specifically applied to the cell cultures at two pivotal time points: at the conclusion of the growth phase (Day 1) and immediately prior to cell sheet delamination at the end of the differentiation phase (Day 3). For each assessment, the culture medium was aspirated, and the cell sheets were gently washed twice with warm Phosphate-Buffered Saline (PBS) to remove any residual medium components. Fresh working solutions were then prepared,

consisting of a final concentration of 2 µM Calcein AM and 2 µg/mL PI. A sufficient volume of this dual-stain solution was added to each culture dish to fully immerse the cell sheet, and the samples were incubated for 20 minutes at 37°C in the dark to allow for complete dye uptake and enzymatic conversion.

Following incubation, the samples were washed again with warm PBS to remove any excess, unbound dye, ensuring a high signal-to-noise ratio. The cell sheets were then submerged in fresh warm PBS, and live-cell imaging was performed using an Eclipse 80i fluorescence microscope (Nikon, Japan). To capture the distinct fluorescent signals, a FITC filter for the green Calcein AM emission and a Texas Red filter for the red PI emission were used. Multiple images were systematically captured at both 4X and 10X objective magnifications to provide a comprehensive and representative view of the cell sheets' viability. The selective nature of these fluorescent probes allowed for a precise and reliable assessment of cell health before the constructs were subjected to further experimental manipulation.

3.1.6. Histology and Immunostaining

Following the fabrication of the 3D constructs, a crucial four-day maturation period (extending from day 3 to day 7) was implemented. This maturation phase allowed for the further development of the engineered tissues, including the establishment of a robust extracellular matrix and the maturation of myotubes. To preserve the structural integrity of the constructs for subsequent microscopic analysis, the samples were first washed three times with Phosphate-Buffered Saline (PBS) to remove any residual media. They were then fixed using a 4% paraformaldehyde solution at 4°C for 12 hours. This process cross-links proteins, effectively preserving cellular morphology and tissue architecture. Post-fixation, the samples were embedded in paraffin blocks, a standard procedure that provides the rigidity necessary for sectioning. The blocks were meticulously sectioned into thin 3 µm slices using a microtome, a thickness that is ideal for detailed cellular and tissue-level examination. These sections were then prepared for both histological and immunostaining procedures to comprehensively evaluate cellular organization and myogenic differentiation.

Hematoxylin and Eosin (H&E) Staining. To gain a foundational understanding of the overall tissue structure, cellular distribution, and morphological integrity, Hematoxylin and Eosin (H&E) staining was performed. This classic histological staining technique utilizes two contrasting dyes. Hematoxylin, a basic dye with a deep blue or purple hue, selectively binds to the acidic components of the cell, such as the nucleic acids within the nucleus and the ribosomes

in the cytoplasm. This staining provides excellent detail of the chromatin structure and nuclear morphology. Conversely, Eosin, an acidic dye, stains the basic cellular components, including the cytoplasm and, most importantly, the extracellular matrix (ECM) proteins, with various shades of pink and red. The striking color contrast between the nuclei and the cytoplasm/ECM enabled the clear visualization of the engineered tissue's architecture, revealing the dense cellular packing and the self-secreted ECM network. This method served as a fundamental assessment of the structural quality of the engineered tissues.

Immunostaining for Myosin Heavy Chain (MHC). To specifically confirm the successful differentiation of C2C12 myoblasts into mature, muscle-like structures, immunostaining for myosin heavy chain (MHC) was conducted. MHC is a principal motor protein and a definitive biomarker for mature skeletal muscle fibers. The tissue sections were first deparaffinized to remove the embedding medium, followed by rehydration. To prevent non-specific binding of the antibodies, which can lead to false-positive signals, the sections were treated with a 10% goat serum blocking solution. The sections were then incubated overnight at 4°C with a primary rabbit anti-mouse MHC antibody. This antibody was meticulously chosen for its high specificity, as it selectively binds to the MHC proteins expressed in the differentiated muscle cells. After the overnight incubation, the sections were thoroughly washed with PBS to remove any unbound primary antibody. A fluorescently labeled anti-rabbit secondary antibody (Alexa Fluor 488) was then applied. This secondary antibody binds to the primary antibody, and its fluorescent tag allows for the visualization of MHC expression under a fluorescence microscope. This approach provided unequivocal evidence of successful muscle cell differentiation and organization within the constructs, thereby verifying the effectiveness of the established differentiation protocol.

3.1.7. Scanning Electron Microscopy (SEM) Imaging

To gain a comprehensive understanding of the structural morphology and microarchitecture of the 3D muscle constructs at the nanoscale, Scanning Electron Microscopy (SEM) was employed. This powerful, high-resolution imaging technique is an indispensable tool in materials science and biological research due to its ability to provide exceptional magnification, depth of field, and detailed topographical information. The specific instrument utilized was a Leo 1530 Gemini scanning electron microscope (Carl Zeiss, Germany).

The preparation of biological samples for SEM requires meticulous steps to preserve their intricate structure and ensure compatibility with the high-vacuum environment of the

microscope. The protocol began with a critical fixation step: the 3D constructs were immersed in a 4% formaldehyde solution for a minimum of 30 minutes at 4°C. Formaldehyde acts as a chemical fixative by cross-linking proteins, thereby arresting all biological processes and stabilizing the cellular and tissue components. Following fixation, the samples underwent a progressive dehydration process using a graded ethanol series. This gradual increase in ethanol concentration systematically replaced all the water within the tissues, a vital step to prevent the collapse of the delicate cellular architecture that would otherwise occur from the surface tension of water during drying.

To eliminate any remaining liquid and prevent structural artifacts, the dehydrated samples were subjected to CO_2 critical point drying (Quorum Technologies, UK). This technique transitions the liquid CO_2 to a gaseous state without passing through the liquid-gas phase boundary, thereby circumventing the damaging effects of surface tension that can cause significant shrinkage and distortion of the sample's microenvironment. Finally, to prepare the specimens for imaging, they were sputter-coated with a very thin layer of gold. This coating served two primary purposes: first, it rendered the non-conductive biological material conductive, which is essential to prevent charge accumulation and image distortion; and second, it enhanced the signal-to-noise ratio, leading to improved imaging resolution. After this process, the average dried sheet thickness was estimated by taking 50 measurements from different regions using ImageJ software.

The fundamental operation of an SEM involves directing a finely focused beam of high-energy electrons across the specimen's surface. The interactions between these electrons and the sample's atoms generate various signals, which are then detected and translated into an image. Secondary electrons, which are dislodged from the specimen's surface, are the primary signal used to form high-resolution topographical images, providing detailed insights into surface features. Backscattered electrons are also generated, offering information on compositional contrast based on the atomic number of the elements present. In addition, the interaction can produce characteristic X-rays, which can be analyzed by Energy-Dispersive X-ray Spectroscopy (EDS) to perform elemental analysis. By leveraging these diverse signals, SEM provided a comprehensive and multi-faceted view of the 3D constructs, enabling a thorough assessment of their morphology, cellular arrangement, and the intricate network of the self-secreted ECM.

3.1.8. Reproducibility of Experiments

All experiments were performed in biological triplicates unless stated otherwise. Each experiment was independently repeated three times under the same conditions to ensure reproducibility and reliability of the results. Data presented in this study therefore represent consistent findings across these independent replicates.

3.2. Results

3.2.1. Cell Sheet and 3D Construct Fabrication

The established protocol, as detailed in Figure 6, successfully induced the formation of cohesive C2C12 cell sheets following a three-day culture period. This period comprised an initial 24-hour growth phase followed by a 48-hour differentiation phase. At the culmination of the differentiation phase on day 3, a remarkable and spontaneous biological event was observed: the cell sheets began to naturally detach from the culture surface. This process initiated at distinct "weak points" along the periphery of the sheet, where cellular adhesion to the plate was visibly reduced. At this critical juncture, the sheets could be manually detached with minimal effort by gently directing a stream of medium from a pipette toward these vulnerable areas. This gentle, non-enzymatic manipulation, which took less than a minute, resulted in the successful release of a complete and structurally intact cell sheet, which then floated freely on the surface of the medium.

A noteworthy observation during the delamination process was the immediate reduction in the size of the detached cell sheets. They visibly contracted, becoming smaller than the original dimensions of the culture plate. This phenomenon is a direct consequence of the high intrinsic cellular tension within the sheet, driven by robust cell-cell and cell-extracellular matrix (ECM) interactions. This finding is consistent with prior observations in the literature concerning scaffold-free tissue engineering [69]. Figure 7a provides a clear visual representation of the weak points that facilitated this efficient delamination process.

The reproducibility and scalability of this protocol were rigorously tested across a range of culture vessel sizes, including 24-well plates, 12-well plates, 6-well plates, 35 mm petri dishes, and 60 mm petri dishes. The method proved highly reliable and reproducible for all these formats. However, a limitation emerged when attempting to scale up to 100 mm petri dishes. The larger sheets exhibited a resistance to spontaneous detachment, making it challenging to obtain a fully intact sheet using the pipetting method alone. This suggests that the delamination

mechanism may be sensitive to the scale, perhaps due to a critical surface area-to-volume ratio or increased tension in the larger constructs. Consequently, for sheets from 100 mm dishes, a sterile cell scraper was required for mechanical delamination on day 3 to ensure a complete harvest.

Upon further incubation at 37°C, the detached cell sheets exhibited another fascinating property: they progressively contracted and curled upon themselves, ultimately forming a compact, three-dimensional (3D) semi-cylindrical structure (Figure 7c). This innate self-assembly capability was then leveraged to fabricate larger and more complex 3D constructs. The protocol involved stacking multiple cell sheets on top of a single "host sheet" that was floating flat on the medium surface. Within 24 hours of co-incubation, the stacked sheets spontaneously integrated into a single, dense structure as the host sheet curled around them.

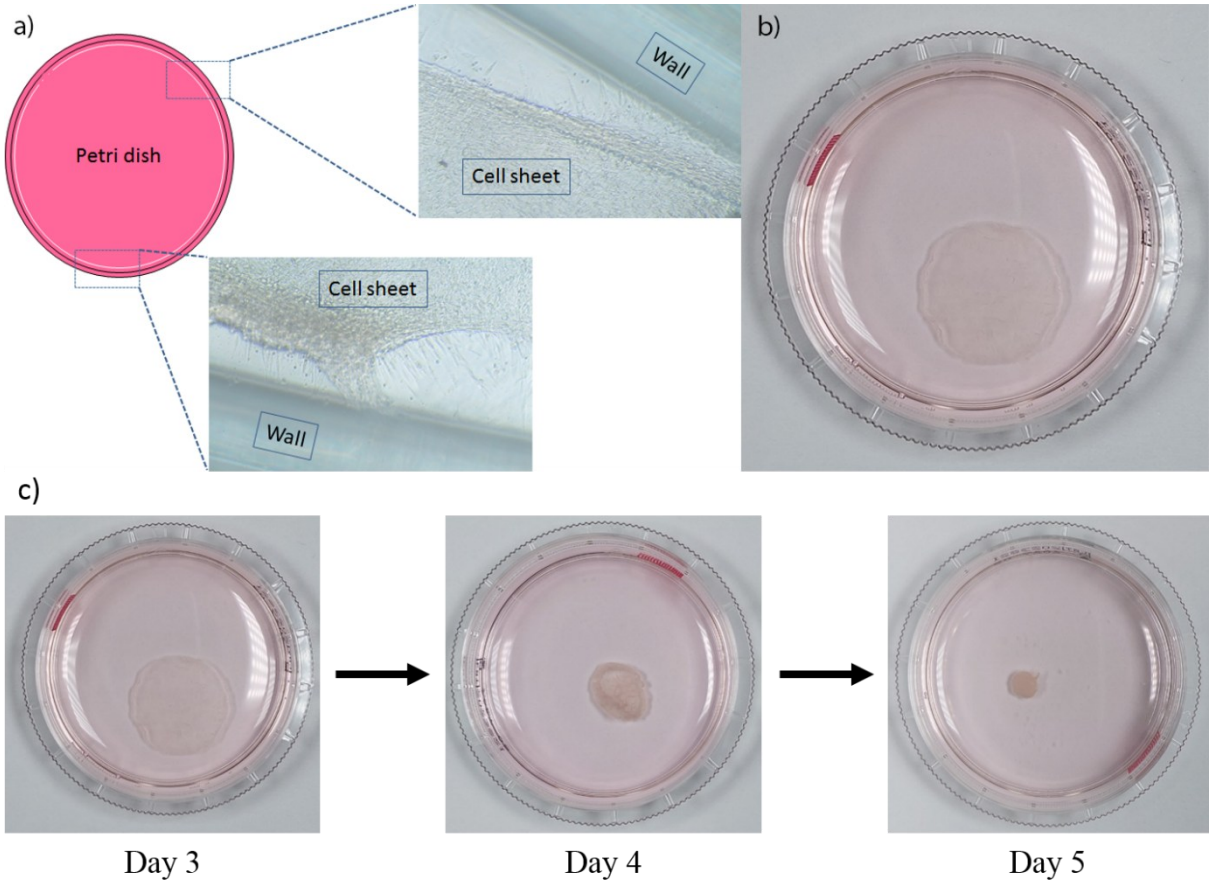

Figure 7 - Procedure of C2C12 cell sheet production, delamination, and size reduction. a) the weak points that appear after the end of differentiation phase. b) A cell sheet just after delamination (35 mm petri dish) c) Size reduction of the cell sheets by time after delamination. This sheet was made in a 35 mm petri dish.

This technique offers significant practical advantages in terms of convenience and time efficiency compared to other scaffold-free methods that require meticulous and time-consuming manual stacking. The scalability of this approach is ultimately dependent on the initial sheet

size and the availability of nutrients. This work demonstrates a robust, practical, and highly efficient method for generating complex 3D muscle constructs, laying a strong foundation for future research.

3.2.2. Cell Viability

To rigorously assess the health and vitality of the engineered C2C12 cell sheets, a fluorescence-based live-dead assay was performed at two key time points: at the conclusion of the initial growth phase (Day 1) and immediately prior to their detachment from the culture surface at the end of the differentiation phase (Day 3). The assay utilized a dual-staining approach with two fluorescent probes: Calcein AM and Propidium Iodide (PI). This methodology provides an unequivocal distinction between viable and non-viable cells based on the integrity of their cell membranes and the presence of intracellular esterase activity.

The results of the comprehensive viability analysis, as illustrated in Figure 8, demonstrated a remarkably high proportion of living cells within the C2C12 monolayers. Microscopic examination revealed a predominant population of cells that exhibited intense green fluorescence, a signal derived from the enzymatic hydrolysis of Calcein AM by intracellular esterases within metabolically active cells. This abundant green staining served as a powerful visual confirmation of the high metabolic activity and robust viability of the cell population. In stark contrast, only a minimal presence of red fluorescence was observed, which corresponds to PI binding to the nucleic acids of cells with compromised membranes. The negligible red signal indicated a very low incidence of cell death throughout the culture period.

The observed dense and uniformly distributed pattern of green fluorescence across the cell sheets strongly suggests the presence of a functionally active and structurally cohesive monolayer. The minimal PI staining not only underscores the low rate of cell death but also provides compelling evidence that the low-serum culture conditions used to induce differentiation did not adversely affect the overall health or membrane integrity of the cells. This favorable outcome is of critical importance, as it confirms the suitability of the established culture protocol in providing a robust and healthy cellular foundation. The high viability and structural integrity of the cell sheets, even after an extended differentiation period, ensure their readiness for subsequent manipulation and use in downstream applications, ranging from further tissue maturation to in-depth functional analyses.

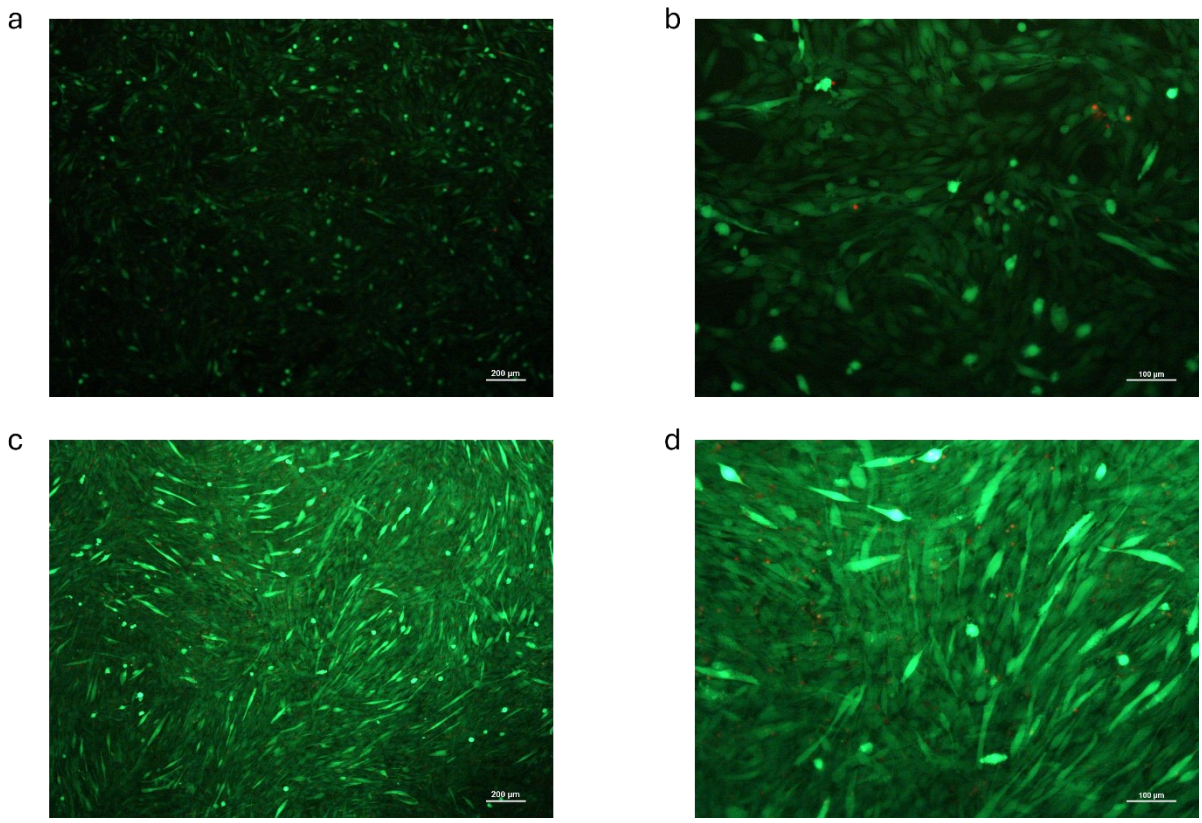

Figure 8 – Live-Dead imaging at different magnifications at a,b) day 1 c,d) day 3 (scale bars indicate 200µm)

3.2.3. Histology And Immunostaining

To comprehensively evaluate the myogenic differentiation and structural organization of the three-dimensional (3D) constructs, both immunostaining and classic histological analyses were performed. This dual approach was essential for providing a multi-faceted view of the tissue's development and integrity.

First immunostaining for Myosin Heavy Chain (MHC), a universally recognized biomarker for late-stage myogenic differentiation, was conducted. In addition, the cell nuclei were visualized by counterstaining with DAPI, a fluorescent dye that binds strongly to DNA. The fluorescence microscopy images, presented in Figures 9a,b, provided compelling evidence of successful myogenic lineage commitment and maturation. A strong and well-distributed expression of MHC throughout the 3D structures was observed, which manifested as an intricate network of bright fluorescent fibers. This robust staining pattern signified the successful formation of muscle-like tissue and demonstrated that the established culture conditions provided a highly conducive microenvironment for the development of functional contractile elements, which are indispensable for muscle tissue integrity. The presence of these clearly defined myosin-positive

regions further reinforced the conclusion that the C2C12 cells had not only differentiated but had also successfully integrated within the complex 3D system.

To complement these findings, Hematoxylin and Eosin (H&E) staining was performed on the constructs after a seven-day maturation period. H&E staining is a gold standard in histology that provides invaluable insight into general tissue morphology and cellular architecture. The H&E-stained sections, shown in Figure 9c, revealed a cohesive and compact tissue structure composed of densely packed, rounded cells. This dense cellular arrangement, a hallmark of scaffold-free tissues, was accompanied by a noticeable accumulation of extracellular matrix (ECM), which appeared as pink-stained regions. The active secretion and deposition of this ECM by the cells is a crucial biological process that provides mechanical support and a stable framework for cellular organization. Interestingly, the H&E analysis also revealed a distinct "crumpled-sheet" architecture within the constructs, with observable spaces between the layered cell sheets. This unique spatial arrangement may offer an advantage by facilitating nutrient and gas exchange, as well as enhancing cell-to-cell communication.

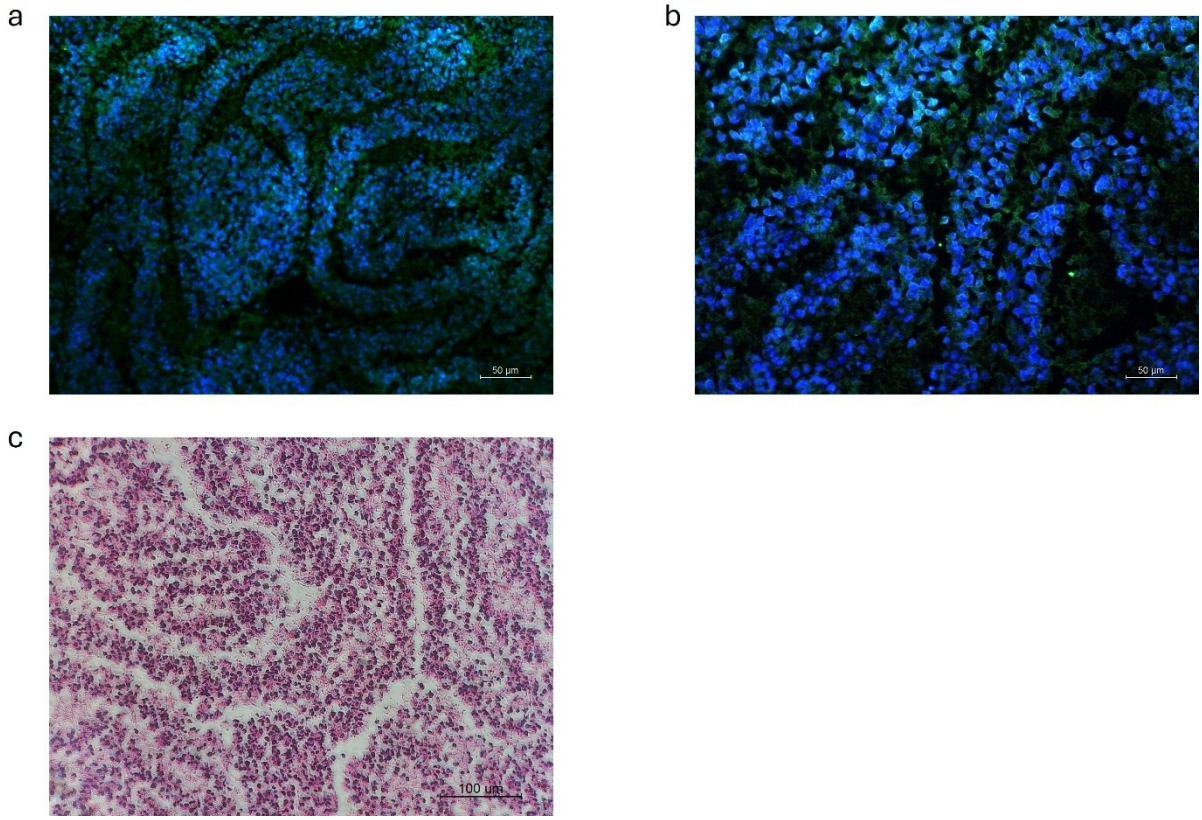

Figure 9 – a,b) Immunostaining images of 3D constructs at different magnifications against myosin heavy chain (scale bars indicate 50µm) c) hematoxylin and eosin imaging of the 3D constructs(scale bar indicates 100µm)

In essence, the combination of strong MHC expression and well-organized tissue architecture confirmed that the engineered 3D constructs provided a structurally and functionally supportive

niche for myogenic differentiation, effectively mimicking key aspects of native muscle tissue development.

3.2.4. SEM Imaging and Microstructural Analysis

To obtain a high-resolution, detailed perspective on the structural morphology and microarchitecture of the engineered 3D constructs, Scanning Electron Microscopy (SEM) was utilized. This powerful technique allowed for a comprehensive visualization of the constructs' surface features and the intricate cellular arrangement within. Before imaging, a rigorous and multi-step sample preparation protocol was executed to preserve the delicate structural integrity of the biological tissues for the high-vacuum environment of the microscope.

First, the samples were immersed in a 4% formaldehyde solution and incubated at 4°C for at least 30 minutes. This chemical fixation step cross-links proteins, effectively arresting all biological processes and stabilizing the cellular and extracellular components. Following fixation, the constructs were systematically dehydrated using a graded ethanol series, a process that gradually replaced the intracellular and interstitial water with ethanol. This critical step was essential to prevent the destructive effects of surface tension forces that would otherwise cause the fragile tissue to collapse and distort during drying. To ensure complete removal of liquid without introducing artifacts, the dehydrated samples were then subjected to CO_2 critical point drying, which transitions the CO_2 from a liquid to a gaseous state without passing through the phase boundary. Finally, to optimize the imaging quality, the specimens were sputter-coated with a thin, electrically conductive layer of gold. This coating not only prevented charge accumulation, which can severely degrade image quality, but also enhanced the signal-to-noise ratio, thereby improving both resolution and contrast.

The SEM images, as presented in Figure 10, provided detailed insights into the constructs' microarchitecture. They revealed a densely packed cellular arrangement with cells appearing rounded and integrated within a rich extracellular matrix (ECM) network. The abundance of this self-secreted ECM suggested a highly active cellular state, which fostered a well-established microenvironment essential for structural cohesion and stability. These findings were entirely consistent with the earlier histological and immunostaining results, which further reinforces the reliability and validity of the structural analyses.

A particularly notable observation was the change in cell morphology immediately following delamination from the culture surface. The cells, which were previously elongated in a monolayer, lost their characteristic spindle shape and transitioned into a more compact, rounded

configuration. This morphological adaptation directly correlated with the observed macroscopic size reduction of the cell sheets post-detachment. This phenomenon suggests that the cells undergo a structural reorganization in response to the removal of the planar culture surface, which ultimately facilitates their self-assembly into a cohesive 3D structure.

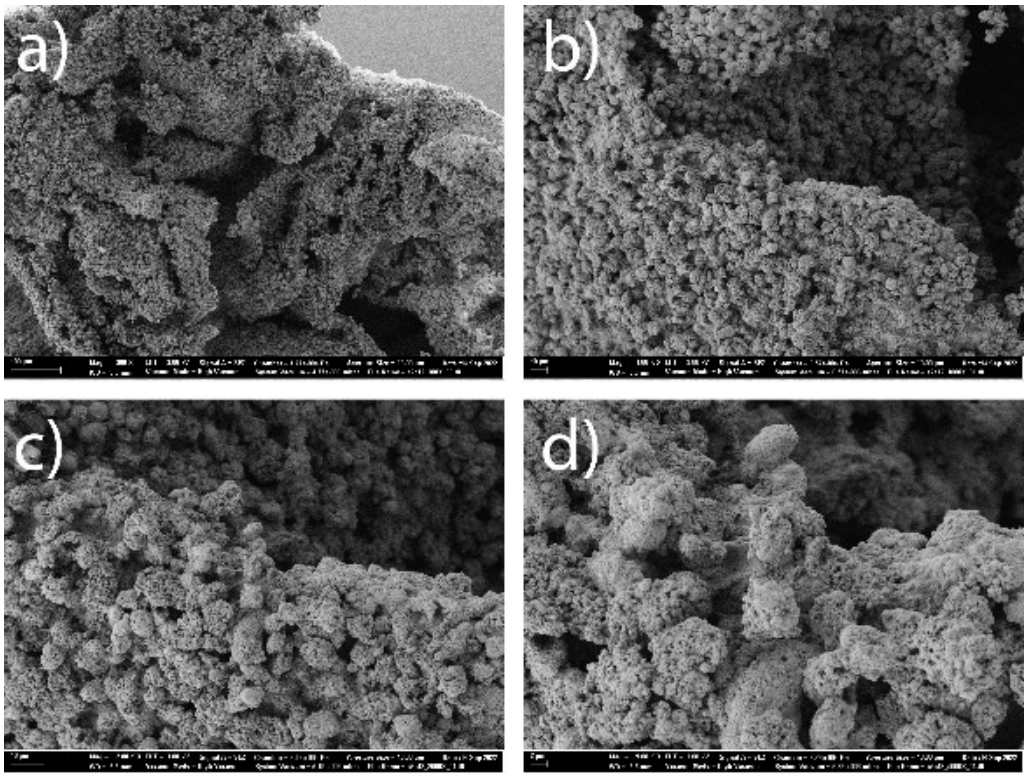

Figure 10 - Scanning electron microscopy of a 3D construct after 7 days in culture a) 300X magnification b) 1000X magnification c) 2000X magnification d) 5000X magnification

In conclusion, the SEM analysis provided a valuable, high-resolution perspective on the micro-level characteristics of the 3D constructs. It confirmed their dense cellular arrangement, abundant ECM enrichment, and the dynamic morphological transitions that follow the delamination process. These observations support the structural soundness of the engineered constructs and suggest potential for future applications in regenerative medicine and bioengineering.

3.3. Chapter Discussion

The first study of this thesis successfully established a novel, scaffold-free protocol for the fabrication of three-dimensional (3D) skeletal muscle constructs. This method represents a significant departure from conventional approaches that typically rely on thermo-responsive or enzymatically degradable surfaces. Instead, the protocol leverages an unexpected cellular response to serum starvation, which triggers the spontaneous delamination of an intact, cohesive

cell sheet. This discovery is particularly advantageous due to its simplicity and cost-effectiveness, as it completely eliminates the need for specialized, expensive substrates.

The observed phenomenon of spontaneous delamination and the subsequent reduction in cell sheet size upon detachment are direct consequences of the high intrinsic cellular tension and robust cell-cell and cell-extracellular matrix (ECM) interactions within the tissue. This finding is consistent with prior research on the mechanical properties of cell sheets [69] and provides evidence consistent with the self-assembling nature of the fabrication technique. The resulting cell sheets are not merely monolayers but are structurally integrated tissues ready for further engineering.

A thorough viability analysis confirmed that the low-serum culture conditions did not compromise cell health. Live-dead assays revealed an a high proportion of viable cells and minimal cell death throughout the entire fabrication process. This outcome is critically important because it ensures that the foundational cellular components of the constructs are robust and primed for long-term survival and functionality. This high viability is a prerequisite for any subsequent engineering or maturation efforts.

Furthermore, histological and immunostaining results provided clear, unequivocal evidence of successful myogenic differentiation within the fabricated 3D constructs. The expression of myosin heavy chain indicated the formation of muscle-like tissue with physiological relevance. The presence of a rich, self-secreted ECM further underscored the ability of the model to support the complex processes of tissue development. Additionally, Scanning Electron Microscopy (SEM) provided a detailed, high-resolution view of the microstructural integrity of the constructs, revealing a dense cellular arrangement and a prominent ECM network. This dense packing and rich ECM are crucial for the mechanical and biochemical functionality of engineered tissues and are hallmarks of a successful scaffold-free approach.

While the protocol is highly reproducible and robust for small-to-medium-sized culture vessels (up to 60 mm petri dishes), a notable limitation emerged during the attempted scale-up to 100 mm dishes. In these larger formats, the spontaneous delamination mechanism was insufficient, requiring mechanical assistance with a cell scraper to harvest intact sheets. This suggests that the delamination process may be sensitive to a specific surface area-to-volume ratio or that larger sheets generate a level of tension that resists spontaneous detachment. Future investigations could focus on optimizing this process for large-scale production without compromising the non-enzymatic nature of the harvest, which is a key advantage of this

method. Overall, this study successfully demonstrates a robust, practical, and highly effective method for generating complex 3D muscle constructs, thereby laying a solid and reliable foundation for subsequent investigations into the environmental and biochemical factors that influence muscle development and function.

4. Chapter Four: Study II - Computer Simulation of Oxygen Transfer

The successful scale-up of engineered tissues, particularly for applications like cultivated meat, hinges on overcoming critical limitations related to nutrient and gas transport. As constructs grow in size and density, diffusion becomes insufficient, leading to oxygen and nutrient starvation in the core and, consequently, cell death. To address this fundamental challenge, this study combines experimental measurements with computational modeling to provide a quantitative understanding of oxygen transport within the scaffold-free 3D muscle constructs. The following sections detail the methods employed to characterize key parameters—including porosity, oxygen uptake rate (OUR), and the effective diffusion coefficient (D_{eff}), which were then used to build a predictive mathematical model.

Oxygen transfer within the 3D cell constructs, a critical limiting factor in thick tissues, was simulated using the finite-element method in COMSOL Multiphysics (v.6.3). Given the semi-cylindrical shape of the cell sheets, the model geometry was simplified to a cylinder immersed in a static culture medium. This allowed the modeling of oxygen transport by molecular diffusion from the surrounding medium, which was assumed to be saturated with atmospheric oxygen. This integrated computational and experimental approach not only identifies a critical size limitation for these constructs but also provides a framework for designing strategies to ensure long-term viability and functionality.

4.1. Methods

4.1.1. Geometry And Governing Equations

To comprehensively model the intricate process of oxygen diffusion within the three-dimensional (3D) skeletal muscle constructs, a mathematical framework based on Fick's second law of mass transfer was employed. This fundamental principle describes how concentration changes over time in response to both diffusion and a sink term representing cellular consumption. Given the semi-cylindrical morphology of the engineered constructs, the governing equation were initially formulated in cylindrical coordinates to accurately capture the system's geometry. The full partial differential equation, which accounts for the spatiotemporal dynamics of oxygen, is expressed as follows:

$$\frac{\partial C_s}{\partial t} = D_{eff}\left(\frac{1}{r}\frac{\partial}{\partial r}\left(r\frac{\partial C_s}{\partial r}\right) + \frac{1}{r^2}\frac{\partial^2 C_s}{\partial \theta^2} + \frac{\sigma^2 C_s}{\sigma Z^2}\right) - OUR \quad (1)$$

Where:

- c_s represents the oxygen concentration within the 3D constructs, measured in units of [mol·L^{-1}].
- D_{eff} is the effective oxygen diffusion coefficient, a critical parameter that accounts for the reduced diffusion rate through the dense cellular and extracellular matrix (ECM) network of the constructs, which is directly influenced by their porosity (ε).
- OUR denotes the oxygen uptake rate of the cells, quantifying the rate at which oxygen is consumed by cellular metabolism, with units of [mol·L^{-1}·h^{-1}].

Due to the inherent assumption of radial symmetry in this model, the governing equation could be simplified by eliminating the angular dependency, reducing the complexity of the computational model while maintaining geometric accuracy in the radial plane:

$$\frac{\partial C_s}{\partial t} = D_{eff}\left(\frac{1}{r}\frac{\partial}{\partial r}\left(r\frac{\partial C_s}{\partial r}\right) + \frac{\sigma^2 C_s}{\sigma z^2}\right) - OUR \quad (2)$$

A significant experimental challenge arose from the inability to directly measure the oxygen concentration profiles along the radial axis, which would have been necessary to solve Equation (2) with appropriate boundary conditions. This practical constraint limited the measurements to a one-dimensional profile along the vertical, or z-axis. To overcome this limitation and enable the calculation of key model parameters from the experimental data, the governing equation was further reduced to a one-dimensional version:

$$\frac{\partial c_s}{\partial t} = D_{eff.}\frac{\partial^2 c_s}{\partial z^2} - OUR \quad (3)$$

This simplification provided a pragmatic and effective framework for determining the effective diffusion coefficient (D_{eff}) and the oxygen uptake rate (OUR) based on the empirical measurements. While this approach necessitates the inherent assumption of uniformity along the radial axis, it was a necessary trade-off that provided a practical pathway to obtaining crucial model parameters and performing realistic simulations of oxygen transport within the constructs.

Despite the use of a 1D approximation for parameter derivation, the final oxygen concentration transfer was simulated using the advanced finite-element method within COMSOL Multiphysics (v.6.3). This robust software enabled incorporating both radial and vertical

dimensions in the simulation, providing a more detailed and spatially heterogeneous model. This cross-validation between the simplified 1D parameter calculations and the more complex 2D COMSOL simulation was crucial for assessing the accuracy of the overall approach. While it is acknowledged that the initial methodological simplification may introduce some degree of error, this integrated approach allowed allowed the study to overcome practical experimental constraints while still providing valuable and actionable insights into the complex oxygen dynamics governing the 3D engineered tissues.

4.1.2. Determination of Construct Porosity

To gain a quantitative understanding of the structural characteristics that govern oxygen transport, it was focused on determining the porosity (ε) of the 3D engineered constructs. Porosity is a critical parameter in the model, as it directly influences the effective oxygen diffusion coefficient (D_{eff}) by defining the fraction of the tissue volume available for molecular transport. Given that the constructs are formed by the crumpling and compaction of multiple cell sheets, the internal porosity is a key determinant of the microenvironment's diffusional properties.

To precisely measure this parameter, micro-computed tomography (μ-CT) was employed, a non-invasive imaging technique that provides high-resolution 3D reconstructions of a sample's internal structure. For this analysis, three constructs of varying thicknesses were fabricated according to the established protocol. Following their formation, the samples were meticulously washed with phosphate-buffered saline (PBS) and then fixed in a 4% formalin solution for 24 hours to preserve their cellular and tissue architecture.

To enhance the contrast between the biological tissue and the void spaces (pores) in the μ-CT scans, the fixed samples were subjected to a staining protocol. They were soaked in an Iodine Potassium Iodide solution (I_2KI) for a period of three days. Iodine is a heavy element that stains biological macromolecules, such as proteins and lipids, significantly increasing their radiopacity and allowing for clear differentiation from the unstained pore spaces. The μ-CT scanning was performed using a μCT 25 system (SCANCO Medical AG, Switzerland) with the following acquisition parameters: a tube voltage of 45 kV, a tube current of 72 μA, and an exposure time of 800 ms.

The raw μ-CT scan data were exported as reconstructed DICOM stacks. These stacks were then processed using two specialized software platforms. For visual and illustrative purposes, the reconstructed volumetric data were imported into 3D Slicer software (v. 5.2.2). For the rigorous

quantitative analysis and the precise calculation of porosity, the DICOM stacks were analyzed in ImageJ software. This process involved segmenting the solid tissue from the void spaces, allowing to calculate the porosity as the ratio of the total void volume to the total construct volume, thereby providing a crucial parameter for the computational model.

4.1.3. Volumetric Mass Transfer Coefficient

To comprehensively model the oxygen transport dynamics within the system, it was essential to quantify the rate at which oxygen is transferred from the gas phase (the incubator atmosphere) into the culture medium. This rate is governed by the volumetric mass transfer coefficient (k_La), a critical parameter that encapsulates the efficiency of oxygen dissolution at the gas-liquid interface. The governing equation for the mass balance of oxygen within a homogenous culture medium, considering both transfer from the gas phase and consumption by cells, is given by:

$$\frac{dc_l}{dt} = K_L a(c^* - c_l) - OUR \quad (4)$$

Here, c_l [mol·L^{-1}] represents the oxygen concentration dissolved in the liquid medium, while c^* [mol·L^{-1}] denotes the saturation concentration of oxygen in the liquid, which is the concentration in equilibrium with the gas phase. The term k_La is the volumetric mass transfer coefficient, which is dependent on a multitude of factors, including the physical properties of the culture vessel, the hydrodynamic conditions of the liquid, and the effective diffusion coefficient of oxygen in the medium. The term OUR represents the oxygen uptake rate of the cells, which acts as a sink for dissolved oxygen.

To isolate and precisely determine the value of k_La without the confounding influence of cellular metabolism, a simplified experimental approach was adopted. By using a cell-free medium, the oxygen consumption term (OUR) was eliminated from the equation. This simplification allowed the study to focus solely on the rate of oxygen transfer at the gas-liquid interface. In this case, the governing equation reduces to:

$$\frac{dc_l}{dt} = K_L a(c^* - c_l) \quad (5)$$

This streamlined approach facilitated the direct calculation of k_La from the experimental data. The measurement was performed by monitoring the real-time oxygen concentration in a cell-free medium using an SDR OxoDish OD24 plate. To determine the saturation concentration of oxygen in equilibrium with the gas phase (c_l^*), Henry's Law was utilized, a fundamental principle that describes the solubility of a gas in a liquid. The Henry's constant for oxygen at a

standard temperature of 25 °C was obtained from established literature sources [70,71]. To account for the temperature variations inherent in the culture conditions (37 °C), the Van't Hoff extrapolation was applied [72], which corrects the Henry's constant for temperature dependence:

$$H_T = H_{T0}.\exp[\frac{-\Delta H_{sol}}{R}(\frac{1}{T}-\frac{1}{T0})] \quad (6)$$

In this equation, H_T and H_{T0} are the Henry's constants at temperatures T and T_0 (in Kelvin), respectively. ΔH_{sol} [J·mol^{-1}] is the enthalpy of dissolution, and R is the universal gas constant [J·mol^{-1}·K^{-1}]. For the purpose of calculations, a reasonable assumption was made, that the effect of medium ionic strength on Henry's constant was negligible, as the variations are typically minor for standard cell culture media. This meticulous approach allowed for an accurate determination of oxygen transfer efficiency in the system, providing a crucial parameter for the computational models.

4.1.4. Oxygen Uptake Rate Determination

To precisely and reliably quantify the Oxygen Uptake Rate (OUR) of the engineered 3D constructs, a key parameter for the computational model, a specialized experimental setup was designed. The primary objective was to isolate the effects of cellular oxygen consumption from other mass transfer phenomena, particularly the complexities associated with the gas-liquid interface. To achieve this, this interface was deliberately eliminated by completely filling the culture plates with medium, ensuring no air bubbles remained. This approach created a closed system where the only source of oxygen loss was cellular consumption, thereby simplifying the mathematical model and allowing for a direct measurement of OUR.

In this sealed environment, where there is no transfer of oxygen from the surrounding air, the governing equation for oxygen mass transfer in the medium, which was initially presented as Equation (4), is significantly simplified. The oxygen concentration in the liquid (c_l) changes solely as a result of cellular consumption, leading to the following streamlined relationship. This rate of consumption, OUR, is a function of both the specific oxygen consumption rate (q_{O2}) of a single cell [mol·cells^{-1}·h^{-1}] and the total cell density (N) of the construct [cells·L^{-1}]. Therefore, the equation can be further expressed as:

$$\frac{dc_l}{dt} = -OUR \xrightarrow{OUR=N.q_{O2}} \frac{dc_l}{dt} = -N.q_{O2} \quad (7)$$

To conduct the measurements, 3D constructs, which had been fabricated in various culture plates according to the established protocol, were carefully transferred to an SDR OxoDish plate. To maintain the airtight conditions essential for the experiment, the lid of the dish was meticulously sealed using a combination of grease oil and Parafilm. This created a hermetic seal that prevented any ingress of atmospheric oxygen. Real-time oxygen concentration within this closed system was then monitored continuously at 15-second intervals. By tracking the linear decrease in oxygen concentration over time, the OUR was directly calculated and, by extension, the specific oxygen consumption rate per cell, providing a critical parameter for validating and informing the computational models.

4.1.5. Effective Oxygen Diffusion Coefficient

To determine the effective oxygen diffusion coefficient (D_{eff}), a key parameter in the model that quantifies the rate of oxygen transport through the dense cellular matrix, the experiments were operated under a steady-state condition. This assumption is crucial as it simplifies the governing equation by eliminating the time-dependent term ($\frac{\partial c_s}{\partial t}$). The justification for this simplification stems from the biological state of the engineered tissues. The experimental measurements were conducted long after the differentiation phase had concluded, a point at which cell proliferation had ceased and the number of cells within the construct had stabilized. Under these conditions, the oxygen consumption rate could be considered constant over time.

In this steady-state scenario, the one-dimensional governing equation for oxygen mass transfer in the solid phase (Equation 3) is reduced to a simplified ordinary differential equation that can be solved analytically. The resulting expression describes the spatial oxygen profile within the construct and is a second-order polynomial with the coordinate origin at the construct's center point:

$$D_{eff.}\frac{\partial^2 c_s}{\partial z^2} = OUR \rightarrow c_s = \frac{OUR}{2D_{eff.}}z^2 + c_{s.min} \quad (8)$$

In this simplified model, $c_{s.min}$ represents the minimum oxygen concentration found at the construct's center along its vertical axis. By fitting the experimentally measured oxygen concentration data against the vertical displacement (z) to this second-order polynomial equation, the effective oxygen diffusion coefficient (D_{eff}) for the 3D constructs could be precisely calculated.

To obtain the necessary experimental data for this calculation—specifically, the oxygen profile along the vertical axis—a highly sensitive TX3 needle-based oxygen sensor (PreSens Precision Sensing GmbH, Germany) was utilized. The needle-sensor was rigidly connected to a syringe pump, which was programmed to move at a very slow and controlled speed of 44.2 µm/s. This exceptionally low speed was vital for ensuring the sensor moved smoothly through the delicate tissue without causing significant disruption and for enabling accurate spatial mapping of the oxygen gradient. Oxygen concentration readings were recorded every second, and with the known movement speed, each oxygen measurement could precisely get correlated with its specific location within the construct. This meticulous procedure was performed on multiple 3D constructs cultured in various plate sizes, including 12-well plates, 35 mm petri dishes, 60 mm petri dishes, and 100 mm petri dishes. The application of this method across different scales ensured that the results were both robust and reproducible, providing a reliable dataset for the calculation of D_{eff}.

4.1.6. Computational Model Validation

To ensure the reliability and predictive power of the computational model, a rigorous validation process was undertaken by directly comparing its outputs with experimentally measured data. The core of this validation focused on a critical parameter for cell survival: the minimum oxygen concentration at the core of the 3D constructs. This value is particularly important because the central region is the most vulnerable to oxygen starvation and, consequently, cellular necrosis. Therefore, a model that can accurately predict oxygen levels in this most challenging area is considered highly robust and trustworthy.

The validation was performed by comparing the minimum oxygen concentration measured at the geometric center of the 3D constructs with the corresponding value generated by the finite element simulations. This direct, quantitative comparison provided a robust confirmation of the model's accuracy. By demonstrating that the computational predictions aligned closely with the empirical observations, the model's reliability in accurately predicting oxygen distribution within the engineered tissues under physiological conditions was confirmed. This validation step is fundamental, as it provides confidence that the model can be used to accurately simulate oxygen dynamics and inform future design strategies aimed at preventing hypoxia and improving cell viability in larger, more complex tissue constructs.

4.1.7. Statistical and Data Analysis

To ensure the statistical robustness and reliability of the findings, all experiments were meticulously conducted in triplicate, unless a different number of repetitions was explicitly noted. This commitment to replication is a cornerstone of rigorous scientific inquiry, as it accounts for inherent biological variability and strengthens the confidence in the conclusions.

For the quantitative analysis of the data and the estimation of key model parameters, a series of advanced analytical techniques were employed. Regression analysis, a powerful statistical tool, was performed using MATLAB (MathWorks). This method allowed the study to systematically identify and quantify the mathematical relationships between key variables, thereby providing profound insights into the underlying biological and physical patterns governing the system. The use of MATLAB's computational capabilities facilitated the efficient processing of large datasets and the precise estimation of model coefficients.

Furthermore, curve fitting techniques were utilized to accurately model and describe the observed experimental data. By fitting the empirical measurements to the proposed mathematical models, the parameter values were optimized, such as the effective diffusion coefficient and oxygen uptake rate, ensuring that the models accurately reflected the real-world behavior of the engineered constructs. This combination of experimental replication and sophisticated data analysis was essential for building a reliable and predictive computational framework.

4.2. Results

The central objective of this computational study was to precisely determine the upper critical size limit for the scaffold-free, three-dimensional (3D) muscle constructs. Identifying this threshold is of paramount importance, as it represents the point at which the constructs' size exceeds the capacity of passive oxygen diffusion from the surrounding culture medium. Beyond this limit, the transport of oxygen to the inner core of the tissue becomes insufficient, leading to a state of hypoxia or even anoxia, which would inevitably compromise cellular viability and functional integrity.

To facilitate the simulation and create a more tractable model, it was first needed to accurately characterize the geometry of the constructs. Through meticulous observation, it was noted that the detached cell sheets naturally curled into a consistent, semi-cylindrical shape. This observation provided the basis for a key simplification in the computational design. To establish a universal relationship between the constructs' dimensions that could be applied across

different culture formats, a systematic analysis was performed. The dimensions of 20 individual constructs derived from a variety of culture vessels were carefully measured, including 12-well plates, 35 mm Petri dishes, 60 mm Petri dishes, and 100 mm Petri dishes.

These direct size measurements, performed using ImageJ software to ensure accuracy and reproducibility, allowed allowed the establishment of a reliable and consistent dimensional relationship. The analysis revealed a consistent ratio of thickness to height, which was determined to be 2.38 ± 0.18. This empirically derived parameter provided the foundation for the geometric approximation in the computational model, enabling accurate simulation of oxygen dynamics with high fidelity. The following results section will detail the findings, which shed light on the physical limitations of these engineered tissues and provide crucial insights for future efforts in scaling up production.

4.2.1. Porosity and Cellular Density

The structural integrity and transport properties of engineered tissues are fundamentally dictated by their porosity, which is the proportion of void space within the construct. In scaffold-based systems, this is primarily determined by the scaffold's architecture. However, in these unique scaffold-free constructs, porosity is a direct manifestation of the cells' ability to self-organize and secrete their own extracellular matrix (ECM). Consequently, the definition of porosity here refers specifically to the void space left unoccupied by the densely packed cells and their surrounding ECM.

To quantitatively assess this critical parameter, micro-computed tomography (μ-CT) was utilized, a powerful imaging modality that allowed for non-invasive, high-resolution 3D analysis. Three representative samples, derived from 35 mm, 60 mm, and 100 mm Petri dishes, were meticulously prepared for scanning. The samples were first stained with a iodine potassium iodide (I_2KI) solution, which served to enhance the contrast between the tissue (stained) and the void spaces (unstained), thereby facilitating accurate segmentation. From each sample's reconstructed μ-CT scan, 50 distinct cross-sectional slices were analyzed using ImageJ software. Then the ratio of the void area (appearing as dark regions) to the total cross-sectional area was calculated. The average porosity across all samples was determined to be 11.95 ± 2.82%. This exceptionally low value is a striking indicator of the constructs' highly compact nature, with minimal open space between the cells.

To gain a deeper understanding of the constructs' composition, the cell density (N) within the tissue was quantified. For this, a total of twelve samples in various dish sizes were cultured, including 24-well plates, 12-well plates, 35 mm Petri dishes, 60 mm Petri dishes, and 100 mm Petri dishes. After five days of culture, the thickness of each construct was measured through image analysis. Following this, the tissues were carefully digested with trypsin, a process that released the individual cells into a suspension, which were then counted. By integrating the total cell count with the previously measured structural dimensions, the cell density for each sample was precisely estimated, with the results visually presented in Figure 11b.

The results revealed an exceptionally high cell density that, remarkably, remained largely consistent across all construct thicknesses. This finding is perfectly aligned with the low porosity measurements and further underscores the tightly packed cellular arrangement within the scaffold-free system. These structural characteristics are a powerful testament to the self-organizing capabilities of the C2C12 cells, which rely solely on their intrinsic biological properties and ECM secretion to build and maintain their cohesive 3D architecture. Overall, this comprehensive computational and experimental analysis provides crucial insights into the structural constraints and unique self-assembly properties of the engineered tissues, which is a key step towards understanding their limitations for future tissue engineering applications.

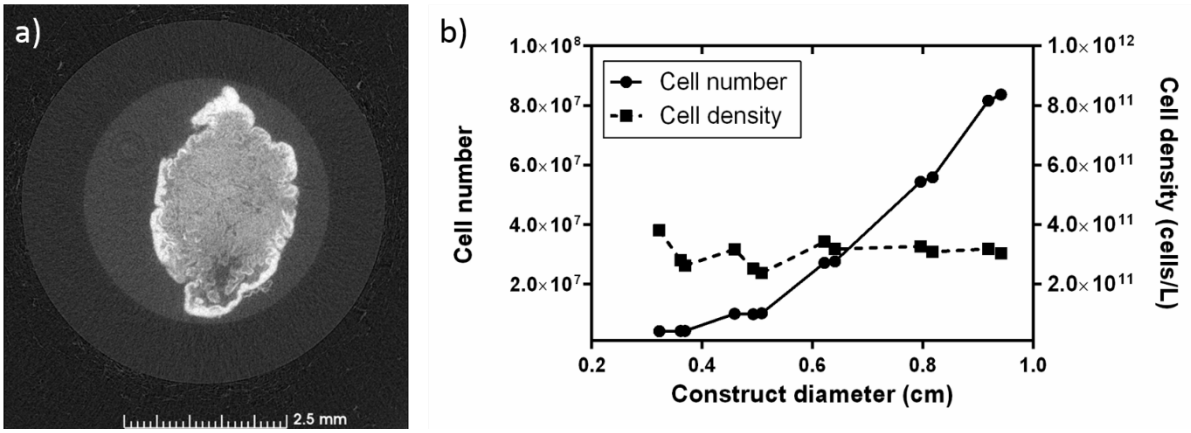

Figure 11 - 3D constructs characterization a) μ-CT scanning image of a 3D construct (dark areas within the construct represent voids) b) cell number and cell density at 5th day of culture relative to the construct thickness

4.2.2. Volumetric Mass Transfer Coefficient (k_La)

To precisely quantify the efficiency of oxygen transfer from the gas phase into the cell culture medium, the volumetric mass transfer coefficient (k_La) was determined. This parameter is a cornerstone of bioprocess engineering, as it represents the rate at which oxygen dissolves into a liquid, a process essential for supplying cells with the oxygen required for metabolism. To isolate this specific phenomenon from the confounding effects of cellular respiration, a targeted

experiment using a cell-free medium was designed. This approach allowed the study to exclusively focus on the physical dynamics of oxygen diffusion at the gas-liquid interface, ensuring that any changes in oxygen concentration were solely attributable to mass transfer.

The experiment was initiated by introducing a pre-warmed medium (37°C) into an SDR OxoDish OD24 plate. To establish a well-defined starting point for the measurements, the medium was first equilibrated in a 50% hypoxic environment for several hours. This critical step reduced the initial dissolved oxygen concentration, providing a clear oxygen deficit that allowed the subsequent re-oxygenation kinetics to be observed with high accuracy. The oxygen concentration was then continuously monitored in real-time at 15-second intervals for a duration of up to 3 hours, providing a rich dataset of oxygen transfer dynamics.

As oxygen transfer in a medium without cells follows a simplified mass balance equation, the experimental data were fitted to Equation 5 (as described in the methods section). To accurately determine the equilibrium oxygen concentration (C^*) in the liquid, a temperature-dependent Henry's law was applied. This involved using the Van't Hoff extrapolation to account for the effect of temperature on oxygen solubility. The resulting experimental oxygen concentration data were then fit to the theoretical model using MATLAB's curve fitting tool. This rigorous fitting process yielded a highly precise k_La value of 0.0022 ± 0.0004 s^{-1}. An example of the excellent agreement between the experimental data and the theoretical model's fitted curve is visually presented in Figure 12. This confirmed the reliability of the model and provided a crucial parameter for all subsequent oxygen simulation studies.

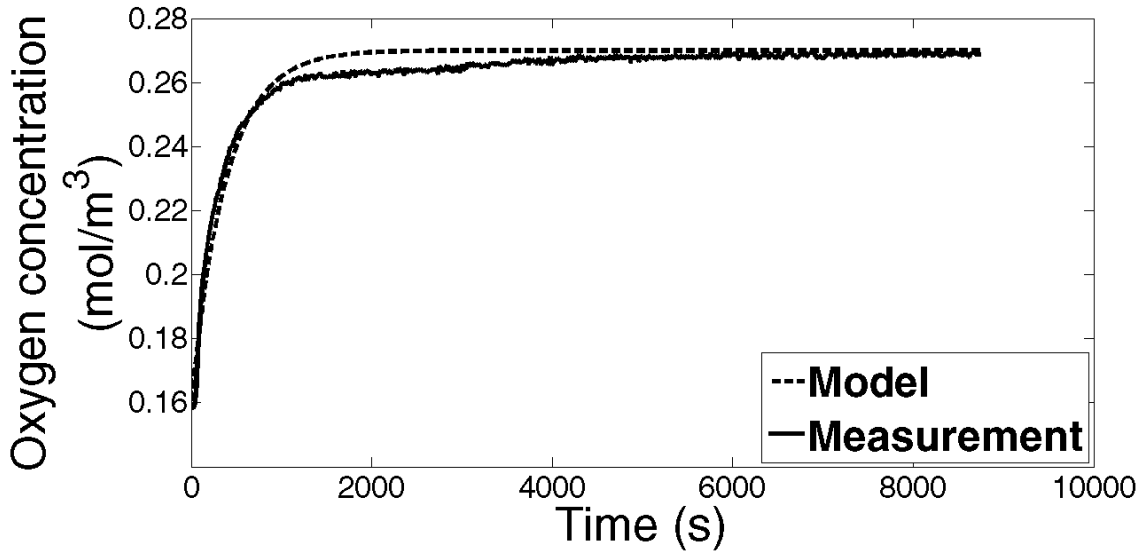

Figure 12 - Fitting experimental data to equation (5) to calculate the K_La value

4.2.3. Oxygen Uptake Rate Determination

To rigorously quantify the metabolic activity of the engineered muscle constructs, it was focused on determining their Oxygen Uptake Rate (OUR). This parameter is a direct measure of the rate at which cells consume oxygen for respiration, providing a vital insight into their metabolic health and functional state within the dense, three-dimensional (3D) environment.

For this evaluation, a total of twelve 3D constructs were meticulously prepared following the established protocol. These constructs, which had been initially formed in 35 mm, 60 mm, or 100 mm Petri dishes to represent different scales, were carefully transferred to an SDR OxoDish OD24 plate. The primary goal of this setup was to create a closed system where oxygen transfer occurred exclusively within the medium and the constructs themselves. This was achieved by completely filling each well with culture media, leaving no air bubbles. By deliberately eliminating the gas-liquid interface, the system was simplified and it was ensured that the measured changes in oxygen concentration were solely due to cellular consumption, thereby isolating this key variable from the complexities of external oxygen exchange.

To further guarantee a truly airtight environment, the lid of the SDR plate was carefully sealed using a combination of grease oil and Parafilm. This meticulous sealing process prevented any external air infiltration, maintaining the integrity of the closed system throughout the measurement period. Oxygen concentration was then continuously and non-invasively monitored in real-time at 15-second intervals. This high-frequency data collection provided a detailed profile of the oxygen depletion curve within the medium.

The collected data were then subjected to rigorous analysis by fitting them to the governing equation for oxygen mass transfer in a closed system (Equation 7), as previously described in the methods section. According to this model, the slope of the linear decrease in oxygen concentration over time directly corresponds to the OUR. The collective results from the twelve constructs yielded an average OUR of $2.08\times10^{-6} \pm 2.18\times10^{-7}$ $mol\cdot L^{-1}\cdot h^{-1}$.By integrating this volumetric OUR value with the previously determined cell density (N) within the constructs, the specific oxygen consumption rate (q_{O2}) could be calculated. This value, which represents the oxygen consumption of a single cell, was found to be $2.02\times10^{-21} \pm 1.42\times10^{-22}$ $mol\cdot cell^{-1}\cdot s^{-1}$. This specific rate provides a standardized metric of metabolic activity, allowing for a more direct comparison with other cell types and tissue models. This detailed quantitative analysis of oxygen consumption is crucial for understanding the metabolic demands of the engineered tissues and for informing future strategies to scale up production while maintaining cellular health.

4.2.4. Oxygen Diffusion Coefficient and Critical Size Limitation

To thoroughly evaluate and quantify oxygen transport within the three-dimensional (3D) muscle constructs, the oxygen concentration profiles along their vertical axis was directly measured. This intricate procedure was performed using a highly sensitive TX3 needle-based oxygen sensor (PreSens Precision Sensing GmbH, Germany). The sensor was precisely controlled by a syringe pump, which allowed it to move downward through the construct's center at an exact and very slow speed of 44.2µm/s. This controlled movement was critical for ensuring accurate spatial mapping of oxygen distribution without causing significant disruption to the delicate tissue. Oxygen concentration data were recorded every second, allowing each measurement to be precisely correlated with its specific depth. This method was applied to multiple constructs cultured in various plate sizes, including 12-well plates, 35 mm, 60 mm, and 100 mm Petri dishes, which provided a comprehensive and robust dataset for analysis.

To determine the effective oxygen diffusion coefficient (D_{eff}), a scientifically sound assumption of a steady-state oxygen transport condition was made. This implies that the oxygen distribution within the tissue had reached a stable equilibrium, with the rate of oxygen supply from the surrounding medium balancing the rate of cellular consumption. This assumption was justified, as the measurements were conducted well after the differentiation phase had concluded, a time when cell proliferation had ceased and the cellular population within the construct was stable. Under these conditions, the time-dependent term in the governing equation could be neglected, simplifying the model to a second-order polynomial (Equation 8). By fitting the experimentally obtained oxygen concentration profiles to this simplified equation, the average D_{eff} value for the 3D constructs was calculated, which was determined to be $1.397\times10^{-11}\pm1.755\times10^{-13}$ $m^2\cdot s^{-1}$.With this experimentally derived parameter in hand, it was proceeded to a powerful computational simulation in COMSOL Multiphysics. The simulation incorporated the experimentally determined parameters, including the volumetric mass transfer coefficient (k_La), the C2C12 oxygen uptake rate (OUR), and the effective diffusion coefficient (D_{eff}). A key feature of the computational approach was the use of a parametric sweep function that systematically varied the construct thickness from 0.1 cm to 1 cm in increments of 0.05 cm. At each simulated thickness, the model calculated the oxygen concentration at the construct's core, a critical point for cell survival. The role of construct porosity was not included as a separate variable in the simulations because its impact on oxygen diffusion was already inherently accounted for within the experimentally determined D_{eff} value.

The results of the simulation were then rigorously cross-validated with the experimental data, as shown in Figure 13a, which compares the predicted oxygen concentrations with the empirical measurements. The model revealed a critical finding: the construct thickness should not exceed 5 mm. Beyond this crucial threshold, the oxygen concentration at the core is predicted to drop to zero, an outcome that would lead to widespread cellular necrosis and a complete loss of tissue function. This result underscores the fundamental importance of controlling construct dimensions to ensure an adequate and continuous oxygen supply. The simulation also provided a more nuanced perspective on oxygen distribution. As construct thickness increased, the oxygen concentration variations along the vertical axis became more pronounced. For example, at a thickness of 0.1 cm, the fluctuation in oxygen saturation remained around a very low 5%, suggesting that smaller constructs offer a more stable and uniform oxygen profile. This finding is particularly relevant for future applications, emphasizing that maintaining a very small construct size and carefully regulating dissolved oxygen levels can lead to a more consistent and healthier microenvironment for the engineered tissue.

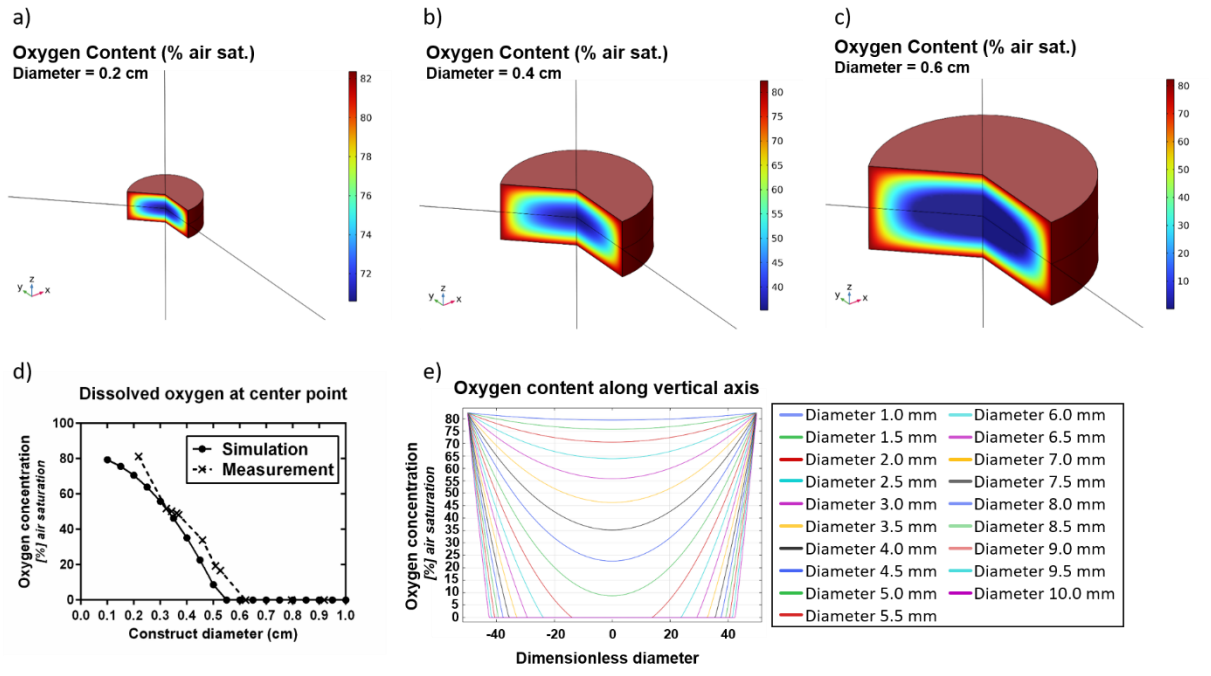

Figure 13 - Effect of Construct Size on Oxygen Concentration Profiles: Insights from 3D Computer Simulation a, b, c) Surface graphs of oxygen concentration in 3D constructs when immersed in media, at thickness 0.2, 0.4, or 0.6 cm d) Validation of computer simulation with experimental data, representing oxygen concentration at construct center point by increasing construct size e) Exploring oxygen content along the vertical axis of constructs at varying thicknesses.

The dramatic relationship between construct thickness and oxygen concentration is further illustrated in the surface plots shown in Figures 13c, 13d, and 13e. These visuals clearly depict a sharp decline in oxygen concentration as thickness increases. This trend is a direct result of

two key factors: the increasing diffusion distance, which slows oxygen transport to the core, and the rising total cellular oxygen consumption within the larger volume of tissue.

The overall correlation between the experimental data and the simulation results was exceptionally strong, achieving a coefficient of determination (R^2) of 0.87. This high value provides a robust validation of the computational model, demonstrating its accuracy and reliability despite the inherent complexities and uncertainties present in any biological system. This successful integration of experimental and computational methods provides a powerful framework for designing scalable and viable engineered muscle tissues.

4.3. Chapter Discussion

The findings presented in this chapter represent a crucial intersection of computational modeling and experimental analysis, providing a definitive answer to a fundamental question in the field: what is the maximum viable size for these specific scaffold-free 3D constructs? The integrated approach here successfully demonstrates a critical size limitation, one primarily dictated by the physical barriers to oxygen transfer. The computational model, meticulously built upon the experimental data, predicts a clear and non-negotiable threshold: the construct's thickness should not exceed 5 mm. Beyond this point, the oxygen concentration at the core is predicted to fall below the levels required to sustain cellular life, leading to the formation of a necrotic core.

This result stands out from general literature findings because it is rooted in parameters specifically tailored to the biological system. System-specific diffusion-related parameters, including the effective diffusion coefficient (D_{eff}) and the oxygen uptake rate (OUR), were experimentally measured and integrated. The excellent coefficient of determination (R^2=0.87) between the simulation outputs and the empirical data provides strong validation for the model's accuracy and predictive power.

A key factor contributing to this size limitation is the unique microstructure of the tissues. The constructs exhibit an exceptionally low porosity of 11.95 ± 2.82% and a remarkably high cell density. This dense cellular packing, a hallmark of the scaffold-free fabrication method, results in a high volumetric oxygen demand (OUR). This high consumption, coupled with the slow diffusion of oxygen through the compact tissue, creates a steep oxygen gradient from the surface to the core. This observation is in perfect agreement with other studies that have identified oxygen consumption as a primary driver of necrotic core formation in dense cell aggregates [2,73].

The implications of these results for the scalability of this specific tissue type are profound and far-reaching. The 5 mm threshold provides a concrete and invaluable design parameter for future efforts in cultivated meat or other tissue engineering applications. It makes it clear that to produce viable tissues of a larger size, one cannot rely solely on passive diffusion. Instead, future work must focus on developing innovative strategies to actively overcome these diffusion barriers. Potential solutions, which have been explored in other tissue engineering contexts, include the integration of microfluidic channels to mimic a vascular network or the incorporation of oxygen-releasing biomaterials.

A recognized limitation of this study was the simplification of the governing equations to a one-dimensional model for the calculation of key parameters. While this approach was a practical necessity due to the experimental constraints, it inherently assumes radial uniformity, which may not fully capture the spatial heterogeneity of oxygen transfer. However, the use of a more complex 2D COMSOL simulation and its successful cross-validation with experimental data significantly mitigated these concerns, providing high confidence in the overall accuracy and utility of the model. In conclusion, this study underscores the critical importance of integrating sophisticated computational modeling with rigorous experimental validation. This powerful symbiotic relationship is essential for optimizing construct design and ensuring long-term cellular survival and function in the challenging environment of engineered 3D tissues.

5. Chapter Five: Study III - Myoglobin Regulation

Achieving the characteristic appearance and taste of conventional meat remains a significant challenge in cultivated meat production. The distinctive red color of skeletal muscle is primarily attributed to myoglobin, a heme-protein that also plays a crucial role in oxygen storage and transport within muscle fibers. Consequently, regulating myoglobin synthesis is a critical step towards creating a consumer-acceptable cultivated meat product. While myoglobin synthesis is known to be influenced by factors such as oxygen availability and mechanical loading, the specific interplay of these cues within dense, scaffold-free tissue constructs has not been fully explored.

This study details a comprehensive investigation of factors influencing myoglobin synthesis in the engineered skeletal muscle constructs. The effects of both biochemical and physical parameters were systematically evaluated. This work explores the influence of specific nutrient supplementation (iron, IGF-I, and creatine), and importantly, the impact of the physical culture environment, including culture vessel size, dissolved oxygen (DO) levels, and mechanical stimulation. The following sections outline the detailed experimental protocols, from cell culture and construct fabrication to myoglobin quantification and complementary analyses, all aimed at identifying the key regulators of this essential protein. The goal of this research is to provide a rational design framework for optimizing functional, aesthetically pleasing, and physiologically relevant muscle tissue for cultivated meat applications.

5.1. Materials and Methods

5.1.1. Inducing Pigmentation

To create a cultivated meat product that is both aesthetically and physiologically similar to conventional meat, it is essential to replicate its characteristic red color. This color is primarily attributed to myoglobin, an intracellular heme-protein found in high abundance in skeletal muscle. Myoglobin's central role is to facilitate the diffusion of oxygen from the cell membrane to the mitochondria, where it is utilized for aerobic respiration. Structurally, myoglobin consists of a single polypeptide chain, known as globin, and a non-protein component called a heme group [74]. The heme group is crucial for its function as it contains a single iron atom (Fe^{2+}) at its core. Given this fundamental structural component, it was hypothesized that increasing the

availability of iron to the cells would serve as a key strategy to potentially upregulate myoglobin synthesis.

To investigate this hypothesis, a set of experiments were designed to test the effect of iron supplementation on myoglobin production in the C2C12 cell constructs. Iron was introduced into the culture medium in the form of ferrous sulfate ($FeSO_4$), a source of bioavailable Fe^{2+} ions. To determine the optimal timing for this supplementation, two distinct experimental groups were established. The first group received iron supplementation from the beginning of the culture, specifically from day 0, while the second group received the iron starting on day 3, immediately following the spontaneous cell sheet delamination. The applied iron concentration was meticulously selected to be 170 µg/dL, which corresponds to 0.011 mM. This concentration was chosen as a physiologically relevant upper limit, mirroring the highest free iron concentration found in human blood serum [57]. The impact of this supplementation was then analyzed through both visual observation and quantitative analysis of the constructs' coloration. The specific experimental groups and their defining characteristics are summarized in Table 1 below.

Table 1 - Study groups to determine the time point to add iron

Study groups	Iron concentration		Starting point for iron addition
	µg/dL	mM	
N	0	0	N/A
d0	170	0.011	Day 0
d3	170	0.011	Day 3 (after delamination)

To determine the optimal iron concentration for myoglobin synthesis, a dose-response study was conducted, systematically investigating a wide range of values. The concentration of 170 µg/dL, representing the highest free iron ion concentration typically found in human blood, was established as the baseline and designated as the 1X concentration. From this reference point, a series of increasing concentrations up to 128X was created, allowing a meticulous evaluation of the effects of both physiological and supraphysiological iron levels on the constructs. This broad range was crucial for identifying a potential saturation point or a level at which iron becomes toxic to the cells.

For each of the defined concentration groups, a total of five 35 mm Petri dishes were used to prepare the cell sheets. Following the established protocol for delamination, the five individual sheets from each group were carefully stacked together to form a cohesive, three-dimensional construct. These newly formed 3D constructs were then cultured in an incubator for a duration

of up to 7 days, during which myoglobin synthesis and other cellular processes were expected to take place. The specific iron concentrations investigated in this part of the study are summarized in Table 2 below, providing a clear overview of the experimental design.

Table 2 - Iron concentrations studied

Study groups	Iron concentration	
	µg/dL	mM
N	0	0
1X	170	0.011
2X	340	0.022
4X	680	0.045
8X	1360	0.090
16X	2720	0.179
32X	5440	0.358
64X	10880	0.716
128X	21760	1.432

To ensure that the iron concentrations used in the myoglobin induction experiments did not have a detrimental effect on cellular health, a quantitative assessment of reactive oxygen species (ROS) levels was performed. ROS are highly reactive metabolic by-products, such as hydrogen peroxide (H_2O_2), that can generate harmful free radicals in the presence of transition metals like iron. This process is most notably described by Fenton's reaction, a chemical cascade that cycles between ferrous (Fe^{2+}) and ferric (Fe^{3+}) iron to produce highly damaging hydroxyl radicals (·OH) [75].

The two key steps of this reaction are:

$$\begin{aligned} Fe^{2+} + H_2O_2 &\rightarrow Fe^{3+} + \cdot OH + OH^- \\ Fe^{3+} + H_2O_2 &\rightarrow Fe^{2+} + H_2O \cdot + H^+ \end{aligned} \quad (5)$$

When the formation of these free radicals outpaces the cell's natural antioxidant defenses, it leads to a state of oxidative stress, which can cause significant cellular damage, lipid peroxidation, and ultimately, programmed cell death (apoptosis) [76].

To confirm that the iron supplementation did not induce these harmful effects, intracellular ROS levels were measured using the dichlorodihydrofluorescein diacetate (DCFH-DA) assay. This assay is a well-established method for quantifying general oxidative stress. The non-fluorescent DCFH-DA probe readily enters the cell, where it is deacetylated by intracellular esterases to form DCFH. In the presence of ROS, DCFH is oxidized to the highly fluorescent compound dichlorodihydrofluorescein (DCF), which can be measured with a microplate reader.

To further investigate the interplay between iron-induced ROS and cellular protection, the role of a potent antioxidant, ascorbic acid (vitamin C), was also explored. Ascorbic acid acts as a reducing agent, which can help to scavenge free radicals and prevent oxidative stress. The effect of ascorbic acid at a range of concentrations, 10, 100, 500, and 1000 μM, was tested to determine its efficacy in mitigating any potential iron-induced oxidative damage. All ROS results were normalized to the cell number, which was determined using the Neutral Red Uptake (NRU) assay. This normalization was crucial for ensuring that the measurements of oxidative stress were a true reflection of the cells' metabolic state, independent of variations in cell count between samples.

Culture vessel size. To investigate the potential influence of physical confinement and cell sheet dimensions on myoglobin content, an experiment was designed that leveraged the scaffold-free fabrication protocol. It was hypothesized that the initial size of the culture vessel, which dictates the surface area available for cell growth and sheet formation, could impact the constructs' subsequent myoglobin expression. To test this, C2C12 cell sheets were produced across a range of different culture vessel types: 24-well plates, 12-well plates, 35 mm Petri dishes, and 60 mm Petri dishes. For this specific analysis, single, unstacked sheets were analyzed to isolate the effect of the initial culture dimensions. Myoglobin content within these single sheets was then meticulously quantified using a highly sensitive myoglobin ELISA kit, providing a precise measure of protein concentration. This approach allowed the correlation between the physical dimensions of the cell sheet and its myoglobin-producing capacity to be established.

IGF-I. Recognizing that Insulin-like Growth Factor-I (IGF-I) is a well-documented promoter of both protein synthesis and myogenesis [39,40], it was sought to determine its specific role in regulating myoglobin synthesis. It was hypothesized that by stimulating muscle cell growth and differentiation, IGF-I would indirectly lead to an increase in myoglobin production. To test this, C2C12 cells were cultured in 12-well plates following the established protocol. Once the differentiation phase began, the cells were treated with a range of IGF-I concentrations, specifically 20, 100, and 500 ng/mL, which were supplemented to the differentiation medium. Following the maturation period, the myoglobin content was rigorously measured in all samples using a myoglobin ELISA kit. This experiment provided quantitative data to either support or refute the hypothesis regarding IGF-I's influence on myoglobin levels.

Creatin. Creatine is an amino acid derivative known to play a vital role in cellular energy metabolism and has been shown to enhance myogenic differentiation and increase the

expression of key growth factors like IGF-I [43]. This evidence led to the hypothesis that creatine supplementation could indirectly upregulate myoglobin synthesis. To investigate this, C2C12 cells were cultivated in 12-well plates using the established protocol. Creatine was then introduced into the differentiation medium at concentrations of 5, 10, and 15 mM. After a period of culture, the myoglobin content of the constructs was meticulously quantified using a myoglobin ELISA kit. This approach allowed the specific impact of creatine supplementation on myoglobin protein levels to be examined, providing valuable insight into its potential as a nutritional additive for cultivated meat production.

DO. To rigorously assess the impact of oxygen concentration on myoglobin synthesis, a multi-pronged experimental approach was pursued, employing both static and dynamic culture systems. This was crucial because myoglobin, a key oxygen-binding protein, is known to be upregulated in low-oxygen environments.

The initial investigation utilized a CO_2 incubator equipped with gas sensors, allowing for precise atmospheric control. The oxygen level was set to a 1% hypoxic environment by continuously injecting nitrogen gas, a stark contrast to the standard atmospheric concentration of 21%. C2C12 myoblasts were seeded into 12-well plates, and the cell sheets were cultivated following the established protocol. Following their spontaneous delamination on day 3, the constructs were immediately transferred back into the same hypoxic incubator for an additional four days of culture, until day 7. To establish a baseline for comparison, a parallel control experiment was conducted in a standard incubator under normoxic conditions (21% O_2). Myoglobin concentrations in both groups were measured at both day 3 and day 7 to capture the temporal effects of the different oxygen regimes.

While a static incubator can control atmospheric oxygen levels, it does not account for the complexities of diffusion within the liquid medium and the 3D constructs themselves. To precisely control the dissolved oxygen (DO) and simulate a more physiologically relevant environment, A DASGIP bioreactor system was employed. This advanced system allowed for the precise regulation and real-time monitoring of key parameters, including DO, pH, and temperature, in an agitated environment.

The introduction of agitation, however, posed a challenge to the established scaffold-free protocol, which relies on a static culture to facilitate spontaneous sheet delamination and 3D construct formation. To overcome this, a hybrid culture approach was adopted. Cell sheets were first produced in 35 mm Petri dishes under standard static conditions until day 3. After

delamination, the sheets were left to self-assemble for an additional 24 hours to form a stable 3D construct. These nascent constructs were then carefully transferred to the DASGIP bioreactor on day 4 to begin the dynamic culture phase, which continued for three days until day 7. This hybrid approach allowed the combination of the advantages of the static fabrication method with the precise control offered by the bioreactor.

Within the bioreactor, a wide range of oxygen levels by maintaining the DO at 2%, 5%, 30%, 50%, or 100% air saturation was investigated. Additionally, to simulate the effect of physical activity and its associated metabolic fluctuations, a variable DO regime was implemented. In this setup, the DO was made to oscillate sinusoidally between a low of 10% and a high of 50% saturation, with each cycle lasting four hours. The temperature for all experiments was maintained at a physiological 37°C, and the pH was regulated at 7.2. Upon completion of the culture period, the myoglobin content of all constructs was quantified using a specialized myoglobin ELISA kit, allowing for a direct comparison of the effects of different oxygenation strategies.

Mechanical Stretching. To more accurately simulate the physiological conditions of muscle activity and to investigate the direct impact of mechanical loading on myoglobin synthesis, a cyclic mechanical stretching regimen was applied to the engineered cell sheets. This approach aimed to replicate the strain experienced by muscle tissue during exercise. The C2C12 cell sheets were first cultured in 100 mm Petri dishes and then non-enzymatically delaminated on day 3, following the standard protocol.

The detached, cohesive sheets were then carefully transferred and rolled around a silicone tube, which served as a flexible scaffold for the stretching system. This tube was aseptically incorporated into an innovative, custom-built mechanical stretching system situated within a DASGIP bioreactor vessel. The system was designed to provide controlled, reproducible strain. One end of the silicone carrying tube was securely fixed to the bottom of the vessel, anchoring it in place. The other end was attached to a silicone diaphragm, which was connected to an external syringe pump via sterile tubing.

The rhythmic back-and-forth motion of the syringe pump generated controlled tension on the elastic silicone tube, subjecting the wrapped cell sheet to cyclical stretching. The stretching cycle consisted of three distinct phases: a 135-second stretching phase, followed by a 30-second pause at maximum stretch, and a 60-second pause at rest. The total displacement at the

maximum stretch point was precisely set to 1 mm. A schematic representation of this innovative stretching system is provided in Figure 14.

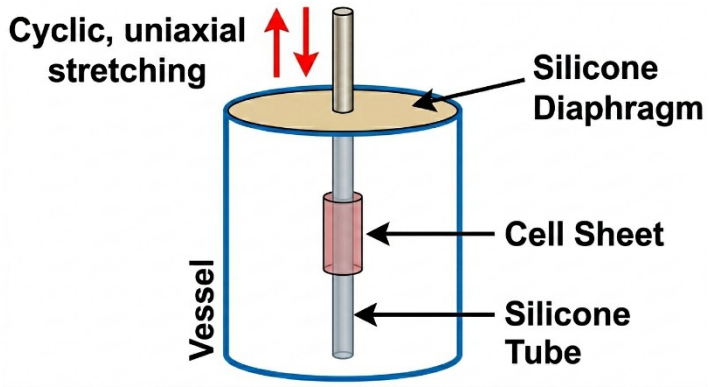

Figure 14 – Schematic representation of the mechanical stretching system

To ensure the cell sheets remained securely attached to the carrying tubes and to protect them from the shear stress induced by the bioreactor's agitator, two distinct methods of fixation were employed:

Alginate Coating Method. After the cell sheet was wrapped around the silicone tube, the entire construct was dipped into a 3% alginate solution for 10 seconds.

The construct was then immediately immersed in a calcium chloride ($CaCl_2$) solution for 30 seconds. This step triggered the ionic cross-linking of the alginate, forming a thin, hydrogel layer that provided a protective coating and securely fastened the cell sheet to the tube without causing cellular damage.

Fibrin Glue Method. Once the sheet was wrapped around the carrying tube, a solution of human fibrinogen was carefully applied to the exterior of the construct.

Immediately following this, a solution of human thrombin was added. Thrombin acted as an enzyme, catalyzing the conversion of fibrinogen into fibrin glue, a robust, biologically compatible adhesive that secured the cell sheet to the tube.

Following the fixation process, the carrying tubes were thoroughly washed with phosphate-buffered saline (PBS) to remove any unbound components before being connected to the stretching system. Upon completion of the stretching regimen, the myoglobin content of the constructs was meticulously quantified using a highly sensitive myoglobin ELISA kit, providing a direct measure of the mechanical stretching's effect on muscle protein synthesis.

5.1.2. Image Analysis and Color Quantification

To achieve a quantitative and objective assessment of the color of the engineered muscle constructs, a standardized image acquisition protocol was established. Images were captured under strictly controlled, aseptic conditions to ensure consistency and minimize environmental variables. A Samsung camera (f/1.8, ISO 25, resolution 3468 x 4624) was used, with its position fixed at a precise distance from the sample. Consistent lighting was provided by two 10 W LED lights, which were strategically placed at opposing positions at a 45-degree angle to eliminate shadows and ensure uniform illumination. This careful control of both camera and lighting parameters was fundamental for obtaining reproducible and reliable images for subsequent analysis.

The captured images were then meticulously analyzed using ImageJ software (v1.54g). For color analysis, the CIELAB color space was utilized, a device-independent and perceptually uniform model defined by the International Commission on Illumination (CIE). CIELAB is a cornerstone of color science and is widely employed in various fields for its ability to accurately represent human color perception [77]. The model quantifies color based on three distinct parameters:

- L^* (Lightness): This parameter ranges from 0 to 100, where a value of 0 corresponds to absolute black and 100 represents pure white.
- a^* (Green-Red Axis): This axis spans from -128 to +127. Negative values indicate a shift towards green, while positive values indicate a shift towards red, a crucial parameter for assessing the reddish hue of myoglobin-containing tissue.
- b^* (Blue-Yellow Axis): This parameter also ranges from -128 to +127, with negative values signifying a tendency towards blue and positive values indicating a shift towards yellow.

To compare the color of the constructs to a reference color (such as that of conventional meat), the delta E (ΔE) metric was employed, which provides a single numerical value for the perceived color difference between two colors. This value is calculated based on the differences in the L^*, a^*, and b^* parameters using the following formula:

$$\Delta E = \sqrt{(L_2^* - L_1^*)^2 + (a_2^* - a_1^*)^2 + (b_2^* - b_1^*)^2} \quad [3]$$

The ΔE value provides a clear, quantitative measure of color difference with well-defined perceptual thresholds. A ΔE of less than 1 indicates a color difference that is nearly invisible to the human eye. Values between 1 and 2 are visible to experts, and differences between 2 and

3.5 are visible to most people. A ΔE value between 3.5 and 5 indicates that the colors are distinctly different, while a value greater than 5 signifies an obvious and highly noticeable color difference.

For the analysis, images were imported into ImageJ, and their color space was converted from the standard RGB model to the CIELAB model using the Color-Space-Converter plugin. The regions of interest (the 3D constructs) were then selected using the Threshold tool, allowing for the isolation of the samples from the background. The CIELAB parameter values for these selected areas were then systematically measured and exported to an Excel spreadsheet for further statistical analysis.

5.1.3. Metabolite Analysis

To gain a deeper understanding of the metabolic activity of the engineered cellular constructs, a quantitative analysis of key metabolites in the culture media was performed. The primary focus of this analysis was to measure both glucose consumption and lactate production, as these two metabolites are critical indicators of cellular energy metabolism and overall health. A high rate of glucose consumption coupled with lactate production can suggest a reliance on anaerobic glycolysis, a common metabolic pathway in dense, hypoxic tissues.

To carry out these precise measurements, a YSI 2900 Biochemistry Analyzer (YSI Inc., USA) was used. This instrument is a reliable tool for enzymatic-based analysis of various substrates in biological fluids. Samples of the culture medium were meticulously collected at predetermined time intervals throughout the experiment. For each distinct sample, a high degree of experimental rigor by collecting two separate replicates was ensured. This step was crucial for accounting for any potential variability in the biological samples themselves.

Before each set of measurements, the YSI 2900 analyzer was carefully calibrated using standard buffers to guarantee the accuracy and precision of the readings. Once calibrated, each individual sample was measured in triplicate by the analyzer. This technical replication was a vital step for minimizing measurement error and ensuring the reliability of the data. By analyzing these metabolic profiles, quantitative insights into the cellular activity and metabolic state of the constructs over time, could be obtained.

5.1.4. Colorimetric Assays

Neutral Red Uptake (NRU) Assay. To accurately and quantitatively assess the number of viable cells in the cultures, a Neutral Red Uptake (NRU) assay was performed. This

colorimetric assay is a well-established and reliable method for determining cell viability and proliferation. The principle of the assay is based on the ability of living cells to actively take up and accumulate the supravital dye, neutral red, within their lysosomes. This process depends on a cell's intact cell membrane and its active metabolic state, making the amount of retained dye a direct proxy for the number of viable cells in a sample.

The experimental procedure was initiated by seeding C2C12 cells into 96-well plates at a density of 5×10^4 cells/cm^2. The plates were then incubated for 24 hours at 37°C in a standard CO_2 incubator to allow the cells to adhere and establish a stable monolayer. Following this attachment period, the cells were washed with Phosphate-Buffered Saline (PBS) to remove any residual culture medium and unbound cells.

A pre-warmed NRU working solution was then prepared by diluting a stock solution (0.4% w/v in PBS) to a final concentration of 50 µg/mL. A volume of 100 µL of this working solution was added to each well. The cells were then incubated with the dye for 3 hours at 37°C, a period that allows sufficient time for the viable cells to actively internalize the dye and sequester it within their lysosomes.

After the incubation, the cells were washed again with PBS to remove any excess or unbound dye. To release the internalized neutral red dye from the lysosomes, 100 µL of an extraction solution was added to each well. This solution was composed of 50% ethanol, 49% deionized water, and 1% glacial acetic acid. To ensure complete and uniform dissolution of the dye from the cells into the extraction solution, the plate was gently agitated on a plate shaker for 10 minutes at room temperature. Finally, the absorbance of the extracted dye in each well was measured at a wavelength of 540 nm using a microplate reader (Infinite® 200 PRO, Tecan, Switzerland). The absorbance value is directly proportional to the number of viable cells in the well.

Myoglobin Content. To ensure a thorough and accurate assessment of the myoglobin content within the engineered muscle constructs, a rigorous and multi-step protocol was implemented. This process involved both the preparation of the 3D tissue structures and the subsequent execution of a highly sensitive immunoassay. The myoglobin concentration in all samples was quantified using a mouse myoglobin ELISA kit (Crystal Chem, USA), a method known for its specificity and precision.

Before the ELISA could be performed, the complex 3D tissue structures required careful digestion to release the intracellular myoglobin. The procedure was initiated by meticulously

washing the constructs with phosphate-buffered saline (PBS) to remove any residual culture medium. Each construct was then weighed using a high-precision 4-digit scale, a critical step that allowed the normalization of the final myoglobin measurements to a per-unit-weight basis, thereby providing a robust metric of myoglobin concentration in the tissue.

Following weighing, the constructs were transferred to individual microcentrifuge tubes. A specified volume of Radioimmunoprecipitation (RIPA) Assay buffer (Thermo Fisher Scientific, USA), a powerful chemical lysis buffer, was added to each tube. To protect the proteins from degradation during the digestion process, the RIPA buffer was supplemented with a 1X Halt Protease Inhibitor Cocktail (Thermo Fisher Scientific, USA). The tubes were then incubated for 30 minutes at 4°C in a ThermoMixer (Eppendorf, Germany). The combination of protease inhibitors and the low temperature was essential for ensuring that the tissue was effectively digested while preserving the integrity and stability of the myoglobin protein.

After incubation, the resulting lysate was centrifuged at 12,000×g for 10 minutes at 4°C. This high-speed centrifugation step served to pellet the cellular debris, leaving a clear supernatant containing the target proteins, including myoglobin. This protein-rich supernatant was then carefully collected and used directly for the subsequent ELISA assay.

The ELISA (Enzyme-Linked Immunosorbent Assay) was performed in strict accordance with the manufacturer's instructions. A standard curve was first generated by preparing a serial dilution of the provided myoglobin standards. Simultaneously, the experimental samples were diluted with the kit's specific dilution buffer to ensure their myoglobin concentration fell within the linear range of the standard curve.

In the first incubation step, 100 µL of each diluted sample or standard was added to the wells of the provided microplates, which were pre-coated with a monoclonal anti-mouse myoglobin antibody. The plates were then incubated for 1 hour at room temperature (RT). During this time, the myoglobin present in the samples specifically bound to the immobilized capture antibody.

Following the initial incubation, the plates were washed three times with the provided wash buffer to remove all unbound substances. After blotting the plate to remove residual wash buffer, 100 µL of an enzyme conjugate was added to each well and incubated for 30 minutes at RT. This enzyme-conjugated antibody specifically bound to the captured mouse myoglobin, creating an enzyme-linked complex. The wells were then washed three more times, and any remaining wash buffer was removed by blotting the plates against a dry towel.

Next, 100 µL of substrate solution was added to each well, and the plates were incubated for 10 minutes at RT in the dark. The substrate reacted with the enzyme conjugate, initiating a color change that was proportional to the amount of captured myoglobin. The enzymatic reaction was then halted by the addition of 100 µL of stop solution, which stabilized the color and allowed for measurement. The optical density (OD) of each well was subsequently recorded at 450 nm using a microplate reader, with a reference wavelength of 630 nm to correct for background absorbance.

A standard curve was generated by plotting the OD values of the standards against their known concentrations. The myoglobin content of the samples was then interpolated from this curve and normalized to the initial tissue weight, with the final results reported as nanograms of myoglobin per milligram of tissue (ng myoglobin/mg tissue).

To provide a physiological benchmark for the results, the myoglobin content of the engineered constructs was compared to that of native mouse muscle. Tissue samples were ethically obtained from the forelimbs of three mice from the mouse pathology facility at Hamburg University. The tissue was pooled at the end of the collection process, and myoglobin content was measured using the identical mouse myoglobin ELISA kit and the same protocol as described above. Since this study involved the use of animal tissue sourced from an established pathology facility, specific ethical approval for animal experimentation was not required. The procurement and use of these tissues for research purposes were in full compliance with institutional guidelines and adhered to standard scientific practices.

Iron Uptake Test. To precisely quantify the cellular uptake of iron and its subsequent accumulation within the engineered constructs, a ferrozine-based colorimetric assay was utilized, a well-established and highly sensitive method for iron detection [78]. This procedure was crucial for directly linking the supplemented iron to its intracellular presence, thereby validating the iron supplementation strategy.

C2C12 cell sheets were first cultured according to the previously developed protocol. Following a seven-day maturation period, the sheets were carefully collected and washed twice with ice-cold Phosphate-Buffered Saline (PBS). This washing step was critical for removing any non-specifically bound or extracellular iron from the constructs. To serve as a control for potential extracellular iron, a separate group of samples was washed with PBS containing 1 mM deferoxamine, a potent iron chelator. Any significant difference in the final iron content between the standard-washed group and the deferoxamine-washed group would indicate the

presence of loosely bound, extracellular iron. After the final wash, the PBS was completely removed, and the samples were stored at −20 °C to preserve their protein content until analysis.

To extract the intracellular iron, the frozen cells were lysed using a 50 mM Sodium Hydroxide (NaOH) solution. The samples were incubated with the lysis buffer for 2 hours on a shaker within a humidified incubator. This method of alkaline lysis effectively disrupts cellular membranes and releases the intracellular contents, including iron-binding proteins. Following lysis, aliquots of the cell lysate were collected for subsequent iron quantification and further experiments.

The total iron content of the cell lysate was determined through a multi-step process. A 100 µL aliquot of the cell lysate was transferred to an Eppendorf tube. To this, 100 µL of 10 mM hydrochloric acid (HCl) and 100 µL of a freshly prepared iron-releasing reagent were added. The iron-releasing reagent was a crucial component, formulated as a 1:1 mixture of 1.4 M HCl and a 4.5% (w/v) potassium permanganate ($KMnO_4$) solution in distilled water. The mixture was then incubated for 2 hours at 60 °C inside a fume hood, as the reaction produces potentially hazardous chlorine gas. This step serves to release iron from its binding proteins and oxidize it to a form suitable for detection.

After the incubation, the tubes were cooled to room temperature, and 30 µL of iron-detection reagent was added to each. This reagent, which was also prepared fresh, contained 6.5 mM ferrozine, 6.5 mM neocuproine, 2.5 mM ammonium acetate, and 1 M ascorbic acid dissolved in distilled water. Ferrozine is a chromogenic reagent that forms a highly colored complex with ferrous iron (Fe_{2+}). The other components were included to optimize the reaction and ensure stability. The mixture was then incubated for 30 minutes at room temperature.

Finally, a specific volume of the colored solution was transferred to a 96-well plate, and the optical density (OD) was recorded at a wavelength of 550 nm using a microplate reader. To quantify the iron content of the samples, a standard curve was generated by preparing and analyzing a serial dilution of a ferric chloride ($FeCl_3$) solution, ranging from 0 to 200 µM, following the exact same protocol. This enabled accurate determination of the iron concentration in the cell lysates by interpolating their OD values from the standard curve.

5.1.5. Fluorescent-Based Assays

DCFH-DA (2′− 7′- dichlorodihydrofluorescein diacetate) Assay. To quantitatively assess the level of intracellular reactive oxygen species (ROS), the 2',7'-dichlorodihydrofluorescein

diacetate (DCFH-DA) assay was employed [79]. This method is a widely accepted and highly sensitive tool for measuring general oxidative stress within living cells. ROS are a class of highly reactive, oxygen-containing molecules that are a natural byproduct of cellular metabolism. While essential in low concentrations for cellular signaling, an excessive accumulation of ROS can overwhelm a cell's antioxidant defenses, leading to a state of oxidative stress. This stress can cause significant damage to macromolecules such as DNA, lipids, and proteins, ultimately compromising cellular function and viability.

The DCFH-DA probe is a non-fluorescent, cell-permeable dye that is an ideal indicator of intracellular ROS. Once it crosses the cell membrane, it is rapidly hydrolyzed by intracellular esterases to form dichlorodihydrofluorescein (DCFH). This new molecule is unable to exit the cell, effectively trapping the probe inside. In the presence of various ROS, the DCFH molecule is then oxidized to its highly fluorescent counterpart, dichlorofluorescein (DCF). The intensity of the resulting green fluorescence is directly proportional to the amount of ROS present, providing a reliable proxy for the level of oxidative stress.

For the experimental procedure, a 10 mM DCFH-DA stock solution was prepared in dimethyl sulfoxide (DMSO) and stored at -20°C in the dark to protect it from light-induced degradation. C2C12 cells were seeded into 96-well plates and supplemented with the various iron concentrations being investigated. They were then incubated overnight at 37°C to allow for proper growth and adherence to the plate surface.

The following day, the cells were carefully washed twice with phosphate-buffered saline (PBS) to remove any residual serum, which could interfere with the assay. The cells were then incubated with a 10 µM working concentration of DCFH-DA diluted in serum-free medium. This incubation was carried out for 60 minutes at 37°C in the dark to prevent any photo-oxidation of the probe.

Upon completion of the incubation, the plates were immediately transferred to a fluorescent microplate reader. The fluorescence intensity was measured at an excitation wavelength of 488 nm and an emission wavelength of 525 nm. The resulting data were exported as relative fluorescence units (RFU), which were then used to quantify and compare the levels of oxidative stress across the different experimental groups. This rigorous methodology ensured whether the iron supplementation had any detrimental effects on the health of the cells.

5.1.6. Statistical Analysis

To ensure the reproducibility and statistical validity of the findings, all experiments were meticulously conducted with a minimum of biological triplicates, unless explicitly stated otherwise. This approach is a cornerstone of rigorous scientific research, as it accounts for inherent biological variability and increases the confidence in the results. The dataset from these replicate experiments was then subjected to a comprehensive statistical analysis. All statistical computations were performed using GraphPad Prism (version 6.1), a powerful and widely-used software for scientific data analysis.

To identify statistically significant differences between the various experimental groups, a one-way analysis of variance (ANOVA) was employed. This test is ideal for comparing the means of three or more independent groups. Following a significant ANOVA result, a Tukey's post hoc test was performed. This specific post hoc analysis is critical because it allows for a simultaneous comparison of all possible pairs of means, while controlling for the family-wise error rate, thereby providing a more conservative and reliable assessment of where the significant differences lie. Any deviations from this standard statistical approach, such as the use of a different test, are explicitly noted within the relevant results sections.

5.2. Results

Since meat color is a key parameter in customer acceptance of cultivated meat products, it was aimed to identify factors that help up-regulating myoglobin in protein level, which is the principal protein responsible for meat color. To do so, several factors, which might affect myoglobin synthesis, have been investigated in this study.

Iron. Myoglobin is a heme-protein with a central iron atom involved in intracellular oxygen transfer which facilitates mitochondrial respiration. It was hypothesized that making iron available to the cells might increase myoglobin synthesis and accumulation in the cells. To investigate this hypothesis, 3D structures were cultured according to the developed protocol and were supplemented with 0.011 mM fresh iron sulphate (FeSO4) on a daily basis, either starting the growth phase (d0) or at the end of the differentiation phase (d3). The constructs were cultured for further maturation in a standard incubator until day 7. A negative control group (N) was also considered, which was not supplemented with iron. The results were evaluated based on visual imaging. Images were captured at defined conditions and analyzed using ImageJ software. CIELAB parameters were measured for each sample and the color change of d0 and d3 samples were compared with the control group using formula [3]. As figure

15 depicts, the 3D structures that were supplemented starting the growth phase (d0), showed the highest color change compared to the control group, with a ΔE around 3, which is visible by most people.

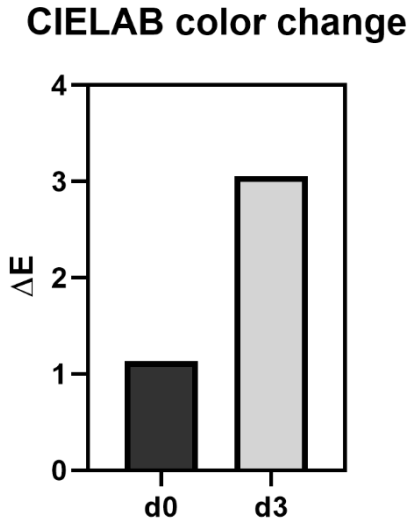

Figure 15 – CIELAB color change indicating the most change for the sample supplemented with iron starting day 0.

It was decided for further experiments to supplement the 3D structures with iron starting the growth phase at day 0. To further investigate the effect of iron on structures color, higher concentrations of iron according to table 2 were studied. It was observed that the cells supplemented with 32X, 64X, and 128X iron experienced reduced cellular proliferation, which was assumed to be a result of reduced pH. To evaluate this assumption, pH was measured for RPMI-1640 medium when supplemented with different concentrations of iron sulfate.

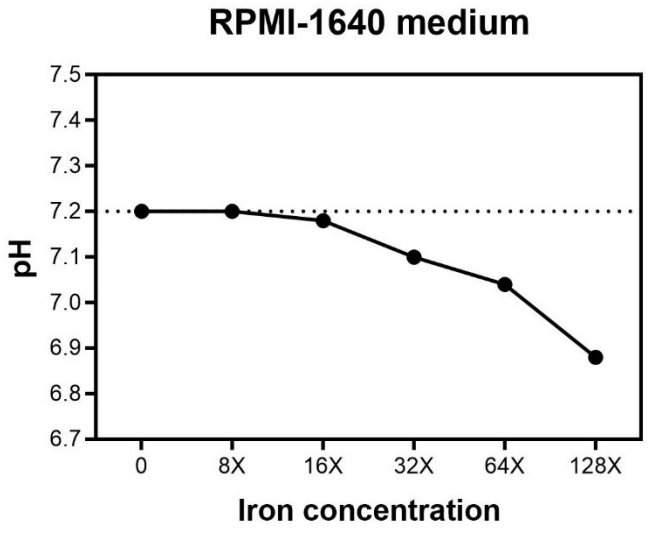

Figure 16 – Medium pH in response to iron sulfate supplementation at various concentrations

As figure 16 shows, pH reduces as iron concentration increases and at concentrations above 32X, pH is acidic. At 32X iron concentration, pH is not acidic but still far from the ideal pH environment for C2C12 cells. Therefore, further experiments at iron concentration above 16X have been discontinued. It was concluded that iron sulfate contributed to medium acidification through hydrolysis. Upon its dissolution in aqueous solutions, Fe^{2+} undergoes hydrolysis, forming $FeOH^{+}$ and releasing protons (H^{+}), which lowers the pH.

$$FeSO_4 \rightarrow Fe^{2+} + SO_4^{2-}$$
$$Fe^{2+} + H_2O \rightleftharpoons FeOH^{+} + H^{+} \quad [4]$$
$$FeOH^{+} + H_2O \rightleftharpoons Fe(OH)_2 + H^{+}$$

Figure 17 depicts the color change in sample supplemented with iron at 1X, 4X, and 16X concentrations. A negative group is also illustrated for comparison.

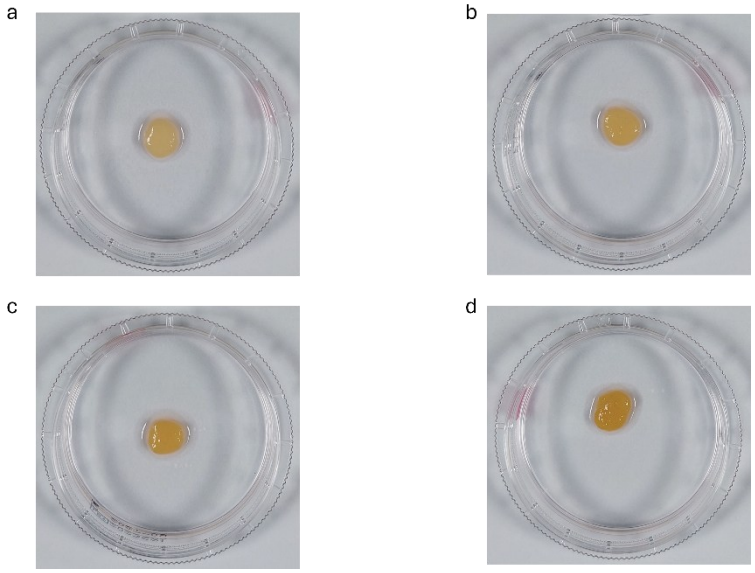

Figure 17 – 3D structures sumplemented with a) no iron, control, b) 1X iron c) 4X iron d) 16X iron

It was observed that by increasing iron concentrations, the color change got stronger. In order to confirm if the color change was due to myglobin synthesis, myoglobin content was measured at each concentration using myoglobin ELISA kit. To do so, C2C12 cells were cultured in 24-well plates based on the developed protocol and supplemented with desired iron concentration. After delamination, three cell sheets were stacked together to form a 3D structure, which was cultured further up to day 7. Samples were weighted and myoglobin content was measured according to the instructions.

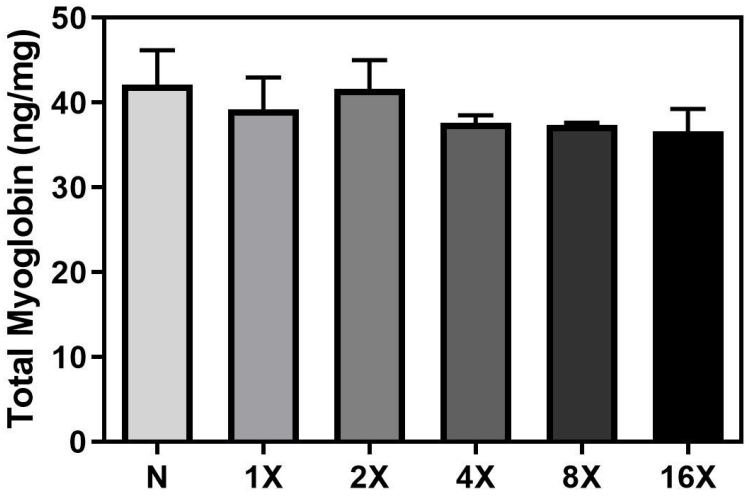

Figure 18 – Myoglobin content of 3D structures supplemented with various iron concentrations

As figure 18 shows, myoglobin protein content did not significantly change by adding or increasing iron concentrations. Thus the color change observed by adding iron sulfate might have another reason. In order to further study the effect of iron, the iron uptake test was performed to investigate whether the supplemented iron is absorbed by the cells or used in protein structures. For this purpose, C2C12 cell sheets were cultured according to the protocol and collected at day 7. A ferrozine-based colorimetric assay was performed to locate the supplemented iron ions. It was observed that iron was not unspecifically bound on extracellular regions since washing the structures with PBS containing the iron chelating agent, deferoxamine, prior to the cell lysis did not make significant changes in the results. Therefore, the supplemented iron could either be absorbed by the cells or washed away with medium changes.

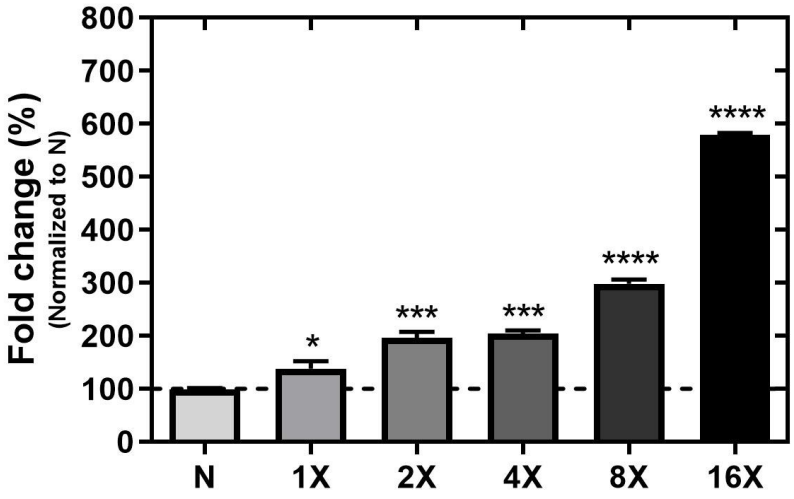

Figure 19 – Iron stored in cell sheets when supplemented with various iron concentrations (data normalized to control)

As figure 19 depicts, the iron stored in cell sheets increased significantly as the supplemented iron concentration increased, where at 16X iron concentration, the iron stored in cells was 6-fold more than the control group. The results were normalized by the control group. Since myoglobin ELISA test revealed that myoglobin content has not significantly changed due to the iron addition, it can be concluded that the iron might be stored in other iron-containing structures inside the cells. One likely destination for the supplemented iron might be ferritins, which are the primary intracellular iron storage proteins, preventing iron toxicity and making it available only when needed. Each ferritin molecule is composed of a hollow structure with 24 sub-units aligned in a spherical arrangement and can hold up to ~4000 iron atom in its core [80]. Another likely destination for the supplemented iron might be mitochondria, which uses iron primarily for heme or iron-sulfur clusters synthesis [81]. In some cases, iron might accumulate in mitochondria, however it leads to increased oxidative stress. In order to verify this hypothesis, the effect of iron addition on reactive oxygen species, as the primary source of oxidative stress, was studied. C2C12 cells were seeded in 96-well plates and supplemented with various iron concentrations and incubated at 37 ^{o}C for an overnight to allow cell attachment. DCFH-DA assay was performed to measure produced ROS in response to iron addition. To ensure accurate quantification of intracellular ROS levels, the fluorescence intensity obtained from the DCFH-DA assay was normalized using both NRU and BCA assay. The NRU assay provides a measure of cell viability, allowing the number of viable cells to be accounted for. Normalizing ROS levels to NRU ensures that differences in ROS signals are not due to changes in cell survival but reflect actual differences in ROS production. The BCA assay quantifies total protein content, serving as an additional normalization factor to account for potential variations

in cell density and protein expression levels. By normalizing ROS fluorescence to total protein, it is ensured that the observed ROS differences are not simply due to variations in biomass. By applying both NRU- and BCA-based normalization, a more comprehensive and reliable assessment of intracellular ROS levels is provided, minimizing the impact of experimental variability. This dual-normalization approach helps differentiate ROS changes resulting from oxidative stress from those arising due to altered cell number or protein content.

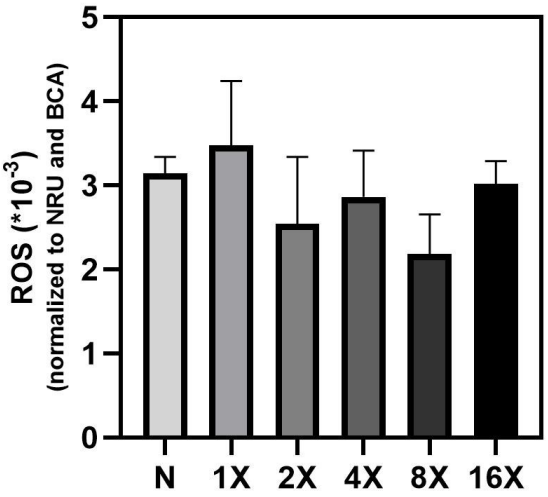

Figure 20 – ROS measurement in response to iron supplementation (data normalized to NRU and BCA assays)

As shown in figure 20 ROS produced in response to iron addition has not experienced significant changes. Therefore, iron has not excessively accumulated in mitochondria, while it could cause increased ROS. As iron stores in ferritins in the form of ferric acid, which has a brownish color is the most likely scenario, which relies good with the observed color changes. However, further investigation of this phenomenon was out of scope of this study, but the authors suggest iron supplementation along with regulation relevant pathways might lead to myoglobin regulation.

Insulin-like Growth Factor-I (IGF-I). It is known that IGF-I promotes cell growth, differentiation, and metabolism. It also promotes C2C12 differentiation into myotubes by activating PI3K/Akt/mTOR pathway [82]. To examine its effect on myoglobin synthesis, C2C12 cells were cultured in 12-well plates according to the developed protocol, and supplemented with various concentrations of IGF-I. However, the results demonstrated that IGF-I did not significantly alter myoglobin synthesis under the tested conditions (figure 21).

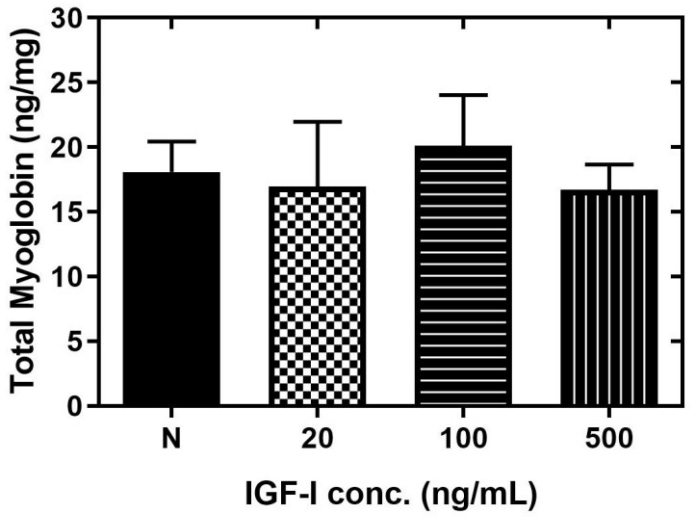

Figure 21 - IGF-I does not directly affect myoglobin protein synthesis.

Creatine. To assess whether creatine supplementation influences myoglobin protein synthesis in C2C12 cells, differentiated myotubes were treated with varying concentrations of creatine and myoglobin levels were quantified using an ELISA assay. The results revealed that myoglobin protein expression remained largely unchanged across all tested conditions (Figure 22). Statistical analysis confirmed that differences between control and creatine-treated groups were not significant ($p > 0.05$).

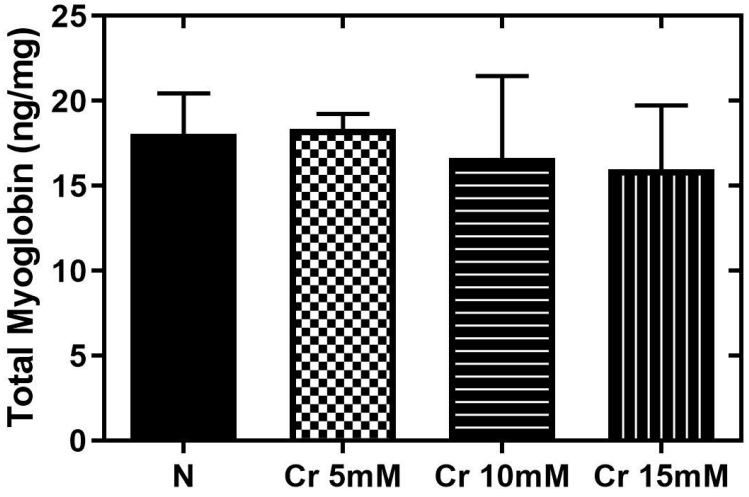

Figure 22 - Creatin supplementation did not directly affect myoglobin protein synthesis.

Culture Vessel Size. It was observed that cell sheet production in different culture vessels cause variations in myoglobin production. Therefore, the effect of vessel size on myoglobin protein content was studied. C2C12 cells were cultured in various vessels of 24-well plate, 12-well

plate, 35mm petri dishes, and 60mm petri dishes according to the proposed protocol and myoglobin content was measured using myoglobin ELISA kit. Figure 23 shows that the size of the vessel in which cell sheets were produced, regulates myoglobin synthesis in protein level. By increasing vessel size, myoglobin content reduces significantly. The highest myoglobin content was observed in smallest vessel size, 24-well plates in this study. Stacking multiple layers of cell sheet, did not affect myoglobin content significantly (data not shown).

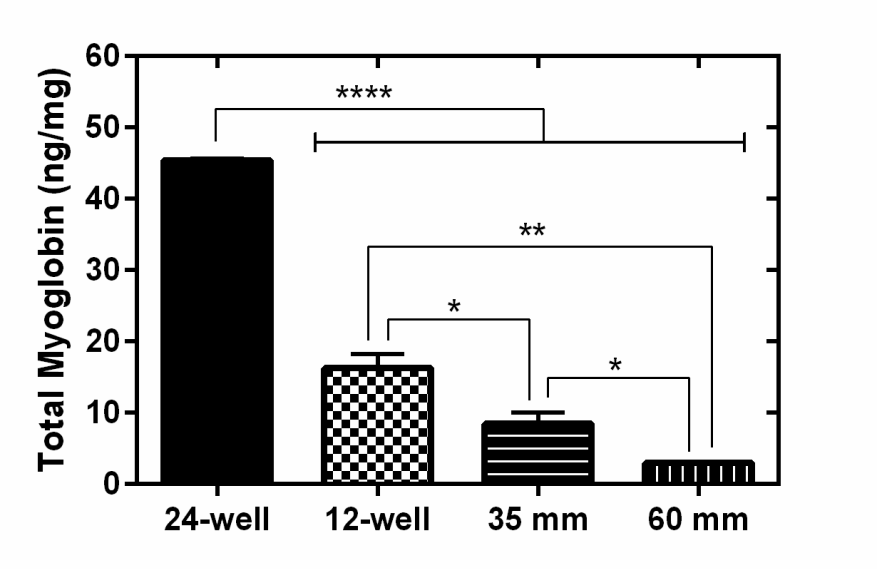

Figure 23 - Culture vessel size affects myoglobin protein synthesis in C2C12 cells.

DO. To investigate the impact of oxygen availability on myoglobin synthesis, C2C12 cell sheets were cultured under either normoxic or hypoxic (1% O_2) conditions. Myoglobin protein content was quantified at two key time points: day 3 (post-delamination) and day 7 (post-maturation). The results indicated that oxygen tension had no significant effect on myoglobin synthesis, as no substantial differences were observed between the normoxic and hypoxic groups at either time point. However, culture duration had a marked influence on myoglobin accumulation. Myoglobin content at day 7 was approximately three times higher than at day 3, suggesting a strong temporal regulation of its expression (Figure 24).

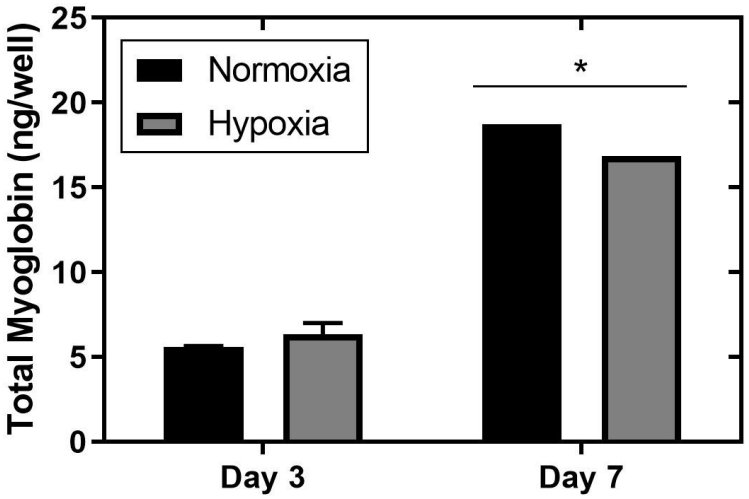

Figure 24 - Myoglobin content in C2C12 cell sheets at day 3 and day 7 under normoxic and hypoxic conditions. Culture duration significantly influenced myoglobin synthesis.

This increase aligns with the distinct phases of cell sheet development. During the initial three days, cells underwent proliferation and differentiation, which primarily set the foundation for myogenic commitment. In contrast, the subsequent four-day maturation phase likely promoted enhanced protein synthesis and cellular adaptation, leading to the observed rise in myoglobin levels. These findings highlight the critical role of maturation time in myoglobin synthesis and suggest that prolonged culture, rather than oxygen availability, is a key factor in optimizing myoglobin accumulation in C2C12 cell sheets.

While hypoxic incubators provide a reduced oxygen environment, cells within static cultures still rely on diffusion for oxygen transport, which may not accurately reflect the intended bulk oxygen concentrations. To better control oxygen availability, myoglobin synthesis was further examined in a DASGIP bioreactor, where DO, pH, and temperature were precisely regulated in an agitated system.

Given that agitation could adversely influence cell sheet development, a hybrid culture approach was used. C2C12 cell sheets were first cultivated in static conditions within 35 mm petri dishes in a standard incubator. After delaminating on day 3, the detached sheets were allowed to mature into 3D constructs for 24 hours. These constructs were then transferred to the dynamic bioreactor system, where they were cultured until day 7 (4 days static + 3 days dynamic).

To assess the impact of oxygen, DO levels were maintained at 2%, 5%, 30%, 50%, or 100% air saturation. Additionally, a variable oxygen regime was tested, simulating exercise-like

conditions by oscillating DO levels between 10% and 50% in a 4-hour cycle. Across all conditions, pH and temperature were kept at 7.2 and 37°C, respectively.

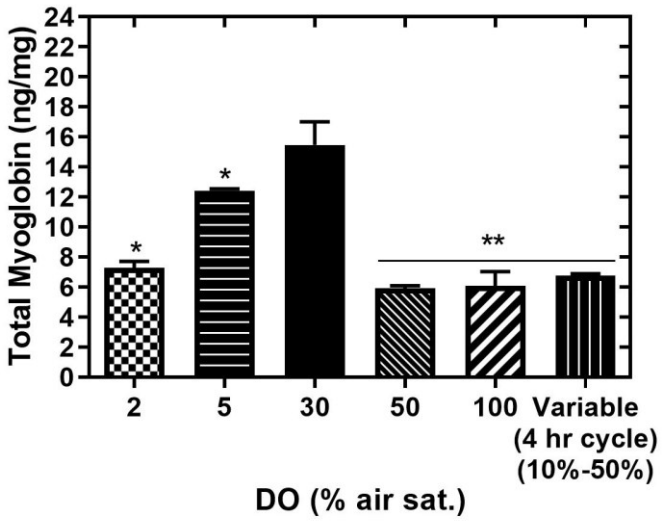

Figure 25 - Myoglobin content in C2C12 cell sheets under different dissolved oxygen (DO) conditions. DO 30% significantly increased myoglobin levels.

Myoglobin content was quantified using an ELISA assay, revealing that DO 30% led to a significant increase in myoglobin levels (figure 25). Notably, neither extreme hypoxia (DO 2–5%) nor mild hypoxia (DO 50–100%) further enhanced myoglobin synthesis. Interestingly, even under fluctuating oxygen conditions, designed to mimic physiological variations seen in muscle activity, myoglobin levels remained unchanged compared to static DO conditions. These findings suggest that a moderate oxygen environment (~30% DO) is optimal for myoglobin synthesis, while both lower and higher DO levels offer no additional benefits.

Mechanical Stretching. To better mimic exercise-like conditions and evaluate their impact on myoglobin synthesis, a mechanical stretching regimen was applied to C2C12 cell sheets. Following the standard protocol, cells were cultured in 100 mm petri dishes and allowed to delaminate on day 3. The detached sheets were then carefully rolled around a silicone tube, which was aseptically secured within a custom-built mechanical stretching system. The stretching cycle consisted of 135 seconds of active stretching, followed by a 30-second hold at maximum stretch and a 60-second relaxation phase. The total displacement at peak stretch was maintained at 1 mm, and DO was kept constant at 30% throughout the experiment. A control group without mechanical stretching was included for comparison.

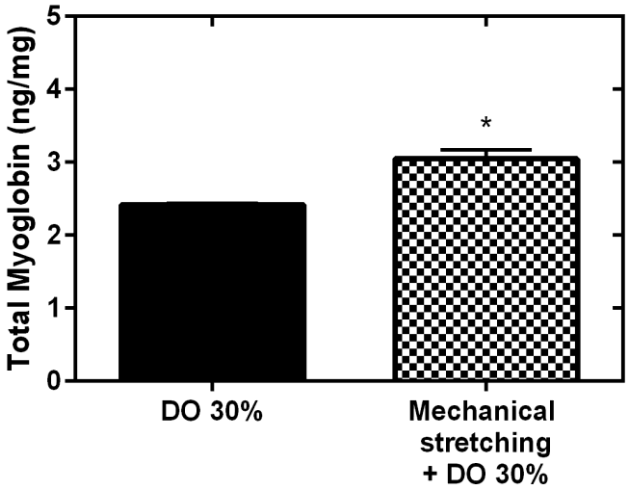

Figure 26 - Myoglobin content in C2C12 cell sheets under 30% DO with and without mechanical stretching. Stretching significantly enhanced myoglobin synthesis.

Myoglobin content was quantified, revealing that the combination of mechanical stretching and 30% DO resulted in a significant increase in myoglobin levels compared to the non-stretched control group (Figure 26). These findings suggest that mechanical strain enhances myoglobin synthesis, likely by activating mechanotransduction pathways that regulate myogenic adaptation. Given that skeletal muscle experiences repeated mechanical loads during physical activity, this result aligns with physiological expectations, reinforcing the importance of both oxygen availability and mechanical stimuli in optimizing myoglobin production.

5.3. Chapter Discussion

The objective of this study was to identify and quantify factors influencing myoglobin synthesis in C2C12 cell constructs, a crucial step toward achieving natural coloration in cultivated meat. The data revealed several key insights regarding metabolic and environmental regulation of this heme-protein.

Contrary to the initial hypothesis, myoglobin protein levels did not significantly increase with iron supplementation, despite a notable visual color change in the constructs. Myoglobin, a heme-protein with a central iron atom, is a plausible target for upregulation via iron supplementation. However, the iron uptake analysis showed a significant increase in intracellular iron concentration with supplementation, suggesting that the absorbed iron was diverted to alternative storage mechanisms rather than myoglobin synthesis. This is consistent with the lack of significant change in reactive oxygen species (ROS) levels, indicating that the iron was likely sequestered in a non-toxic form, such as in ferritin molecules, which are known

to have a brownish hue. These findings suggest that while iron is essential for myoglobin, its availability alone is insufficient to drive synthesis.

The effects of creatine and IGF-I on myoglobin synthesis were also explored, but neither supplementation significantly altered myoglobin protein content under the tested conditions. This result is surprising given that both are known to promote myogenesis and protein synthesis in C2C12 cells [39,40,43]. This suggests that the pathways they influence may not directly upregulate myoglobin at the protein level, or that the specific experimental parameters used were not conducive to a measurable effect.

In contrast, the physical culture environment played a decisive role in myoglobin regulation. Myoglobin content was found to be inversely correlated with the size of the culture vessel, with the highest levels observed in the smallest 24-well plates. This finding is particularly important as it suggests that cell sheet size, or a parameter directly linked to it, is a critical regulator of myoglobin synthesis. The increased cellular density and subsequent cell-to-cell contact within the smaller vessels may create a microenvironment that is more conducive to myoglobin production. This is in agreement with studies that highlight the importance of physical cues and cell-to-cell signaling in promoting myogenesis and protein accumulation [2].

Furthermore, the investigation into the effects of oxygen availability highlighted a nuanced relationship. While static culture in a hypoxic incubator did not yield a significant increase in myoglobin, a moderate dissolved oxygen (DO) concentration of ~30% in a precisely controlled bioreactor environment did. This underscores the limitations of static diffusion-based oxygen supply and the critical need for a controlled, agitated system to study cellular oxygen requirements. The temporal increase in myoglobin content from day 3 to day 7, regardless of the oxygen condition, also indicates that maturation time is a primary factor in myoglobin accumulation.

The final element of this study, mechanical stretching, provided a crucial link between environmental and physiological stimuli. When combined with the optimal 30% DO, a cyclic stretching regimen significantly increased myoglobin levels. This finding aligns with the physiological response of skeletal muscle, where mechanical loading during exercise promotes myogenic adaptation and protein synthesis. These results suggest a synergistic effect between mechanical stimulus and a moderate oxygen environment in maximizing myoglobin production, activating mechanotransduction pathways that regulate myogenic adaptation.

In conclusion, this study demonstrates that myoglobin synthesis is not simply regulated by the presence of key components like iron but is highly dependent on both maturation time and the physical and chemical microenvironment. The significant impact of culture vessel size, a specific, moderate DO level (30%), and the application of mechanical stretching are novel and valuable findings that can guide future efforts in cultivated meat production.

6. Chapter Six: General Discussion and Outlook

In this study, it was investigated how various parameters influence myoglobin synthesis in C2C12 cell sheets, aiming to better understand the factors that regulate oxygen-binding protein expression in muscle-like tissue models. These findings provide valuable insights into the relationship between oxygen concentration, mechanical stimulation, etc. and myoglobin production. By analyzing these effects, this study contributes to the broader understanding of muscle cell metabolism but also open new possibilities for optimizing *in vitro* muscle tissue models for biomedical applications.

6.1. Integration of Findings Across Studies and Literature Review

A protocol was successfully established to produce C2C12 cell sheets which can be further stacked together or round up to form 3D structures. As C2C12 cells are mouse myoblasts with differentiation potential to myotubes, a differentiation phase was necessary following a growth phase. Cell sheets exhibited a self-delamination ability after the differentiation phase, which facilitated the process and was reproducible in various culture vessel types, including 24-well plates, 12-well plates, 35mm, 60mm, and 100mm petri dishes. However, it was observed that sheet delamination happened to be easier at smaller culture vessels. Up to 60mm petri dishes, it was easily possible to speed up the delamination procedure by pushing media using pipettes at the "week points" (figure 7); however, in order to delaminate the sheets in 100mm petri dishes a mechanical force using scrappers was essential. This observation led to the assumption that culture vessel type alters the cell sheet production process. It was later observed that culture vessel size plays a crucial role in myoglobin regulation, as myoglobin protein content was significantly higher in smaller vessels (figure 23). Therefore, it was concluded that the surface-to-circumference-ratio of the cell sheets affects their protein synthesis pathways, which is suggested to be further confirmed by studying other muscle specific proteins like actin contractile proteins. The findings on progressive shrinkage of cell sheets after delamination can also be explained by the presence of contractile forces influenced by cytoskeletal rearrangements, which mimics *in vivo* muscle tissue development, where muscle fibers self-organize into compact structures over time.

In order to study the cellular metabolism in the course of cell sheet development, cellular metabolites namely glucose and lactate were measured on a daily basis in a 5-day period. It was observed that glucose levels decreased sharply during the differentiation phase following a

near-zero value on day 3, where self-delamination occurred (figure 27). Glucose levels increased afterwards in the maturation phase. A similar but reverse pattern was observed for lactate production, where its levels peaked on day 3. These observations led to the conclusion that the self-delamination process relates to altered cellular metabolism.

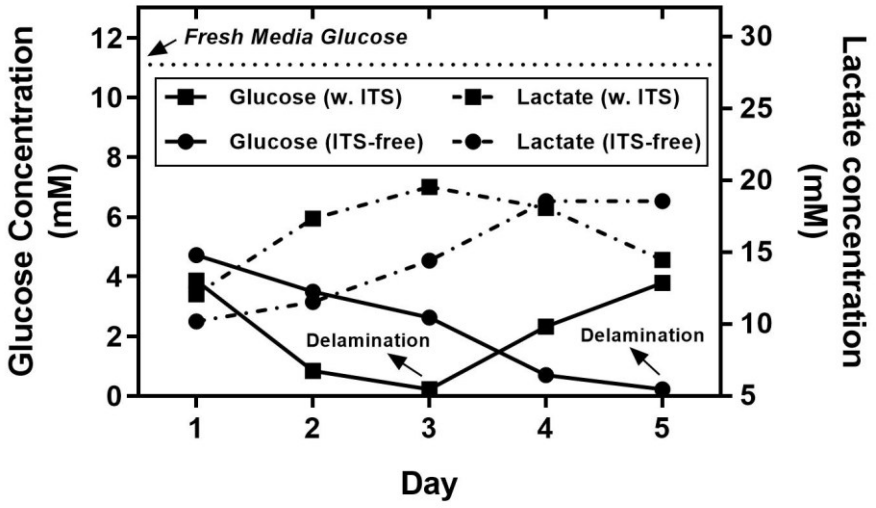

Figure 27 - Glucose and lactate levels in C2C12 cell culture over time with and without ITS supplementation. In the presence of ITS, glucose depletion occurs rapidly by day 3, while in its absence, depletion is delayed until day 5 (differentiation phase is longer). Lactate accumulation follows a similar trend, indicating enhanced glycolytic activity in ITS-supplemented conditions. These findings confirm the role of cellular metabolism in cell sheet delamination.

To further confirm this idea, cellular metabolites were recorded in the absence of ITS, which is a common supplement in C2C12 cell proliferation and differentiation and plays a key role in cellular metabolism. Briefly, insulin stimulates glucose uptake via GLUT4 transporters [83] and promotes anabolic pathways and building up large molecules. Transferrin facilitates iron transport and is essential for mitochondrial function, and selenium is a cofactor which protects cells from oxidative stress. It was observed that glucose levels in the absence of ITS also depleted but at a slower rate, reaching a near-zero value at day 5, following by sheet delamination. In other words, ITS accelerated the differentiation phase, leading to rapid glucose consumption and enhanced differentiation efficiency, and confirming the role of cellular metabolism in cell sheet delamination.

To investigate the effect of sharp glucose depletion during differentiation phase on cell viability, live-dead assay performed at days 1 and 3. It was observed that the cells were viable to a large extent at the end of differentiation phase with only a few dead cells, and numerous elongated myotubes were visible, confirming myogenic differentiation process (figure 8). Due to the limited dye penetration after sheet delamination and formation of compact 3D constructs, a live-dead assay could not be performed at later stages. However, the presence of MHC-positive

myotubes and DAPI-stained nuclei suggests that cells were viable and undergoing differentiation within the constructs. Future studies incorporating alternative viability assays, such as metabolic activity-based assessments (e.g., MTT, PrestoBlue) or improved live-dead imaging techniques, could provide a more comprehensive evaluation of cell survival.

The developed approach approach to cell sheet production offers a unique advantage over traditional methods by eliminating the need for enzymatic or temperature-responsive surface modifications. Unlike enzymatic detachment, which often compromises extracellular matrix integrity and weakens cell-cell junctions, the presented method preserves these structures, potentially improving the mechanical strength and functional properties of the sheet. Another key benefit is the ease of handling, particularly for substrates up to 60 mm in diameter. With these, delamination can be achieved simply by manipulating the culture medium at the edges, making the process less invasive. This stands in contrast to conventional methods that rely on temperature-responsive surfaces or manual peeling, which require additional processing steps and specialized materials. The ability to detach sheets without disrupting their structure may also facilitate downstream applications such as stacking and 3D tissue formation.

However, challenges arise with larger substrates, where mechanical assistance is required for complete delamination. The use of a scraper, while effective to some extent, introduces inconsistencies and risks partial damage to the sheet. This highlights a potential limitation in scalability, particularly for applications requiring larger tissue constructs. Further refinements, such as optimizing the substrate surface properties or modifying culture conditions, may help overcome this constraint. One notable observation in the present system is the tendency of delaminated sheets to shrink and form three-dimensional structures. This phenomenon was further confirmed by SEM imaging and immunostaining results, which provided deeper insights into the morphological changes occurring during and after delamination. Immunostaining revealed that just before detachment, the cells within the sheet exhibited a randomly elongated morphology. However, after delamination and subsequent maturation, SEM imaging showed that the cells had transitioned into a more rounded morphology, indicating compaction and contraction of the sheet. These observations strongly support the hypothesis that cellular rearrangement and cytoskeletal remodeling contribute to the overall shrinkage of the sheet. The shrinkage behavior presents both opportunities and challenges. On one hand, it could be harnessed to create self-organizing tissue constructs that mimic natural tissue morphology without requiring external scaffolds. On the other hand, this spontaneous contraction poses difficulties in applications where maintaining a precise predefined geometry

is crucial, such as engineered muscle grafts or patterned tissue models for regenerative medicine. To fully exploit this phenomenon while mitigating its drawbacks, further investigations are needed to understand the underlying biophysical and biochemical mechanisms driving sheet shrinkage. Factors such as cell contractility, extracellular matrix composition, and intercellular adhesion likely play a role in determining the extent of contraction.

Cell sheet engineering has been explored by various research groups for a wide range of tissue applications. One of the most well-established methods was introduced by Okano et al., who developed a thermo-responsive polymer-based approach for generating cardiomyocyte sheets aimed at myocardial tissue reconstruction [84]. Over time, their method evolved to address the challenge of stacking multiple layers, as sheet-to-sheet adhesion required an extended period of 20–30 minutes. To overcome this, they later refined their protocol by introducing centrifugation at forces between 12–34*g, which significantly reduced adhesion time to just three minutes [10]. This optimization marked an important advancement in the field, enabling faster and more efficient multilayer tissue construction.

Alternative approaches to cell sheet fabrication have also been investigated. Yamamoto et al. explored the use of magnetic fields to generate C2C12 myoblast sheets while eliminating the need for thermo-sensitive substrates [85]. However, they encountered significant limitations, most notably, the severe shrinkage of the sheets over time, which prevented them from maintaining their intended shape during prolonged culture. In response to this issue, they developed an innovative strategy: instead of producing flat sheets, they created cell rings around a silicone plug under magnetic fields. These rings were then hooked onto two pins for further culture, leading to the formation of dense, aligned skeletal muscle tissue structures.

Beyond muscle and cardiac applications, Okano et al. have also advanced the field of vascularized tissue engineering. By incorporating endothelial cells into their cardiomyocyte sheets, they successfully generated vascularized cardiac tissue [86]. Their work demonstrated that patterned cell sheets could be used to control the orientation of vascular structures, paving the way for more complex, functional tissue constructs with integrated blood vessel networks.

A more recent study by Shahin-Shamsabadi et al. introduced a method for C2C12 cell sheet production that closely resembles the approach developed in this study, albeit with minor variations [69]. Notably, their method does not rely on conventional thermo-sensitive polymers or enzymatic detachment techniques. This demonstrates that alternative, simpler methods can

also facilitate cell sheet formation, reinforcing the idea that myoblasts can spontaneously organize into sheets under specific culture conditions.

The method used in the present work was developed after an observation on C2C12 cell cycle behavior, revealing that these cells can form sheets under certain conditions without the need for external surface modifications. While it is not claimed that this approach surpasses all existing methods or leads directly to a commercially viable product, it served as a useful platform for studying factors that regulate myoglobin synthesis, an essential consideration for cultivated meat production. Further research will help refine the technique and expand its potential applications in both regenerative medicine and food biotechnology. Beyond cultivated meat, this system holds potential as a tissue model for drug screening and disease studies. The ability to form stackable layers may allow for the creation of physiologically relevant models that better mimic native tissue organization, providing a more accurate platform for testing pharmaceutical compounds. Additionally, the self-delaminating nature of the sheet could make it an attractive option for scaffold-free tissue engineering, where preserving native ECM is crucial for transplantation and regenerative medicine applications.

Further research could explore the underlying mechanisms driving spontaneous delamination and the impact of different culture conditions on sheet properties. Additionally, optimizing handling techniques for larger sheets would be beneficial for expanding the potential applications of this method.

Following the biological considerations and principles underlying cell sheet engineering, it is equally important to address the physical and environmental parameters that critically influence the success of 3D tissue constructs. Among these parameters, oxygen availability plays a pivotal role, as it dictates the maximum construct size. Therefore, understanding and predicting oxygen transport within engineered constructs is essential for optimizing their design and ensuring long-term cell viability. To this end, a computational simulation was performed to model oxygen diffusion and consumption within the 3D constructs. The goal was to estimate the maximum permissible construct thickness that maintains an adequate oxygen concentration at the core region, thereby preventing anoxia.

The simulation was built upon key experimentally determined parameters, including the k_La. In this study, the k_La value was estimated by fitting the experimental oxygen concentration profiles to the simulation model, yielding a value of $0.0022 \pm 0.0004\ s^{-1}$. Previous studies have reported k_La values under various experimental conditions [87,88]. For instance, in 48-well plates, the

k_La for oxygen transfer was determined using an empirical equation, with values reaching 0.008 s^{-1} (or 28.92 h^{-1}) at a shaking speed of 650 rpm. This highlights the significant role of agitation in enhancing oxygen transfer. Interestingly, despite the absence of agitation in the setup, the observed k_La values were in a similar range to those in studies where active mixing was introduced. This suggests that other factors, such as vessel geometry and surface properties, may contribute to oxygen transfer efficiency in static conditions. However, direct comparisons should be made cautiously, as empirical models introduce additional complexity by incorporating multiple variables that may not be explicitly accounted for in the present system.

In addition to the volumetric mass transfer coefficient, the oxygen uptake rate (OUR) and the specific oxygen consumption rate (qO_2) of the cells within the 3D constructs were also determined by fitting the experimental oxygen concentration data. The OUR and qO_2 were measured as $2.08 \times 10^{-6} \pm 2.18 \times 10^{-7}$ mol.L^{-1}.h^{-1} and $2.02 \times 10^{-21} \pm 1.42 \times 10^{-22}$ mol.$cells^{-1}$.s^{-1}, respectively.

Previous studies have reported that C2C12 cells in monolayer culture exhibit a significantly higher qO_2 value of 3.7×10^{-18} mol·$cell^{-1}$·s^{-1} [89,90]. This disparity suggests that the transition from 2D to 3D culture significantly influences oxygen consumption, likely due to changes in cellular metabolism, diffusion limitations, or altered microenvironmental conditions within the constructs. These findings highlight the complex interplay between cell organization, oxygen diffusion, and metabolic activity in 3D constructs. Further studies are needed to unravel the dynamics of oxygen consumption throughout different phases of construct maturation, which could provide valuable insights into optimizing engineered tissue models and regenerative medicine applications.

the effective diffusion coefficient (D_{eff}) within the 3D constructs was also calculated to be $1.397 \times 10^{-11} \pm 1.755 \times 10^{-13}$ m^2·s^{-1}, which is approximately two orders of magnitude lower than the diffusion coefficient of oxygen in water. This significant difference can be attributed to the structural and compositional characteristics of the constructs. As shown in Figure 10, the 3D constructs exhibited exceptionally high cell density, which played a major role in impeding oxygen diffusion. The densely packed cellular structure created a complex microenvironment where oxygen molecules faced greater resistance while navigating through the intricate network of cells and extracellular matrix. This limited oxygen movement, resulting in a much lower diffusion coefficient compared to a more open environment like water. In addition to high cell density, the porosity of the constructs was measured at only 11.95%, meaning that very few void spaces were available for oxygen to pass through. This lack of open pathways further

restricted oxygen diffusion, compounding the effects of cell density. With fewer available routes, oxygen had to traverse a tightly packed structure, significantly slowing its transport.

The combination of elevated cell density and low porosity provides a clear explanation for the reduced oxygen diffusion coefficient observed in the 3D constructs. These findings underscore the importance of microstructural properties in influencing mass transport within engineered tissues. Understanding these diffusion limitations is essential for optimizing tissue engineering strategies, ensuring sufficient oxygen supply for cell viability and function in complex 3D environments.

Fiedler et al. utilized Lattice Monte Carlo simulations to assess the oxygen diffusion coefficient in solid porous scaffolds fabricated using techniques like robocasting, sol-gel foaming, and foam replication [91]. Their model assumed that scaffold pores were entirely occupied by newly formed tissue resembling brain, muscle, or lung. All scaffolds were composed of a PCL polymer matrix, where the material itself acted as a diffusion barrier, restricting oxygen penetration to the pore spaces. Among the fabrication methods, foam replication yielded scaffolds with the highest diffusion coefficient, measured at approximately 1.3-1.4 × 10^{-9} m^2/s when filled with muscle tissue. This value is nearly two orders of magnitude higher than the diffusion coefficient determined in this study. The disparity can be attributed to the significantly greater porosity of foam-replicated scaffolds, which ranged between 89.7% and 91.2%—nearly 7.5 times higher than that of the 3D structure developed in this study. The relationship between diffusion coefficient, material porosity, and mechanical properties is well-documented. Cheema et al. demonstrated that decreasing collagen scaffold density results in a reduction of the oxygen diffusion coefficient [92]. Additionally, scaffold crosslinking, which enhances mechanical integrity, is associated with a lower diffusion rate. However, while Cheema et al. investigated material density's influence on diffusion, they did not account for oxygen consumption by cells, assuming it to be negligible in early time points.

The simulation results clearly demonstrated that as the thickness of the 3D construct increased, the oxygen concentration at the center progressively declined. This trend underscores the critical influence of construct dimensions on internal oxygen availability, which in turn directly impacts cell viability and function. The simulation achieved a coefficient of determination (R^2) of 0.87 when compared to the experimental data, indicating a good level of agreement despite the inherent complexity of the system. Nonetheless, several sources of error must be acknowledged when interpreting these results.

Two primary sources of error were identified. First, the governing equations were simplified due to the inability to measure oxygen profiles radially within the 3D construct. Consequently, a three-dimensional model was reduced to a one-dimensional approach, focusing on vertical oxygen transport. While this introduced some approximations, it enabled the determination of key parameters, such as OUR and k_La. Second, the assumption that the 3D construct could be modeled as a cylinder with a diameter-to-height ratio of 2.38 ± 0.18 introduced another potential source of error. This assumption was based on the automated fabrication process, but geometric simplifications may have led to discrepancies. Advanced tissue engineering techniques, such as 3D bioprinting, could enhance shape precision, thereby reducing these errors and improving simulation accuracy.

Based on the simulation findings, a maximum construct thickness of 5 mm was identified as the threshold beyond which the oxygen concentration at the center drops to critically low levels. This outcome highlights the necessity of incorporating this size limitation into all subsequent experimental designs to ensure adequate oxygen supply and maintain cellular viability. Guided by this constraint, the study next focused on investigating the regulation of myoglobin expression within the 3D constructs.

As iron plays a central role in the structure of myoglobin, it was hypothesized that supplementing C2C12 myoblast cultures with iron might stimulate myoglobin synthesis. Upon the addition of a defined concentration of ferrous iron (referred to as 1X), the color of the 3D constructs changed from warm beige to mustard brown. This color shift was quantitatively assessed using the CIELAB color space, a method widely used in the meat industry [74,93,94] and recommended by the American Meat Science Association (AMSA) for standardized color measurements [95]. Notably, when iron supplementation was initiated at the onset of the growth phase, the resulting color change was threefold more pronounced compared to iron addition after sheet delamination at the end of the differentiation phase (Figure 15).

To further investigate the influence of iron, concentrations ranging from 1X to 16X were tested. Concentrations above 16X were excluded, as they led to a decrease in medium pH, creating an acidic environment that compromised cell viability. A concentration-dependent enhancement in color intensity was observed, reaching a golden-brown hue at 16X (figure 17). To determine whether this color change was attributable to increased myoglobin production, the myoglobin content of the constructs was quantified using an ELISA kit (figure 18). However, no significant increase in myoglobin levels was detected, suggesting that the observed color change was likely due to other factors.

Reactive oxygen species (ROS) levels measured via the DCFH-DA assay showed no significant increase with iron supplementation, indicating that excess iron was not accumulating in mitochondria. In contrast, ferritin levels—indicative of intracellular iron storage—were significantly elevated, up to six fold at 16X iron concentration. Since ferritin stores ferric iron, which is brown in color, this accumulation likely accounts for the observed visual changes. Consequently, while the CIELAB colorimetric method provided useful initial insights, it was deemed insufficient for evaluating myoglobin content. Subsequent experiments therefore relied on the more specific ELISA-based quantification of myoglobin to assess the effects of various conditions on its expression.

Previous studies have suggested that the presence of sufficient iron is essential for promoting myoglobin synthesis [96,97]. However, to the best of current knowledge, this is the first study to report that iron supplementation alone does not significantly increase myoglobin content in C2C12 myoblasts, indicating that additional factors may be required in combination with iron to induce myoglobin expression effectively.

Another strategy proposed to enhance myoglobin levels in cultured meat constructs is the direct addition of heme proteins such as hemoglobin or myoglobin. For example, Simsa et al. reported that supplementing cultures with these proteins enhanced cell proliferation and altered the color of muscle-like structures derived from bovine satellite cells, as measured using the CIELAB method [93]. Nevertheless, the resulting color still fell short of replicating that of natural meat. Moreover, the direct addition of purified myoglobin is not considered economically viable, as it substantially increases production costs.

In this context, the objective of this study was to optimize the culture environment using a process engineering approach to promote endogenous myoglobin synthesis in muscle-derived cell sheets, rather than relying on external heme supplementation.

In parallel to iron supplementation, the role of insulin-like growth factor I (IGF-I) was also investigated, given its involvement in promoting myogenic differentiation. Specifically, Florini et al. demonstrated that IGF-I induces the expression of the myogenin gene, a key regulator of terminal differentiation, at concentration of 40 ng/mL [98,99]. Based on this, it was hypothesized that IGF-I might enhance myoglobin synthesis, either directly or through its differentiation-promoting effects. However, the results showed that IGF-I treatment at concentrations of 20, 100, and 500 ng/mL did not significantly affect myoglobin protein content in the 3D C2C12 constructs (figure 21). This observation aligns with findings by Peters et al.,

who reported that IGF-I at 100 ng/mL actually decreased myoglobin gene expression in differentiated C2C12 myotubes, despite its protective effects against hypoxia-induced atrophy [100]. Moreover, Witt et al. observed that while early IGF-I stimulation (after 2 days) could transiently upregulate myogenic markers such as MEF2 and ACTN2 in rat satellite cells, prolonged stimulation (7 days) did not sustain this effect [101]. These findings suggest a temporal component to IGF-I signaling in myogenic differentiation and potentially in myoglobin regulation, where its early benefits may not translate into long-term increases in functional muscle-specific proteins like myoglobin. Taken together, these findings indicate that although IGF-I is a potent differentiation factor, it does not act as a positive regulator of myoglobin synthesis under the current experimental conditions. This reinforces the notion that the regulation of myoglobin expression is multifactorial and cannot be effectively modulated by IGF-I alone, at least not in 3D muscle constructs. Future investigations should consider combinatorial treatments or temporally controlled stimulation to better mimic the complex signaling environment of *in vivo* myogenesis.

Given its known effects on muscle physiology and gene expression, the potential of creatine supplementation to enhance myoglobin synthesis in the 3D C2C12 constructs was also explored. Creatine is widely recognized not only as an energy buffer in muscle metabolism but also as a modulator of differentiation pathways. Louis et al. reported that 5 mM creatine significantly increased the expression of myogenic regulatory factors such as MyoD, myogenin, and MRF-4 after 72 hours of treatment, alongside elevated IGF-I levels and enhanced myotube protein content [102]. It was also reported that these effects are mediated via activation of p38 MAPK and Akt/PKB signaling, both crucial for myogenic progression [103]

Motivated by these findings, it was hypothesized that creatine might indirectly support or even upregulate myoglobin production, particularly in a 3D context where metabolic demand and differentiation cues differ from traditional 2D cultures. However, contrary to expectations, the results showed that creatine supplementation at 5, 10, and 15 mM did not lead to any significant increase in myoglobin protein content (figure 22). This discrepancy raises important questions. While creatine clearly promotes myogenic differentiation, as supported by the literature, this does not necessarily translate into elevated myoglobin synthesis. One possible explanation lies in the divergence between markers of structural differentiation (such as myogenic regulatory factors) and functional muscle-specific proteins like myoglobin, which may require distinct or additional regulatory inputs. Moreover, differences in experimental design, such as 3D versus 2D culture systems, oxygen tension, or exposure time, could play a crucial role in modulating

the outcome of creatine treatment. Present findings thus suggest that, similar to IGF-I, creatine alone is not sufficient to enhance myoglobin production in engineered muscle tissues. This underlines the complexity of replicating natural muscle maturation *in vitro* and the need for multi-factorial strategies that go beyond classical differentiation cues.

While single-factor supplementation with iron, IGF-I, or creatine did not yield the expected increase in myoglobin synthesis, it was further investigated whether physical or spatial culture parameters might influence this outcome. Surprisingly, a pronounced effect was observed when varying the size of the culture vessel. Despite identical cell densities, medium composition, and incubation conditions, the myoglobin protein content in C2C12 cell sheets cultured in 24-well plates was nearly 15-fold higher compared to those grown in standard 60 mm Petri dishes.

To current knowledge, no previous study has directly reported such a strong link between culture vessel size and myoglobin synthesis. The underlying mechanism remains speculative but could relate to several physical factors. One potential explanation is the reduced surface-to-volume ratio in smaller wells, which may lead to more stable nutrient and oxygen gradients across the sheet. Furthermore, edge effects may play a role: in smaller vessels, the distance between the sheet center and its edge is shorter, possibly increasing the influence of edge-associated factors like oxygen diffusion, mechanical tension, or paracrine signaling. Another plausible factor might involve accumulation of autocrine or paracrine signals in smaller volumes. In confined environments, secreted factors could reach higher local concentrations and act more efficiently to promote myogenic maturation and protein expression. Additionally, smaller vessels may promote a more uniform and compact cell sheet formation, influencing the overall tissue architecture and cellular communication dynamics. This observation highlights that beyond biochemical stimuli, the physical context of the culture system can have a profound impact on muscle-specific protein synthesis and should be carefully considered in tissue engineering approaches aiming to replicate functional muscle phenotypes.

Following the observation that physical culture parameters such as vessel size significantly influenced myoglobin content in C2C12 cell sheets, the study next focused on oxygen availability, a well-established regulator of muscle respiratory proteins. Hypoxia has long been associated with increased myoglobin synthesis *in vivo*. For instance, Reynafarje reported that high-altitude natives exhibited significantly higher muscle myoglobin content compared to sea-level individuals, suggesting an adaptive enhancement in oxygen storage capacity [104]. Similarly, Widmer et al. demonstrated that blind mole rats, which live in chronically hypoxic subterranean environments, have approximately three times higher myoglobin levels than

surface-dwelling white rats [105]. These findings point toward hypoxia as a potent physiological stimulus for myoglobin production. A study by Terrados et al. further supported this by showing that one-legged training under hypobaric hypoxia in humans led to increased myoglobin content in muscle biopsies, compared to training under normoxic conditions [106].

Motivated by these findings, it was investigated whether exposing the engineered 3D muscle constructs to *in vitro* hypoxia would elicit a similar effect. Initial experiments using a hypoxic chamber (1% O_2) did not result in significant differences in myoglobin content when compared to normoxic conditions (figure 24). However, a clear temporal increase in myoglobin was observed from day 3 to day 7 of culture, with levels increasing up to threefold. Since day 3 marked the end of the differentiation phase and delamination of the sheets, this suggested that maturation rather than oxygen level was the dominant driver of myoglobin expression during this stage.

To gain deeper insights into the specific role of oxygen, a fully controlled bioreactor system (DASGIP) was employed, allowing precise regulation of DO, pH, and temperature, parameters that are not tightly controlled in standard hypoxic chambers. In hypoxic chambers, only ambient gas composition is adjusted, often leading to variable oxygen diffusion rates across the medium, particularly in static cultures. In contrast, the bioreactor setup enabled precise modulation of dissolved oxygen (DO) levelswithin the culture medium, ensuring stable and reproducible conditions. Using this system, sheets under various chronic oxygenation levels (2%, 5%, 30%, 50%, and 100% air saturation) were cultured. Notably, DO at 30% air saturation resulted in a threefold increase in myoglobin content, identifying it as an optimal oxygenation level for promoting myoglobin synthesis in the engineered muscle sheets (figure 25). An intermittent hypoxic regimen oscillating between 10% and 50% air saturation in 4-hour cycles was also explored. Surprisingly, this condition did not enhance myoglobin synthesis, despite the fact that the optimal 30% DO fell within this range. A similar observation was reported by Herawati et al., where intermittent hypoxia initially increased myoglobin expression but later triggered an adaptive downregulation, likely as a protective mechanism to sustained stress [107].

Taken together, the results highlight that moderate, chronic hypoxia (30% DO), rather than extreme or oscillating hypoxic conditions, most effectively promoted myoglobin synthesis in C2C12-based 3D muscle constructs. These findings emphasize the importance of finely tuned oxygen delivery, rather than simply reducing oxygen levels, and underscore the utility of controlled bioreactor systems in elucidating such complex physiological responses.

Building upon the observed benefits of moderate hypoxia, the study next explored whether mechanical stimulation could further enhance myoglobin synthesis under optimal oxygen conditions. To test this, C2C12 cell sheets were cultured at 30% DO and subjected to cyclic mechanical stretch by rolling them around a silicone tube mounted inside the bioreactor and connected to a custom-built stretching device. The system applied a 1 mm total displacement with a 135-second cycle time, mimicking gentle, rhythmic muscle motion. Remarkably, this combination of mechanical loading and moderate hypoxia led to a 25% increase in myoglobin content compared to static sheets cultured at 30% DO alone. These findings suggest that myoglobin synthesis is not only sensitive to biochemical cues such as oxygen tension but also responsive to biomechanical stimuli. While hypoxia alone can promote a myogenic adaptation, the added effect of mechanical stretch appears to synergistically stimulate myoglobin production, possibly by simulating a more physiologically relevant environment akin to working muscle.

This dual effect is supported by previous *in vivo* findings. Kanatous et al. showed that exposing mice to 10% hypoxia for three weeks led to increased myoglobin expression in active, working heart muscle, but no change in the slow-twitch soleus and even a decrease in the non-working tibialis anterior [15,108,109]. These results align with the observation that oxygen deprivation alone may not be sufficient; rather, it is the combination of metabolic demand (e.g., mechanical load) and hypoxic signaling that optimally drives myoglobin expression.

In summary, the findings identify four key parameters that influence myoglobin protein synthesis in C2C12 cell sheets:

- **Culture vessel size:** Smaller formats like 24-well plates significantly increased myoglobin levels, potentially due to altered surface-to-volume ratios or edge effects.
- **Culture time:** Myoglobin content increased substantially during the maturation phase, highlighting the importance of extended culture beyond differentiation.
- **Dissolved oxygen:** A controlled DO of 30% air saturation was found to be optimal for enhancing myoglobin expression.
- **Mechanical stimulation:** When combined with 30% DO, cyclic stretch further amplified myoglobin synthesis by an additional 25%.

These insights provide a robust framework for engineering muscle tissue with enhanced oxygen-binding capacity and may offer valuable strategies for optimizing bioartificial muscle systems or studying skeletal muscle physiology under controlled *in vitro* conditions.

6.2. Concluding Remarks

In this study, an integrated approach to engineering 3D skeletal muscle-like tissues using C2C12 cells was presented, with a particular focus on enhancing myoglobin protein synthesis as a marker of muscle functionality. The work was divided into three main parts. First, a straightforward and reproducible protocol to generate C2C12 cell sheets was developed that undergo spontaneous detachment from the culture surface, enabling the formation of 3D constructs without the need for external scaffolds or enzymatic harvesting. These structures were then morphologically and functionally characterized, laying the groundwork for subsequent analyses.

In the second part, computational modeling to simulate oxygen diffusion across the thickness of these cell-dense 3D tissues was employed. The goal was to understand how oxygen availability changes toward the core and to determine the critical thickness beyond which hypoxic stress might impair cellular function or viability. This step was essential for informing the design of later experiments and ensuring physiological relevance in the *in vitro* systems.

Finally, a variety of biochemical, physical, and mechanical parameters were systematically examined that could impact myoglobin expression, applying an engineering lens to the optimization of culture conditions. These investigations included supplementation with known modulators like iron, creatine, and IGF-I, as well as adjustments to physical parameters such as vessel dimensions, oxygen levels, and mechanical stimulation. Among these, four key factors, culture vessel size, culture time, dissolved oxygen levels, and mechanical loading, were identified, that significantly influenced myoglobin protein content. These findings emphasize the importance of tailoring the microenvironment when the goal is to enhance the functional maturation of muscle-like tissues, whether for tissue engineering, pharmacological studies, or cultivated meat applications.

6.3. Future Directions

The work presented in this thesis has established a robust, scaffold-free protocol for fabricating C2C12 muscle constructs and has provided fundamental insights into the critical factors governing their development and functionality. Looking ahead, this research lays a solid foundation for several key avenues of future inquiry, with the ultimate goal of developing scalable and physiologically relevant models for cultivated meat production.

Optimizing Scale-Up and Vascularization. A central challenge identified in this work is the scalability of the constructs. The spontaneous delamination of C2C12 cell sheets, while useful

for scaffold-free 3D formation, is still poorly understood and deserves deeper investigation at the mechanistic level. Additionally, the influence of vessel geometry on myoglobin synthesis appears to be more than a simple scaling effect, suggesting a need to study how spatial constraints, edge effects, or nutrient gradients may interact to shape cellular responses. While the spontaneous delamination method is effective for small-scale applications, its limitations with larger culture vessels and the identified oxygen diffusion barrier for constructs exceeding 5 mm thickness must be addressed. Future research should focus on developing a non-enzymatic, mechanically assisted delamination method that is compatible with large-scale bioreactor systems, ensuring a consistent and cost-effective harvest.

To overcome the oxygen transfer limitation, a primary focus should be on integrating vascular-like networks within the constructs. This could involve co-culturing C2C12 cells with endothelial cells to promote self-assembly of capillary-like structures. Alternatively, advanced biofabrication techniques, such as 3D printing, could be used to directly engineer perfusable microfluidic channels into the tissue, creating an artificial circulatory system that supplies oxygen and nutrients to the construct's core. Such advancements would not only enable the production of larger, thicker tissues but also provide a more physiologically accurate model for studying muscle metabolism and function.

Elucidating Myoglobin Regulation Pathways. The findings on myoglobin synthesis, particularly the inverse correlation with culture vessel size and the synergistic effect of mechanical stretching and dissolved oxygen (DO), open up new areas of research. The next logical step is to delve into the underlying molecular mechanisms.

Future studies should use a multi-omics approach, combining transcriptomics (RNA sequencing) and proteomics (mass spectrometry), to identify the specific genes and protein pathways that are activated in response to these physical and chemical cues. For example, investigating the mechanotransduction pathways triggered by cyclic stretching could reveal novel targets for enhancing protein synthesis. Additionally, further research is needed to understand why supplemented iron is not efficiently incorporated into myoglobin but is instead sequestered in ferritin. A deeper understanding of the interplay between iron transport, storage, and myoglobin synthesis would be crucial. Strategies could include the use of small-molecule activators or gene-editing techniques to upregulate the expression of key enzymes in the heme biosynthesis pathway, thereby forcing the absorbed iron toward myoglobin production.

Assessing Maturation and Functional Fidelity. Finally, while this thesis demonstrated successful myogenic differentiation and myoglobin synthesis, a comprehensive analysis of the long-term functional fidelity of the constructs is essential. Future work should incorporate more advanced functional assays, such as force contraction measurements and calcium signaling analysis, to quantify the mechanical properties and contractile functionality of the engineered muscle. Comparing these functional metrics to those of native muscle tissue would provide a clear benchmark for success. Moreover, a sensory analysis, including taste, texture, and color, could help bridge the gap between scientific progress and consumer perception.

By pursuing these directions, the research initiated in this thesis can build upon the current foundational work toward more scalable approaches for producing cultivated muscle tissue, potentially contributing to the development of sustainable future food systems.

7. Chapter Seven: References

[1] Bach AD, Beier JP, Stern-Staeter J, Horch RE, Bach AD. Skeletal muscle tissue engineering. vol. 8. 2004.

[2] Jana S, Levengood SKL, Zhang M. Anisotropic Materials for Skeletal-Muscle-Tissue Engineering. Advanced Materials 2016;28:10588–612. https://doi.org/10.1002/adma.201600240.

[3] Koning M, Harmsen MC, Van Luyn MJA, Werker PMN. Current opportunities and challenges in skeletal muscle tissue engineering. J Tissue Eng Regen Med 2009;3:407–15. https://doi.org/10.1002/term.190.

[4] Dong R, Ma PX, Guo B. Conductive biomaterials for muscle tissue engineering. Biomaterials 2020;229. https://doi.org/10.1016/j.biomaterials.2019.119584.

[5] De Pieri A, Rochev Y, Zeugolis DI. Scaffold-free cell-based tissue engineering therapies: advances, shortfalls and forecast. NPJ Regen Med 2021;6. https://doi.org/10.1038/s41536-021-00133-3.

[6] Stevens KR, Kreutziger KL, Dupras SK, Korte FS, Regnier M, Muskheli V, Nourse MB, Bendixen K, Reinecke H, Murry CE. Physiological function and transplantation of scaffold-free and vascularized human cardiac muscle tissue. Proceedings of the National Academy of Sciences 2009;106:16568–73.

[7] Fujita H, Shimizu K, Yamamoto Y, Ito A, Kamihira M, Nagamori E. Fabrication of scaffold-free contractile skeletal muscle tissue using magnetite-incorporated myogenic C2C12 cells. J Tissue Eng Regen Med 2010;4:437–43. https://doi.org/10.1002/term.253.

[8] Shimizu T, Yamato M, Kikuchi A, Okano T. Cell sheet engineering for myocardial tissue reconstruction. Biomaterials 2003;24:2309–16. https://doi.org/10.1016/S0142-9612(03)00110-8.

[9] Takahashi H, Okano T. Cell Sheet-Based Tissue Engineering for Organizing Anisotropic Tissue Constructs Produced Using Microfabricated Thermoresponsive Substrates. Adv Healthc Mater 2015;4:2388–407. https://doi.org/10.1002/adhm.201500194.

[10] Hasegawa A, Haraguchi Y, Shimizu T, Okano T. Rapid fabrication system for three-dimensional tissues using cell sheet engineering and centrifugation. J Biomed Mater Res A 2015;103:3825–33. https://doi.org/10.1002/jbm.a.35526.

[11] Ordway GA, Garry DJ. Myoglobin: An essential hemoprotein in striated muscle. Journal of Experimental Biology 2004;207:3441–6. https://doi.org/10.1242/jeb.01172.

[12] Suzuki T, Imai K. Evolution of myoglobin. CMLS, Cell Mol Life Sci 1998;54:979–1004.

[13] Larson AM, Hamilton K, Mykles D. THESIS TEMPORAL EXAMINATION OF MYOGLOBIN AND MYOSIN HEAVY CHAIN EXPRESSION PATTERNS IN VITRO Submitted by. Colorado State University, 2020.

[14] Weller,' PA, Price,' M, Isenberg H, Edwards YH, Jeffreys" AJ. Myoglobin Expression: Early Induction and Subsequent Modulation of Myoglobin and Myoglobin mRNA during Myogenesis. Mol Cell Biol 1986;6:4539–47.

[15] Kanatous SB, Mammen PPA. Regulation of myoglobin expression. Journal of Experimental Biology 2010;213:2741–7. https://doi.org/10.1242/jeb.041442.

[16] Vlecken DH, Testerink J, Ott EB, Sakalis PA, Jaspers RT, Bagowski CP. A critical role for myoglobin in zebrafish development. International Journal of Developmental Biology 2009;53:517–24. https://doi.org/10.1387/ijdb.082651dv.

[17] Langer R, Vacanti JP. Tissue Engineering. Science (1979) 1993;260:920–6.

[18] Khademhosseini A, Langer R. A decade of progress in tissue engineering. Nat Protoc 2016;11:1775–81. https://doi.org/10.1038/nprot.2016.123.

[19] Langer RS, Vacanti JP. TISSUE ENGINEERING: THE CHALLENGES AHEAD. Sci Am 1999;280:86–9.

[20] Reddy MSB, Ponnamma D, Choudhary R, Sadasivuni KK. A comparative review of natural and synthetic biopolymer composite scaffolds. Polymers (Basel) 2021;13. https://doi.org/10.3390/polym13071105.

[21] Naderi H, Matin MM, Bahrami AR. Review paper: Critical issues in tissue engineering: Biomaterials, cell sources, angiogenesis, and drug delivery systems. J Biomater Appl 2011;26:383–417. https://doi.org/10.1177/0885328211408946.

[22] Zhao J, Griffin M, Cai J, Li S, Bulter PEM, Kalaskar DM. Bioreactors for tissue engineering: An update. Biochem Eng J 2016;109:268–81. https://doi.org/10.1016/j.bej.2016.01.018.

[23] Zaszczyńska A, Moczulska-Heljak M, Gradys A, Sajkiewicz P. Advances in 3D printing for tissue engineering. Materials 2021;14. https://doi.org/10.3390/ma14123149.

[24] Murphy S V., De Coppi P, Atala A. Opportunities and challenges of translational 3D bioprinting. Nat Biomed Eng 2020;4:370–80. https://doi.org/10.1038/s41551-019-0471-7.

[25] Mathur V, Agarwal P, Kasturi M, Srinivasan V, Seetharam RN, Vasanthan KS. Innovative bioinks for 3D bioprinting: Exploring technological potential and regulatory challenges. J Tissue Eng 2025;16. https://doi.org/10.1177/20417314241308022.

[26] Zhao Y, Yan Wang E, Lai FB, Cheung K, Radisic M. Organs-on-a-chip: a union of tissue engineering and microfabrication. Trends Biotechnol 2022;41:410–24.

[27] Bakhshandeh B, Ranjbar N, Abbasi A, Amiri E, Abedi A, Mehrabi MR, Dehghani Z, Pennisi CP. Recent progress in the manipulation of biochemical and biophysical cues for engineering functional tissues. Bioeng Transl Med 2023;8. https://doi.org/10.1002/btm2.10383.

[28] Handschin C, Mortezavi A, Plock J, Eberli D. External physical and biochemical stimulation to enhance skeletal muscle bioengineering. Adv Drug Deliv Rev 2015;82:168–75. https://doi.org/10.1016/j.addr.2014.10.021.

[29] Somers SM, Spector AA, Digirolamo DJ, Grayson WL. Biophysical stimulation for engineering functional skeletal muscle. Tissue Eng Part B Rev 2017;23:362–72. https://doi.org/10.1089/ten.teb.2016.0444.

[30] Shimizu T, Yamato M, Kikuchi A, Okano T. Cell sheet engineering for myocardial tissue reconstruction. Biomaterials 2003;24:2309–16. https://doi.org/10.1016/S0142-9612(03)00110-8.

[31] Matsuda N, Shimizu T, Yamato M, Okano T. Tissue engineering based on cell sheet technology. Advanced Materials 2007;19:3089–99. https://doi.org/10.1002/adma.200701978.

[32] Fujita H, Shimizu K, Nagamori E. Novel method for fabrication of skeletal muscle construct from the C2C12 myoblast cell line using serum-free medium AIM-V. Biotechnol Bioeng 2009;103:1034–41. https://doi.org/10.1002/bit.22318.

[33] Takahashi H, Shimizu T, Nakayama M, Yamato M, Okano T. The use of anisotropic cell sheets to control orientation during the self-organization of 3D muscle tissue. Biomaterials 2013;34:7372–80. https://doi.org/10.1016/j.biomaterials.2013.06.033.

[34] Nagamine K, Kawashima T, Sekine S, Ido Y, Kanzaki M, Nishizawa M. Spatiotemporally controlled contraction of micropatterned skeletal muscle cells on a hydrogel sheet. Lab Chip 2011;11:513–7. https://doi.org/10.1039/c0lc00364f.

[35] Hasegawa A, Haraguchi Y, Shimizu T, Okano T. Rapid fabrication system for three-dimensional tissues using cell sheet engineering and centrifugation. J Biomed Mater Res A 2015;103:3825–33. https://doi.org/10.1002/jbm.a.35526.

[36] Nagamori E, Ngo TX, Takezawa Y, Saito A, Sawa Y, Shimizu T, Okano T, Taya M, Kino-oka M. Network formation through active migration of human vascular endothelial cells in a multilayered skeletal myoblast sheet. Biomaterials 2013;34:662–8. https://doi.org/10.1016/j.biomaterials.2012.08.055.

[37] Ngo TX, Nagamori E, Kikuchi T, Shimizu T, Okano T, Taya M, Kino-oka M. Endothelial cell behavior inside myoblast sheets with different thickness. Biotechnol Lett 2013;35:1001–8. https://doi.org/10.1007/s10529-013-1174-x.

[38] Chen S, Kawazoe N, Chen G. Biomimetic Assembly of Vascular Endothelial Cells and Muscle Cells in Microgrooved Collagen Porous Scaffolds. Tissue Eng Part C Methods 2017;23:367–76. https://doi.org/10.1089/ten.tec.2017.0088.

[39] Bach A. A new approach to tissue engineering of vascularized skeletal muscle. J Cell Mol Med 2006;10. https://doi.org/10.2755/jcmm010.003.14.

[40] Levenberg S, Rouwkema J, Macdonald M, Garfein ES, Kohane DS, Darland DC, Marini R, Van Blitterswijk CA, Mulligan RC, D'Amore PA, Langer R. Engineering vascularized skeletal muscle tissue. Nat Biotechnol 2005;23:879–84. https://doi.org/10.1038/nbt1109.

[41] Kim JJ, Hou L, Huang NF. Vascularization of three-dimensional engineered tissues for regenerative medicine applications. Acta Biomater 2016;41:17–26. https://doi.org/10.1016/j.actbio.2016.06.001.

[42] Gilbert-Honick J, Grayson W. Vascularized and Innervated Skeletal Muscle Tissue Engineering. Adv Healthc Mater 2020;9. https://doi.org/10.1002/adhm.201900626.

[43] Carrier RL, Rupnick M, Langer R, Schoen FJ, Freed LE, Vunjak-novakovic G. Perfusion Improves Tissue Architecture of Engineered Cardiac Muscle. Tissue Eng 2002;8.

[44] Vollert I, Seiffert M, Bachmair J, Sander M, Eder A, Conradi L, Vogelsang A, Schulze T, Uebeler J, Holnthoner W, Redl H, Reichenspurner H, Hansen A, Eschenhagen T. In vitro perfusion of engineered heart tissue through endothelialized channels. Tissue Eng Part A 2014;20:854–63. https://doi.org/10.1089/ten.tea.2013.0214.

[45] Cerino G, Gaudiello E, Grussenmeyer T, Melly L, Massai D, Banfi A, Martin I, Eckstein F, Grapow M, Marsano A. Three Dimensional Multi-Cellular Muscle-Like Tissue Engineering in Perfusion-Based Bioreactors. Biotechnol Bioeng 2016;113:226–36. https://doi.org/10.1002/bit.25688/abstract.

[46] Jiang S, Zheng Y, Xia H, Liu Z, Rao S, Wang Y, Sun H, Lu X, Xie C. Oxygen-Releasing Hydrogels for Tissue Regeneration. Adv Nanobiomed Res 2024;4. https://doi.org/10.1002/anbr.202300133.

[47] Suvarnapathaki S, Nguyen A, Goulopoulos A, Camci-Unal G. Oxygen-Generating Scaffolds for Cardiac Tissue Engineering Applications. ACS Biomater Sci Eng 2023;9:409–26. https://doi.org/10.1021/acsbiomaterials.2c00853.

[48] Mozafari M, Barbati ME. Oxygen-generating biomaterials for cardiovascular engineering: unveiling future discoveries. Drug Discov Today 2024;29. https://doi.org/10.1016/j.drudis.2024.104135.

[49] McMurtrey RJ. Analytic models of oxygen and nutrient diffusion, metabolism dynamics, and architecture optimization in three-dimensional tissue constructs with applications and insights in cerebral organoids. Tissue Eng Part C Methods 2016;22:221–49. https://doi.org/10.1089/ten.tec.2015.0375.

[50] Cioffi M, Küffer J, Ströbel S, Dubini G, Martin I, Wendt D. Computational evaluation of oxygen and shear stress distributions in 3D perfusion culture systems: Macro-scale and micro-structured models. J Biomech 2008;41:2918–25. https://doi.org/10.1016/j.jbiomech.2008.07.023.

[51] Coletti F, Macchietto S, Elvassore N. Mathematical modeling of three-dimensional cell cultures in perfusion bioreactors. Ind Eng Chem Res 2006;45:8158–69. https://doi.org/10.1021/ie051144v.

[52] Ordway GA, Garry DJ. Myoglobin: An essential hemoprotein in striated muscle. Journal of Experimental Biology 2004;207:3441–6. https://doi.org/10.1242/jeb.01172.

[53] Brunori M, Bourgeois D, Vallone B. The structural dynamics of myoglobin. J Struct Biol 2004;147:223–34. https://doi.org/10.1016/j.jsb.2004.04.008.

[54] Ordway GA, Garry DJ. Myoglobin: An essential hemoprotein in striated muscle. Journal of Experimental Biology 2004;207:3441–6. https://doi.org/10.1242/jeb.01172.

[55] Brunori M, Bourgeois D, Vallone B. The structural dynamics of myoglobin. J Struct Biol 2004;147:223–34. https://doi.org/10.1016/j.jsb.2004.04.008.

[56] Wittenberg JB, Wittenberg BA. Myoglobin function reassessed. Journal of Experimental Biology 2003;206:2011–20. https://doi.org/10.1242/jeb.00243.

[57] Gros G, Wittenberg BA, Jue T. Myoglobin's old and new clothes: From molecular structure to function in living cells. Journal of Experimental Biology 2010;213:2713–25. https://doi.org/10.1242/jeb.043075.

[58] Datar I, Betti M. Possibilities for an in vitro meat production system 2010;11:13–22. https://doi.org/10.1016/j.ifset.2009.10.007.

[59] Tuomisto HL, Teixeira De Mattos MJ. Environmental impacts of cultured meat production. Environ Sci Technol 2011;45:6117–23. https://doi.org/10.1021/es200130u.

[60] Sinke P, Swartz E, Sanctorum H, van der Giesen C, Odegard I. Ex-ante life cycle assessment of commercial-scale cultivated meat production in 2030. International Journal of Life Cycle Assessment 2023;28:234–54. https://doi.org/10.1007/s11367-022-02128-8.

[61] Sharma S, Thind SS, Kaur A. In vitro meat production system: why and how? J Food Sci Technol 2015;52:7599–607. https://doi.org/10.1007/s13197-015-1972-3.

[62] Acevedo CA, Orellana N, Avarias K, Ortiz R, Benavente D, Prieto P. Micropatterning Technology to Design an Edible Film for In Vitro Meat Production. Food Bioproc Tech 2018;11:1267–73. https://doi.org/10.1007/s11947-018-2095-4.

[63] Ben-Arye T, Shandalov Y, Ben-Shaul S, Landau S, Zagury Y, Ianovici I, Lavon N, Levenberg S. Textured soy protein scaffolds enable the generation of three-dimensional bovine skeletal muscle tissue for cell-based meat. Nat Food 2020;1:210–20. https://doi.org/10.1038/s43016-020-0046-5.

[64] Ramachandraiah K. Potential development of sustainable 3d-printed meat analogues: A review. Sustainability (Switzerland) 2021;13:1–20. https://doi.org/10.3390/su13020938.

[65] Choudhury D, Tseng TW, Swartz E. The Business of Cultured Meat. Trends Biotechnol 2020;38:573–7. https://doi.org/10.1016/j.tibtech.2020.02.012.

[66] Pandurangan M, Kim DH. A novel approach for in vitro meat production. Appl Microbiol Biotechnol 2015;99:5391–5. https://doi.org/10.1007/s00253-015-6671-5.

[67] Bomkamp C, Skaalure SC, Fernando GF, Ben-Arye T, Swartz EW, Specht EA. Scaffolding Biomaterials for 3D Cultivated Meat: Prospects and Challenges. Advanced Science 2022;9:1–40. https://doi.org/10.1002/advs.202102908.

[68] David Yaffe, Ora Saxel. Serial passaging and differentiation of myogenic cells isolated from dystrophic mouse muscle. Nature 1977;270:725–7. https://doi.org/https://doi.org/10.1038/270725a0.

[69] Shahin-Shamsabadi A, Selvaganapathy PR. π-SACS: PH Induced Self-Assembled Cell Sheets without the Need for Modified Surfaces. ACS Biomater Sci Eng 2020;6:5346–56. https://doi.org/10.1021/acsbiomaterials.0c01073.

[70] Burkholder JB, Sander SP, Abbatt JPD, Barker JR, Huie RE, Kolb CE, Kurylo MJ, Orkin VL, Wilmouth DM, Wine PH. Chemical Kinetics and Photochemical Data for Use in Atmospheric Studies, Evaluation No. 19. JPL Publications 19-5 2020:1–153.

[71] Sander R. Compilation of Henry's law constants (version 5.0.0) for water as solvent. vol. 23. 2023. https://doi.org/10.5194/acp-23-10901-2023.

[72] Smith FL, Harvey AH. Avoid common pitfalls when using Henry's law. Chem Eng Prog 2007;103:33–9.

[73] Henry C.H. Ko, Bruce K. Milthorpe, Clive D. McFarland. 2014 - Engineering thick tissues – The vascularisation problem. HCH Ko European Cells and Materials 2007;14:1–19.

[74] El-Din Ahmed Bekhit A, Morton JD, Bhat ZF, Zequan X. Meat colour: Chemistry and measurement systems. Encyclopedia of Food Chemistry, Elsevier; 2018, p. 211–7. https://doi.org/10.1016/B978-0-08-100596-5.22419-0.

[75] Kastanek F, Spacilova M, Krystynik P, Dlaskova M, Solcova O. Fenton Reaction–Unique but Still Mysterious. Processes 2023;11. https://doi.org/10.3390/pr11020432.

[76] Pizzino G, Irrera N, Cucinotta M, Pallio G, Mannino F, Arcoraci V, Squadrito F, Altavilla D, Bitto A. Oxidative Stress: Harms and Benefits for Human Health. Oxid Med Cell Longev 2017;2017. https://doi.org/10.1155/2017/8416763.

[77] Fairchild MD. Color Appearance Models (3rd edition). John Wiley & Sons; 2013.

[78] Riemer J, Hoepken HH, Czerwinska H, Robinson SR, Dringen R. Colorimetric ferrozine-based assay for the quantitation of iron in cultured cells. Anal Biochem 2004;331:370–5. https://doi.org/10.1016/j.ab.2004.03.049.

[79] Benedetti S, Catalani S, De Stefani S, Primiterra M, Fraternale A, Palma F, Palini S. A microplate-based DCFH-DA assay for the evaluation of oxidative stress in whole semen. Heliyon 2022;8. https://doi.org/10.1016/j.heliyon.2022.e10642.

[80] Arosio P, Elia L, Poli M. Ferritin, cellular iron storage and regulation. IUBMB Life 2017;69:414–22. https://doi.org/10.1002/iub.1621.

[81] Seo AY, Xu J, Servais S, Hofer T, Marzetti E, Wohlgemuth SE, Knutson MD, Chung HY, Leeuwenburgh C. Mitochondrial iron accumulation with age and functional consequences. 2008.

[82] Rommel C, Bodine SC, Clarke BA, Rossman R, Nunez L, Stitt TN, Yancopoulos GD, Glass DJ. Mediation of IGF-1-induced skeletal myotube hypertrophy by PI(3)K/Akt/mTOR and PI(3)K/Akt/GSK3 pathways. vol. 3. 2001.

[83] Leto D, Saltiel AR. Regulation of glucose transport by insulin: Traffic control of GLUT4. Nat Rev Mol Cell Biol 2012;13:383–96. https://doi.org/10.1038/nrm3351.

[84] Shimizu T, Yamato M, Kikuchi A, Okano T. Cell sheet engineering for myocardial tissue reconstruction. Biomaterials 2003;24:2309–16. https://doi.org/10.1016/S0142-9612(03)00110-8.

[85] Yamamoto Y, Ito A, Kato M, Kawabe Y, Shimizu K, Fujita H, Nagamori E, Kamihira M. Preparation of artificial skeletal muscle tissues by a magnetic force-based tissue

engineering technique. J Biosci Bioeng 2009;108:538–43. https://doi.org/10.1016/j.jbiosc.2009.05.019.

[86] Sakaguchi K, Shimizu T, Okano T. Construction of three-dimensional vascularized cardiac tissue with cell sheet engineering. Journal of Controlled Release 2015;205:83–8. https://doi.org/10.1016/j.jconrel.2014.12.016.

[87] Sieben M, Giese H, Grosch JH, Kauffmann K, Büchs J. Permeability of currently available microtiter plate sealing tapes fail to fulfil the requirements for aerobic microbial cultivation. Biotechnol J 2016;11:1525–38. https://doi.org/10.1002/biot.201600054.

[88] Ihling N, Berg C, Paul R, Munkler LP, Mäkinen MEL, Chotteau V, Büchs J. Scale-down of CHO cell cultivation from shake flasks based on oxygen mass transfer allows application of parallelized, non-invasive, and time-resolved monitoring of the oxygen transfer rate in 48-well microtiter plates. Biotechnol J 2023;18. https://doi.org/10.1002/biot.202300053.

[89] Wagner BA, Venkataraman S, Buettner GR. The rate of oxygen utilization by cells. Free Radic Biol Med 2011;51:700–12. https://doi.org/10.1016/j.freeradbiomed.2011.05.024.

[90] Guarino RD, Dike LE, Haq TA, Rowley JA, Pitner JB, Timmins MR. Method for determining oxygen consumption rates of static cultures from microplate measurements of pericellular dissolved oxygen concentration. Biotechnol Bioeng 2004;86:775–87. https://doi.org/10.1002/bit.20072.

[91] Fiedler T, Belova I V., Murch GE, Poologasundarampillai G, Jones JR, Roether JA, Boccaccini AR. A comparative study of oxygen diffusion in tissue engineering scaffolds. J Mater Sci Mater Med 2014;25:2573–8. https://doi.org/10.1007/s10856-014-5264-7.

[92] Umber Cheema, Zimei Rong, Omar Kirresh, Alexander J. MacRobert, Pankaj Vadgama and Brown RA. Oxygen diffusion through collagen scaffolds at defined densities: implications for cell survival in tissue models. J Tissue Eng Regen Med 2012;6:77–84. https://doi.org/10.1002/term.402.

[93] Simsa R, Yuen J, Stout A, Rubio N, Fogelstrand P, Kaplan DL. Extracellular heme proteins influence bovine myosatellite cell proliferation and the color of cell-based meat. Foods 2019;8. https://doi.org/10.3390/foods8100521.

[94] Mancini RA, Hunt MC. Current research in meat color. Meat Sci., vol. 71, 2005, p. 100–21. https://doi.org/10.1016/j.meatsci.2005.03.003.

[95] Hunt M, King A. AMSA Meat Color Measurement Guidelines. Illinoise: American Meat Science Association; 2012.

[96] Fraeye I, Kratka M, Vandenburgh H, Thorrez L. Sensorial and Nutritional Aspects of Cultured Meat in Comparison to Traditional Meat: Much to Be Inferred. Front Nutr 2020;7. https://doi.org/10.3389/fnut.2020.00035.

[97] M.J. Post, J.-F. Hocquette. New Sources of Animal Proteins: Cultured Meat. Woodhead Publishing; 2017.

[98] Florini JR, Ewton DZ, Roof SL. Insulin-Like Growth Factor-I Stimulates Terminal Myogenic Differentiation by Induction of Myogenin Gene Expression. 1991.

[99] Florini JR, Ewton DZ, Magri KA. Hormones, growth factors, and myogenic differentiation. vol. 53. 1991.

[100] Peters EL, van der Linde SM, Vogel ISP, Haroon M, Offringa C, de Wit GMJ, Koolwijk P, van der Laarse WJ, Jaspers RT. IGF-1 attenuates hypoxia-induced atrophy but inhibits myoglobin expression in C2C12 skeletal muscle myotubes. Int J Mol Sci 2017;18. https://doi.org/10.3390/ijms18091889.

[101] Witt R, Weigand A, Boos AM, Cai A, Dippold D, Boccaccini AR, Schubert DW, Hardt M, Lange C, Arkudas A, Horch RE, Beier JP. Mesenchymal stem cells and myoblast differentiation under HGF and IGF-1 stimulation for 3D skeletal muscle tissue engineering. BMC Cell Biol 2017;18. https://doi.org/10.1186/s12860-017-0131-2.

[102] Louis M, Van Beneden R, Dehoux M, Thissen JP, Francaux M. Creatine increases IGF-I and myogenic regulatory factor mRNA in C 2C12 cells. FEBS Lett 2004;557:243–7. https://doi.org/10.1016/S0014-5793(03)01504-7.

[103] Deldicque L, Theisen D, Bertrand L, Hespel P, Hue L, Francaux M. Creatine enhances differentiation of myogenic C 2 C 12 cells by activating both p38 and Akt/PKB pathways. Am J Physiol Cell Physiol 2007;293:1263–71. https://doi.org/10.1152/ajpcell.00162.2007.-In.

[104] Baltazar Reynafarje. Myoglobin content and enzymatic activity of muscle and altitude adaptation'. J Appl Physiol 1962;17:301–5. https://doi.org/10.1152/jappl.1962.17.2.301.

[105] Widmer HR, Hoppeler H, Nevo E, Richard Taylor, Weibel ER. Working underground: Respiratory adaptations in the blind mole rat. Physiology 1997;94:2062–7.

[106] Terrados N, Jansson E, SYLVfiN C, Kaijser L, Sylvan C. Is hypoxia a stimulus for Synthesis of oxidative enzymes and myoglobin. J Appl Physiol 1990;68:2369–72.

[107] Herawati M, Wardaya, Mulyawan W, Farhan FS, Ferdinal F, Jusman SWA, Sadikin M. Expression of Hypoxia-Inducible Factor-1α and Myoglobin in Rat Heart as Adaptive Response to Intermittent Hypobaric Hypoxia Exposure. Hayati 2017;24:131–5. https://doi.org/10.1016/j.hjb.2017.08.010.

[108] Kanatous SB, Mammen PPA, Rosenberg PB, Martin CM, White MD, Dimaio JM, Huang G, Muallem S, Garry DJ. Hypoxia reprograms calcium signaling and regulates myoglobin expression. Am J Physiol Cell Physiol 2009;296:393–402. https://doi.org/10.1152/ajpcell.00428.2008.-Myoglobin.

[109] Wittenberg BA. Both hypoxia and work are required to enhance expression of myoglobin in skeletal muscle. Focus on "Hypoxia reprograms calcium signaling and regulates myoglobin expression." Am J Physiol Cell Physiol 2009;296. https://doi.org/10.1152/ajpcell.00002.2009.